Corrosion Evaluation of 13Cr (AISI 420) Stainless Steel: Synergic Effects of Environmental Factors and Microstructure

By

© Mostafa Kazemipour

A Thesis

Submitted to the School of Graduate Studies

In partial fulfillment of the requirements for the degree of

Master of Mechanical Engineering

Faculty of Engineering and Applied Science

Memorial University of Newfoundland

St. John’s, NL

May 2020

This page is intentionally left blank

Abstract

13 Cr (AISI 420) martensitic stainless steel, widely used as an oil country tubular goods (OCTG), is sensitive to localized corrosion especially in the harsh downhole environment of oil and gas wells. The corrosion behavior of the material is determined by both the materials' intrinsic characteristics and environmental conditions. Accordingly, in the first part of the study, the corrosion properties of the 13Cr stainless steel were studied using response surface methodology in three different environmental parameters of temperature, pH, and chloride concentration at the ranges of 22-80°C, 4-7, and 1000-22000 mg/Lit. , respectively. The results were provided as a quadratic model correlating the materials pitting potential to the parameters. In the second part, the effect of the microstructure and micro-phase constituents of the steel on its corrosion performance was investigated. The results showed that a defect-free and partially tempered microstructure containing delta ferrite as a highly concentrated region of chromium could have suitable corrosion properties.

Keywords: 13 Cr (AISI 420) stainless steel, Response surface methodology, Microstructural characterization, Corrosion properties

Acknowledgments

The current thesis has been completed with the help, support, and guidance of a number of great people.

First, I would like to express my deep and sincere gratitude to my parents and my family for giving me a continuous love, kindness, and encouragement in my life and providing a happy and comfortable environment for my growth.

I am really fortunate that I have had a great supervisor, Dr. Ali Nasiri, whom I would like to express my special appreciation and gratitude. I have learned a lot from him during my research and studies so that without his encouragement and support this thesis would have been insurmountable.

I am always thankful to SUNCOR for the provision of funding and a workspace permitting me to develop my research.

I am grateful to my colleagues in my research group. Their friendship, along with our collective struggles , made for valuable input and provided constant sources for inspiration in my research.

I also want to express my gratitude to the labs technicians at Memorial University, whose contributions were instrumental in the completion of this thesis through their expertise to help in building necessary equipment for the experiments.

To my parents

Table of Contents

List of Tables

List of Figures

Acronyms and Abbreviations

CRA	Corrosion Resistant Alloy
SCC	Stress Corrosion Cracking
OCTG	Oil Country Tubular Goods
SSC	Sulfide Stress Cracking
GDP	Gross Domestic Product
HIC	Hydrogen Induced Cracking
SOHIC	Stress Oriented Hydrogen Induced Cracking
SWC	Stepwise Cracking
HPIC	Hydrogen Pressure Induced Cracking
SEM	Scanning Electron Microscopy
API	American Petroleum Institute
YS	Yield Strength
PREV	Pitting Resistance Equivalent
OCP	Open Circuit Potential
WE	Working Electrode
CE	Counter Electrode
RE	Reference Electrode
PDP	Potentiodynamic Polarization
ASTM	American Society for Testing and Materials
AC	Alternating Current
EIS	Electrochemical Impedance Spectroscopy
DOE	Design of Experiment
CPP	Cyclic Potentiodynamic Polarization
CPE	Constant Phase Element
OM	Optical Microscopy
XRD	X-Ray Diffraction
EDX	Energy Dispersive X-ray Spectroscopy
RSM	Response Surface Methodology
ANOVA	Analysis of Variance
SLM	Selective Laser Melting
BCC	Body Centred Cubic
FCC	Face Centred Cubic
BCT	Body Centred Tetragonal
AISI	American Iron and Steel Institute

JCPDS	Joint Committee on Powder Diffraction Standards
E_{Corr}	Corrosion Potential
I_{Corr}	Corrosion Current
E_{Pit}	Pitting Potential
R_{Sol}	Solution Resistance
R_{ct}	Charge Transfer Resistance
pH	Hydrogen Ion Concentration
°C	Degrees Celsius
ppm	Parts per Million
ppb	Parts per Billion
mm	Millimetre
kPa	kilopascal
ISO	International Standard Organization
MPa	Mega Pascal
wt%	Weight Percent
PREN	Pitting Resistance Equivalent
cm	Centimeter
gr	Gram
KSI	Kilo Pounds per Square Inch
PSI	Pounds per Square Inch
min	Minute
A	Ampere
Lit	Liter
nm	Nano-meter
sec	Second
V	Voltage
Hz	Hertz
deg	Degree
mg	Milligram

Chapter 1. Introduction

Corrosion is one of the most important natural phenomena in the world which is the result of electrochemical interactions between materials and the environment. This process is almost seen all around the world and matters in terms of economic and environmental aspects [1]. One of the places in which corrosion can appear as a big issue is oil and gas industries where materials used for production and transportation of the products work in contact with different harsh corrosive environments [2,3]. In order to deal with this issue, many different corrosion-resistant materials have been developed in recent decades. Corrosion-resistant alloys (CRA) are the most common materials used in the environment of oil and gas wells where high service temperatures and pressure, corrosive gases (H_2S and CO_2), chemicals with different pH, and high chloride concentration act together to create a harsh corrosive environment [4]. One of the main CRA materials is stainless steel containing at least 12wt% of chromium element in their chemical composition which grants the steels corrosion protection through covering the surface with a thin layer of chromium oxide [5]. While, this layer usually protects the steels against general corrosion, in the harsh environment containing different aggressive chemicals, the protective layer may locally break down at some weak points and lead to a type of corrosion called pitting corrosion [6,7]. Simultaneous action of the pitting process and the environment stresses facilitate the condition for initiation and propagation of cracks in the steels, called stress corrosion cracking (SCC) which is one of the common reasons for the failures in oil and gas industries [6,8]. Among all types of the stainless steels used in this area, 13Cr (AISI 420) with a martensitic microstructure is widely used in oil and gas harsh downhole environment due to its good mechanical and corrosion properties in sweet and sour environment and less cost compared with other types such as duplex stainless steels [4]. Two groups of the parameters, namely, the environmental factors and materials properties including microstructure, tensile strength, H_2S/CO_2 partial pressures, pH, temperature, chloride concentration of the environment affect mainly the corrosion behavior at oil and gas environment and give the ability to predict the service life of the oil country tubular goods (OCTG) [9,10]. For instance, in sweet environment, increasing the temperature can influence the corrosion rate through changing the chemical composition of the corrosion products on the steels surface [11]. In the environment, the corrosion rate is higher at lower pH and higher CO_2 partial pressures

[11]. In addition, in the mentioned environment, the effect of chloride concentration on the corrosion has been controversial. While some concluded that chloride content does not significantly change the corrosion behavior, others pointed out that even a small amount of chloride can be harmful to the passivity of the steel [11]. It is obvious that the chloride effect still needs more investigation [12]. 13Cr stainless steel shows less corrosion resistance at elevated temperatures (>120-150°C) [13,14]. Many studies also have been performed at different H_2S partial pressure, pH, and temperature [15–17]. However, due to the synergetic interaction of the parameters, the effect of various factors on the corrosion behavior of the martensitic stainless steel remains complicated [18]. The corrosion behavior of stainless steel in a specific environment is also highly dependent on the microstructure and the microphase constituents [19]. The improvement of the corrosion and mechanical properties of the 13Cr stainless steels may be obtained through chemical composition and microstructural modifications. It is shown that adding some elements such as Mo and Ni to the composition of 410 stainless steel can modify its resistance to sulfide stress cracking (SSC) [20–22]. In the case of martensitic stainless steels, quench and tempering are the main heat treatment processes to control the amount of the main phase elements in the microstructure including martensite, carbides, retained austenite, etc. Excellent properties can be obtained by tailoring the amount of each phase by heat treatment methods [23,24]. The effect of each heat treatment parameter, also the fraction of each phase in the corrosion properties of martensitic stainless steels are not well known [25]. For example, while higher austenitizing temperatures can improve pitting resistance, it escalates the corrosion rate [26,27].

Although there has been extensive research works on the types of corrosion, their acting mechanisms, the influence of the environmental factors, and microstructural study of martensitic stainless steels, lack of a comprehensive study and model consisted of all affecting environmental parameters and micro-phase constituents in 13Cr stainless steel corrosion is obvious. Therefore, the objectives of the current research are defined as (1) Developing a model describing the exact role of each environmental factor and then optimization of the model to gain the worst and the best conditions; (2) Trying to find the phases function in the microstructure so that presenting a more developed heat treatment procedures would be possible. The materials used in all the studies are 13Cr (AISI420) stainless steel and the corrosion studies are performed using two common electrochemical methods, i.e., potentiodynamic polarization and electrochemical impedance

spectroscopy. The effect of the H_2S/CO_2 partial pressures is discarded in the research which is known as the research limitation.

Chapter 2. Literature Review

2.1 Corrosion fundamentals

According to the definitions presented during decades, corrosion simply can be defined as the degradation of the material due to the impact of the environment [28]. Different types of materials can be affected by corrosion including concrete, wood, plastic, polymer, and metal. However, metals are the most important materials exposed to corrosion [29]. The degradation usually is categorized into two processes: (a) Non-aqueous (dry) where metals are degraded directly due to the chemical attack and interaction with a dry environment such as oxidizing gases (CO_2, O_2, Sulphur, etc.) either at room, temperature or high temperature and (b) aqueous (wet) corrosion where metals are degraded by electrochemical reactions occurring at low or high-temperature liquid environments (electrolyte) [30,31]. Corrosion also defines as reverse extractive metallurgy as it is depicted in Fig. 2.1 as an example of steel [28].

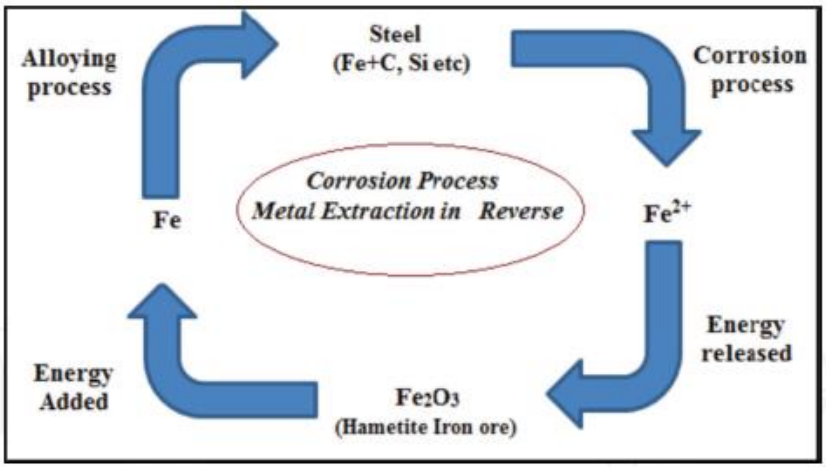

Fig. 2.1. Corrosion defined as a reverse cycle of steel production (taken from [32]).

The life cycle of plain steel can be seen in Fig. 2.1. Iron is most available in nature in the stable form of hematite (Fe_2O_3). The compound will be transformed into steel by consuming energy. According to the thermodynamic laws, metals tend to go to low energy states which are the most stable. Therefore, during a corrosion process, the internally stored energy released again and steel transforms to rust which is literally the same compound as hematite [28,33].

2.1.1 Principles of electrochemical corrosion

Fig. 2.2 shows a simple schematic of wet corrosion cell including two similar or dissimilar metals which are immersed in a solution while they are electrically connected.

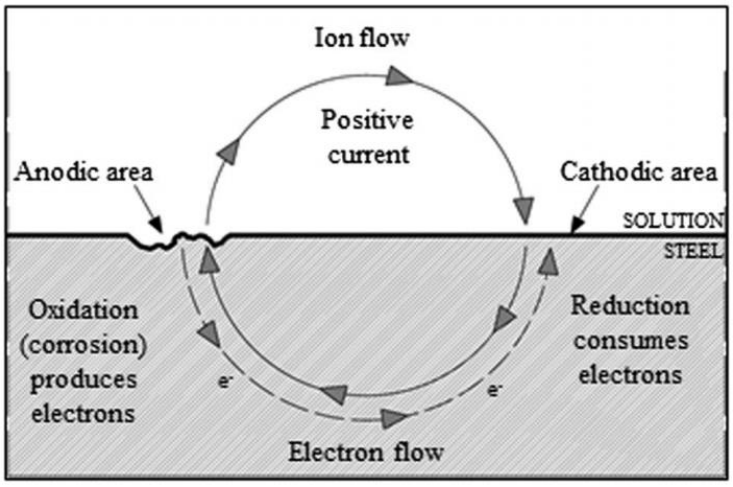

Fig. 2.2. Schematic of a typical corrosion cell (taken from [34]).

A corrosion cell basically has four essential components of anode, cathode, electrolyte (solution), and an electrical connection between anode and cathode parts [28]. An electrochemical reaction also includes mass and charge transfer phenomenon, so that mass (ions and atoms) are transferred between the metals (anode or cathode) and the electrolyte and the electrical charge is transferred between atoms and ions during an electrochemical reaction [35]. Anode which is the more reactive metal (less standard electrochemical potential) than the cathode is dissolved into electrolyte according to the following reaction:

$$M \rightarrow M^{z+} + ze^{-} \qquad (2.1)$$

Where M is a metal, z is the number of electrons taken from each metallic atom and equals the valence capacity of the metal. Due to the insolubility of the produced electrons into the electrolyte, they move toward the cathode through an electrical connection. Cathode side which is less reactive than anode and is not corroded takes up these electrons and during a reduction or cathodic reaction on its surface consumes them. The electrons are consumed for two common main reactions taking place on the cathode surface during corrosion :

Hydrogen evolution:

$$2H^+ + 2e^- \rightarrow H_2 \qquad (2.2)$$

And oxygen reduction in which dissolved oxygen reacts and consumes electrons to produce hydroxyl ions:

$$2H_2O + O_2 + 4e^- \rightarrow 4OH^- \qquad (2.3)$$

Electrolyte is an electrically conductive solution, which charged ions can move in. It is an environment in which dissolved anode ions with positive charge get away from the anode surface.

The fourth part of a complete corrosion cell is the electrical connection which is responsible for carrying electrons from anode to cathode. In a real condition of metallic corrosion, obviously, a separate electrical connection is not required [35]. Herein, the location of anode and cathode are on the same metal but different positions with different electrochemical potentials. Various potential values on the same metal surface are due to the inhomogeneity on the surface or local variations in the electrolyte [36].

2.2 Corrosion in oil and gas fields

The demand for oil and gas as the main energy sources has been increased from 75 in 2000 to 120 million oil barrels per day in 2030 and gas consumption will double during this period [37]. Pipelines play an important role and are central in oil and gas production and transportation from upstream well production sites to downstream destinations of refineries and power stations, where all over the path, corrosion has been always a potential hazard. For instance, risers and flowlines are two important parts of the oil and gas production system. The former is used for transportation of oil, gas, and water from downhole environment to wellhead platforms and the latter transports the products from well platform to the post-treatment facilities such as reservoirs [38,39]. It has been the main concern that the pipelines work in a suitable condition to ensure safe mass production and transportation of oil and gas and prevent any environmental pollution. However, the integrity of the pipelines can be damaged by corrosion. Different chemical species from external (e.g. Oxygen, Chloride ion in deep-sea environment) and internal environment (H_2S, CO_2, organic acids) of the pipelines could cause corrosion and subsequent leakage of the product and failure of the infrastructures [40]. If the water content increases so that the wells productions wet the pipeline metal surface and electrochemical reactions are established, the dissolved H_2S and CO_2 gases would be able to accelerate corrosion by lowering the fluid pH [38]. The main purpose

of dealing with corrosion is safety and avoidance of its consequence because CO_2 and H_2S which are common in oil fields fluids are poisonous for both human and marine beings [40]. In addition, corrosion-related failures, which cover 70% of all oil and gas pipeline failures, could take much cost. There have been different studies on the corrosion cost in many countries such as USA, UK, Japan, Australia, etc., in the past decades [41–43]. 58% of all corrosion-related failures are caused by internal corrosion [44]. Table 2.1 presents a comprehensive analysis of different failure reasons and their frequencies in oil and gas equipment [45].

According to the economic studies, the cost of corrosion in pipelines for a country, particularly in industrialized ones, is around 3.5% of its gross domestic product (GDP) [45]. For instance, in the US, the expenses of corrosion are totally more than 1.372 billion USD per year among which a big portion belongs to pipelines corrosion [40]. The studies show that 589 and 463 million USD were spent in corrosion issues for the surface pipeline infrastructures and downhole tubing equipment, respectively [46].

Table 2.1. Different failure origins in oil and gas equipment (taken from [45]).

Type of failure	Frequency (%)
Corrosion (all types)	33
Fatigue	18
Mechanical damage/overload	14
Brittle fracture	9
Fabrication defects	9
Welding defects	7
Others	10

Many factors can influence corrosion in pipelines including dissolved H_2S and CO_2 gases in the fluid, the temperature of the environment, fluid flow velocity, composition and chemistry and wetting condition of the flowing oil and water, surface condition of the steel pipelines, and the presence of the microorganisms which can induce corrosion. Any change in the above-mentioned parameters could alter the corrosion rate and properties of the pipeline steels as well as the characteristics and compactness of the corrosion product formed on the surfaces. Due to the increase in the volume percentage of water in the fluid inside the pipes over time, the surfaces change from oil wetted to water wetted and therefore the electrochemical reactions run. Over the period, the activity of the microorganisms increases as well. This phenomenon has made the

internal corrosion of the pipelines a serious issue [47]. For instance, the Canadian Association of petroleum producers in 2009 reported that internal corrosion has been the main responsible for all pipeline failures (see Fig. 2.3) [48]. In a pipeline flow, if CO_2 only exists and the fluid contains a water phase, $FeCO_3$ forms on the steel surface as a compact and adherent corrosion product layer, which can act as a barrier against the diffusion of corrosive species to the steel substrate. The formation of this barrier layer can be easier at higher temperatures and pH values. However, if the fluid contains both CO_2 and H_2S, FeS forms more and easier than $FeCO_3$ and needs lower temperatures to be formed. However, this corrosion product layer is not dense, contains porosity, and is electrically conductive so that cannot protect the subsurface steel. Therefore, corrosion of pipelines at the presence of a combination of CO_2, H_2S, and free water can be severe and should constantly be monitored and controlled by chemical agents such as corrosion inhibitors [49].

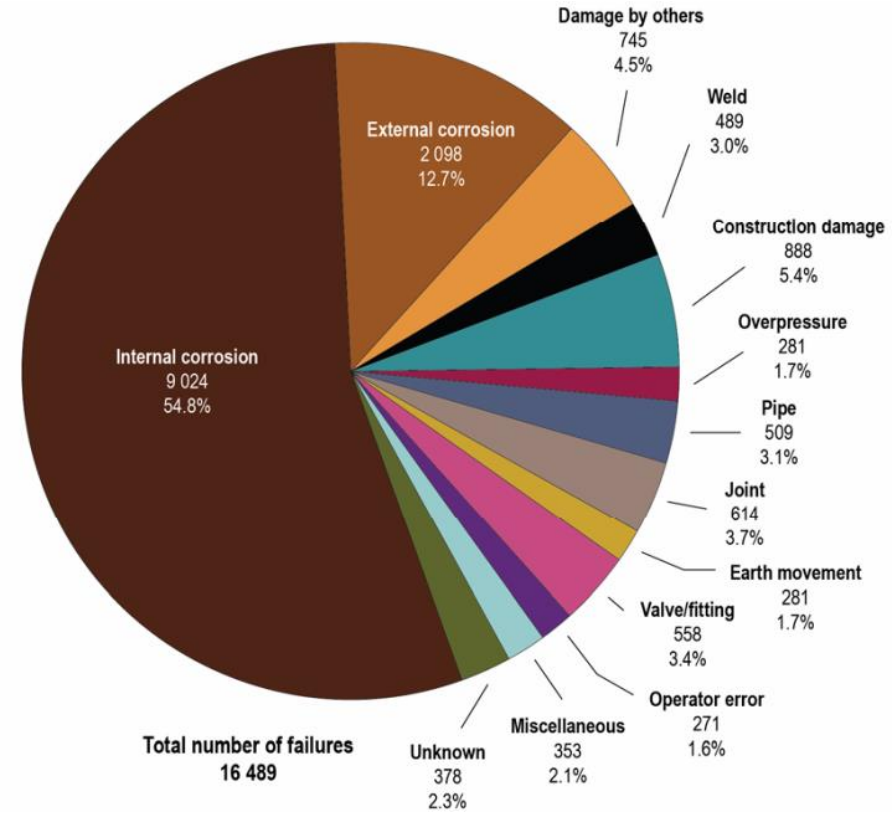

Fig. 2.3. Percentages & causes of all pipeline failures between 1990 to 2012 reported in Alberta. Canada (taken from [48]).

2.3 Corrosion types in the oil and gas industry

Corrosion in the oil and gas industry can be classified in different forms. In can be categorized based on the appearance of the corroded site, corrosion mechanism, the agent caused the corrosion, industry section view, and the method adopted for corrosion prevention. In oil and gas industry corrosion types introduce according to its causes as sweet (CO_2 corrosion), sour (H_2S corrosion), galvanic, crevice, microbial, and stress corrosion cracking [50,51]. Nesic [52] has classified the corrosion types and the frequencies as shown in table 2.2 according to the failures data recorded by Britoil from 1978 to 1988.

Table 2.2. Frequency of occurrence of different forms of corrosion (taken from [52]).

Type of failure	Frequency (%)
CO_2 related corrosion	28
H_2S related corrosion	18
Preferential weld	18
Pitting corrosion	12
Erosion corrosion	12
Galvanic corrosion	6
Crevice corrosion	3
Stress corrosion	3

In this section, some types of corrosion, which are common in oil and gas tubing materials, will be discussed.

2.3.1 Oxygen corrosion

Oxygen as a kind of chemical species with high oxidant power and a tendency to quick reaction with metals is responsible for many cases of corrosion in the oil industry. The concentration of Oxygen is typically very low at the depths of more than 100 meters. Its solubility in water or brines is very low and its concentration at stagnant water is 7-8 ppm so that the resulted corrosion rate would be 0.25 mm/year. This value can increase more than 15mm/year at turbulent conditions. Nonetheless, it can enter during the injection waters at surface processing and storage. Oxygen also can get into the wells' fluids due to leakage in the casing and through a flaw in pump sealing,

vents, etc. Oxygen accepts electron during cathodic reactions and causes anodic dissolution of metals [53–55]. The dissolution of oxygen also escalates the corrosive effects of H_2S and CO_2 gases. The form of Oxygen attack mainly refers to instant pitting corrosion and uniform corrosion that can be seen in different areas [46,56]. Fig. 2.4 shows an example of an Oxygen attack. Anodic and cathodic reactions related to Oxygen corrosion are as follows [40]:

$$Fe \rightarrow Fe^{2+} + 2e^{-} \qquad Anodic\ Reaction \qquad (2.4)$$

$$O_2 + 2H_2O + 4e^{-} \rightarrow 4OH^{-} \qquad Cathodic\ Reaction \qquad (2.5)$$

Since oxygen presence even at concentrations as low as 5 ppb could be destructive for steels, some treatments are necessary to prevent oxygen corrosion. The treatments are using inhibitors, scavengers (e.g. sodium sulfide, sodium bisulfite, hydrazine, etc.), and mechanical deaerator. In the off-shore environment, counter-current gas stripping towers are normally used. At the first step mechanical deaerator is used to diminish Oxygen concentration to low levels and then oxygen scavengers remove it up to low traces [54,57].

Fig. 2.4. A pipe affected by oxygen corrosion (taken from [46]).

2.3.2 CO_2 (Sweet) corrosion

The most recognized type of corrosion in oil and gas production and transportation is CO_2 corrosion. This type of corrosion can cause failure at oil and gas equipment, particularly in downhole tubing. For the first time, sweet corrosion was reported in the 1940s in Texas gas wells. CO_2 gas (dry CO_2) by itself is not corrosive at normal temperatures of oil and gas production

systems, however, when the gas is dissolved in water, it can cause corrosion in high rates through electrochemical reactions with steel [2,58].

Inhibitors can be effective to control and prevent CO_2 corrosion however, if the conditions of high temperature and high pressure of the downhole environment rules, they would be ineffective [40].

2.3.2.1 CO_2 corrosion mechanism

Oil and gas produced in wells usually contain a high amount of CO_2 gases. The gas existed in the produced hydrocarbon fluids, dissolves into the water and forms carbonic acid based on the reactions as follows:

$$CO_2(g) \rightarrow CO_2(aq) \qquad (2.6)$$

$$CO_2(g) + H_2O(l) \leftrightarrow H_2CO_3(aq) \qquad (2.7)$$

The main cathodic reactions in this type of corrosion are presented at Eqs. 2.8-2.10 and the only anodic one, which is on the steel surface, can be identified as iron dissolution at Eq. 2.11:

$$2H_2CO_3(aq) + 2e \leftrightarrow H_2(g) + 2HCO_3^-(aq) \qquad (2.8)$$

$$2HCO_3^-(aq) + 2e \leftrightarrow H_2(g) + 2CO_3^-(aq) \qquad (2.9)$$

$$2H^+(aq) + 2e \leftrightarrow H_2(g) \qquad (2.10)$$

$$Fe(s) \leftrightarrow Fe^{2+}(aq) + 2e \qquad (2.11)$$

The corrosion product which is formed according to the Eqs. 2.12-2.14, is iron carbonate ($FeCO_3$) that is soluble in water, but limited. If it exceeds the limit of the solubility, the product precipitates on the surface. The factors changing the solubility limit include pH, temperature, and CO_2 partial pressure. This corrosion product can cover the surface and protect it from further corrosion and decreases the corrosion rate. According to the environmental conditions, the scale layer is broken and pitting corrosion can take place.

$$Fe^{2+}(aq) + CO_3^{2-}(aq) \leftrightarrow FeCO_3(s) \qquad (2.12)$$

$$Fe^{2+}(aq) + 2CO_3H^-(aq) \leftrightarrow Fe(CO_3H)_2(s) \qquad (2.13)$$

$$Fe(CO_3H)_2(s) \leftrightarrow FeCO_3(s) + CO_2(g) + H_2O(l) \qquad (2.14)$$

2.3.2.2 CO_2 corrosion damages

The types of damages caused by CO_2 are classified based on the shape of the damage in general (uniform) corrosion and three types of localized corrosion including pitting corrosion, mesa attack, and flow-induced localized corrosion [59].

Pitting corrosion (see Fig. 2.5a) typically takes place in stagnant or low-velocity fluid flow and in gas producing wells can be seen in the positions with a temperature about the dew point. The formed pits are not evenly distributed, however occasionally found either adjacent to steel surface inclusions or starting point of mesa attack [60–62]. Generally speaking, pitting susceptibility of steels alters by changing the environmental factors. For instance, an increase in the temperature and chloride (Cl^-) concentration could escalate the pitting corrosion susceptibility. Schmitt et al. [63–65] studied the effect of temperature, chloride concentration, usage of corrosion inhibitors, and the nature of anions and cations in the environments, on the pitting corrosion of low alloy steels and iron when they are undergone CO_2 corrosion. They showed that, in CO_2 environment, all the studied alloys might be damaged by pitting corrosion in its own right environmental conditions. In another investigation, Videm et al. [66,67] found that in CO_2 corrosion, Cl^- concentration does not play a significant role in pitting corrosion of carbon steel.

Mesa corrosion (see Fig. 2.5b) is a type of localized corrosion observed in the environment with low to medium fluid flow velocity. In these flow conditions, the protective iron carbonate scale formed on the surface is unstable and might be pealed off. In this type of corrosion, the uncovered areas by corrosion products act as anode regions, and the adjacent regions are the cathode. The corroded area morphology is either long grooves or flat-bottomed local steps with sharp edges without protective corrosion scales, which is different from erosion-corrosion morphology [59]. Mesa corrosion is highly dependent on fluid composition [68]. Ikeda, et al., [69] proposed that mesa attack could start due to the disturbing effect of Fe_3O_4 on $FeCO_3$ protective film formation. Therefore, the poor formation of the iron carbonate film can act similar to locally destructed film as a prone location to mesa attack.

This type of corrosion is normally in the temperature range of 60 to 90 ^oC, where the protective film may not form enough to protect the subsurface in all situations [70].

If the internal surface of a pipe is damaged by pits or mesa attack, flow-induced localized corrosion initiates in high fluid flows conditions (see Fig. 2.5c). The pits and locally corroded sites in mesa attack and also the particular risen geometries of the environment can make local turbulence in the flow and then this form of corrosion develops. The local turbulent flow may also destroy the protective corrosion product film and prevent the reformation of the scales [63–65].

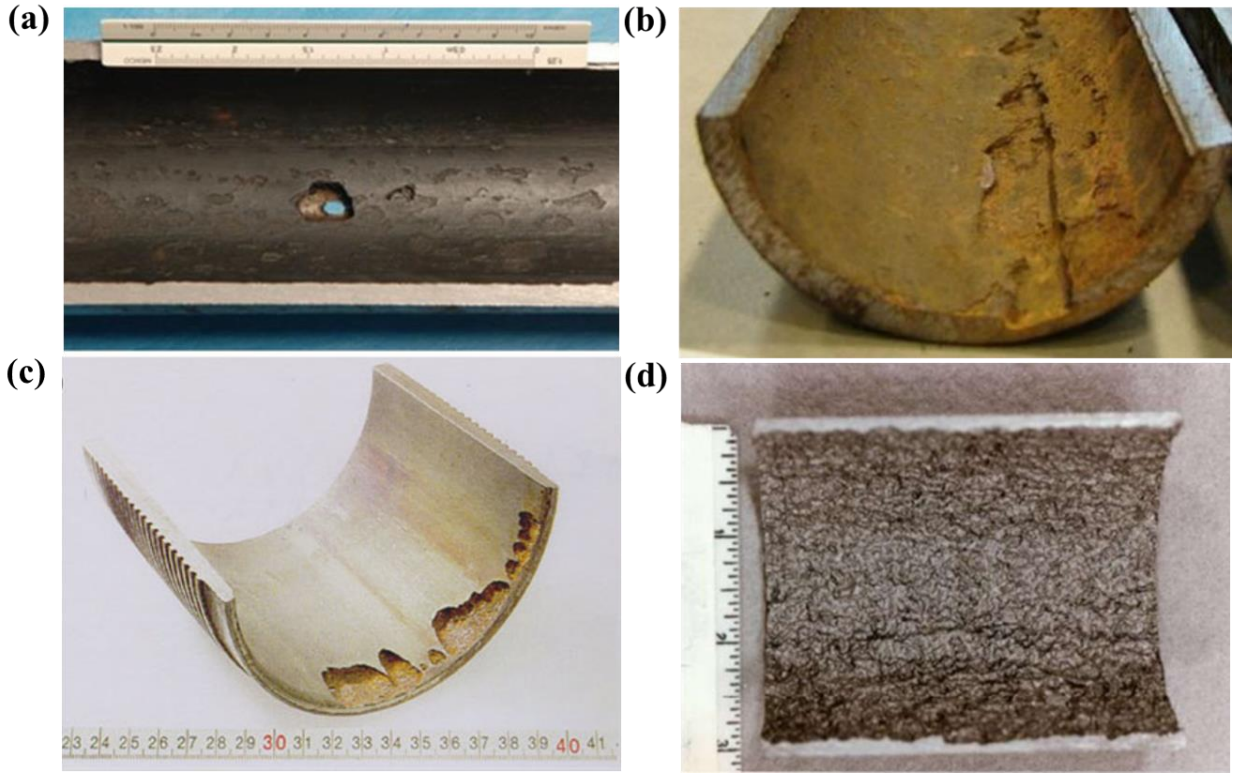

Fig. 2.5. (a) Pitting corrosion (b) Mesa attack (c) Flow-induced localized corrosion (d) Uniform corrosion (taken from [56,71]).

2.3.2.3 Factors controlling CO_2 corrosion

Sweet corrosion and its severity are affected by many factors including environmental, physical, and metallurgical parameters. The main important parameters are listed as follows:

- CO_2 partial pressure

- Temperature

- pH

- Water chemistry

- Steel composition and surface properties

- Fluid characteristics (velocity and dynamics)

All the abovementioned parameters can affect the corrosion severity through influencing corrosion product layer formation and characteristics. The parameters are not dependent, but interdependent and have interactive impact on the corrosion in many ways [2,71]. In this study, the focus has been placed only on the main environmental factors due to their inherent effect on the corrosion properties of the fluid phase on the sweet corrosion [2].

2.3.2.3.1 The effect of CO_2 partial pressure

According to many studies, CO_2 partial pressure is an important factor in corrosion rate and pH control and measurements [2]. Assuming the conditions not leading to the formation of any corrosion product on the steel surface, an increase in the CO_2 partial pressure results in higher corrosion rate due to the increase in the amount of carbonic acid (H_2CO_3) and consequently promoting the following cathodic reaction:

$$2H_2CO_3 + 2e^- \leftrightarrow 2H^+ + 2HCO_3^- \qquad (2.15)$$

Fig. 2.6 shows the dependency of the corrosion rate on the partial pressure of CO_2. As shown, the increasing trend is up to 10 bar and then corrosion rate growth lowers because at higher pressures of CO_2, the concentration of some species such as bicarbonate and carbonate ions increases in the fluid, which in turn promotes the corrosion product precipitation on the surface and prevents more corrosion [72].

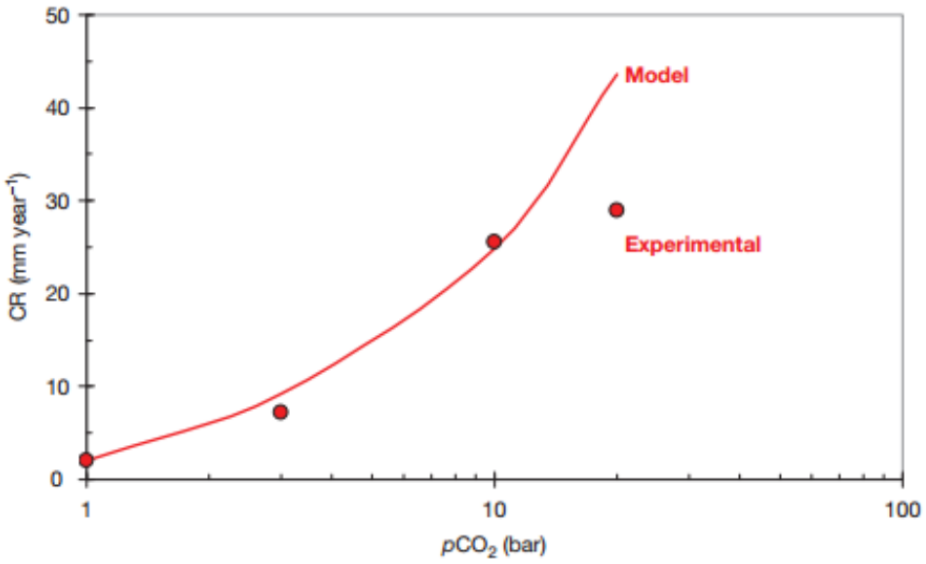

Fig. 2.6. The model and experimental results of the effect of CO_2 partial pressure on the steel corrosion rate at Temp. 60°C and pH=5 (taken from [73]).

2.3.2.3.2 The effect of temperature

Temperature strongly influences all the phenomena involved in the corrosion, including corrosion product film (nature, properties, and morphology), chemical species transportation in the fluid, and chemical and electrochemical reactions at bulk or interface of the metal with the solution. Temperature can either decrease or increase the corrosion rate of the steels depending on its effect on the solubility of the corrosion products. By increasing the temperature (above 80°C), particularly at higher pH values, the solubility of $FeCO_3$ in the solution diminishes and tends to precipitate. However, at sites where the corrosion product layer breaks down, the corrosion can be localized and proceed. At low temperatures, increasing temperature leads to higher corrosion rates due to the higher mobility of the species, higher mass transfer rate, and slow scaling precipitation [74,75]. The temperature can also interactively influence the impact of CO_2 partial pressure (See Fig. 2.7). As shown in Fig. 2.7, at higher CO_2 pressures, the maximum corrosion rate occurs at lower temperature ranges [71].

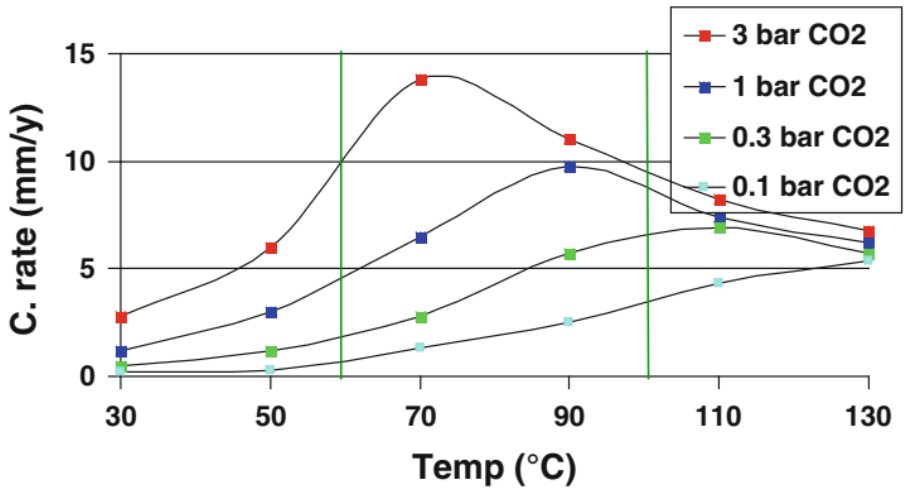

Fig. 2.7. Effect of temperature and CO_2 partial pressure on the corrosion rate of a low alloyed carbon steel (taken from [71]).

2.3.2.3.3 The effect of environment pH

pH is the index for H^+ concentration in the environment. As an important factor, it affects the corrosion product formation and the electrochemical reactions [55]. In addition, Hydrogen reduction (see Eq. 10) by itself is one of the main cathodic reaction occurs in the CO_2 corrosion process. At pH values lower than 4, and low CO_2 partial pressures, the reduction reaction of H^+ is the main cathodic reaction in the environment and carbonic acid reduction can be ignored. Therefore, the pH value is directly determining the corrosion rate. Increasing pH values decreases the solubility of iron ions (Fe^{2+}) and increases the precipitation of iron carbonate film. This leads to lower corrosion rates which are not a linear reduction. For instance, when pH changes from 5 to 6, the reduction of Fe^{2+} is 20 times more than that for 4 to 5 (see Fig. 2.8) [59,61,68]. Increasing pH in the environment containing CO_2 is a technique to reduce the corrosion rate, however, high precipitation rate can also block the pipes in service [72].

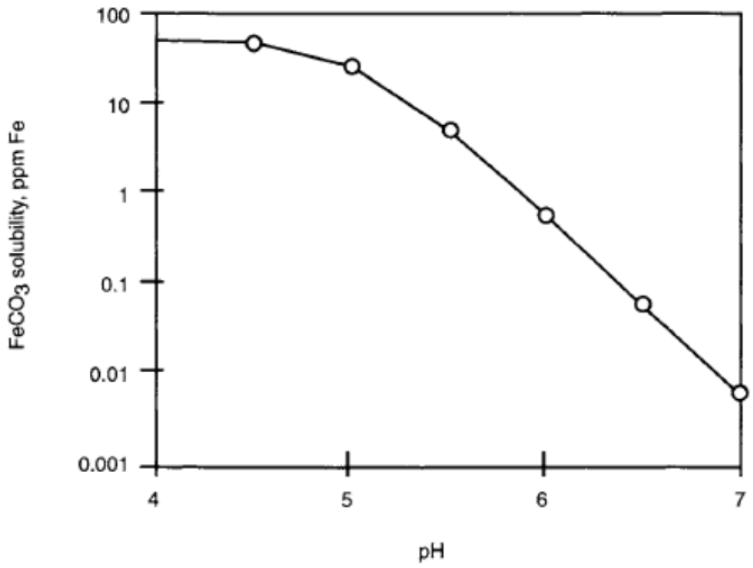

Fig. 2.8. The solubility of $FeCO_3$ vs pH value at Temp. 40°C and CO_2 pressure of 2 bar (taken from [73]).

2.3.3 H_2S (sour) corrosion

Hydrogen sulfide combined with water in the wet area can degrade the steels in oil and gas equipment and facilities, which is called sour corrosion and can make the pipeline steels embrittlement (see Fig. 2.9) [76]. Hydrogen sulfide is not corrosive by itself; however, when it dissolves in water becomes a weak acid and consequently a source of H^+. The corrosion product of sour corrosion is iron sulfide (FeS_x) which is not in a single form, i.e. it can be in different types of amorphous ferrous sulfide, cubic ferrous sulfide, mackinawite, smythite, etc [77]. Iron sulfide scale can act as a corrosion barrier at low temperatures that can decrease the corrosion rate [51]. The overall reaction presenting H_2S corrosion is as the following equation [78]:

$$H_2S + Fe + H_2O \leftrightarrow FeS_x + 2H + H_2O \qquad (2.16)$$

Sun et al. [79] suggested a more detailed mechanism for iron sulfide corrosion based on the formation of mackinawite corrosion film. The reactions involved in the proposed mechanism are shown in Fig. 2.10.

Fig. 2.9. A pit formed by sour corrosion (taken from [56]).

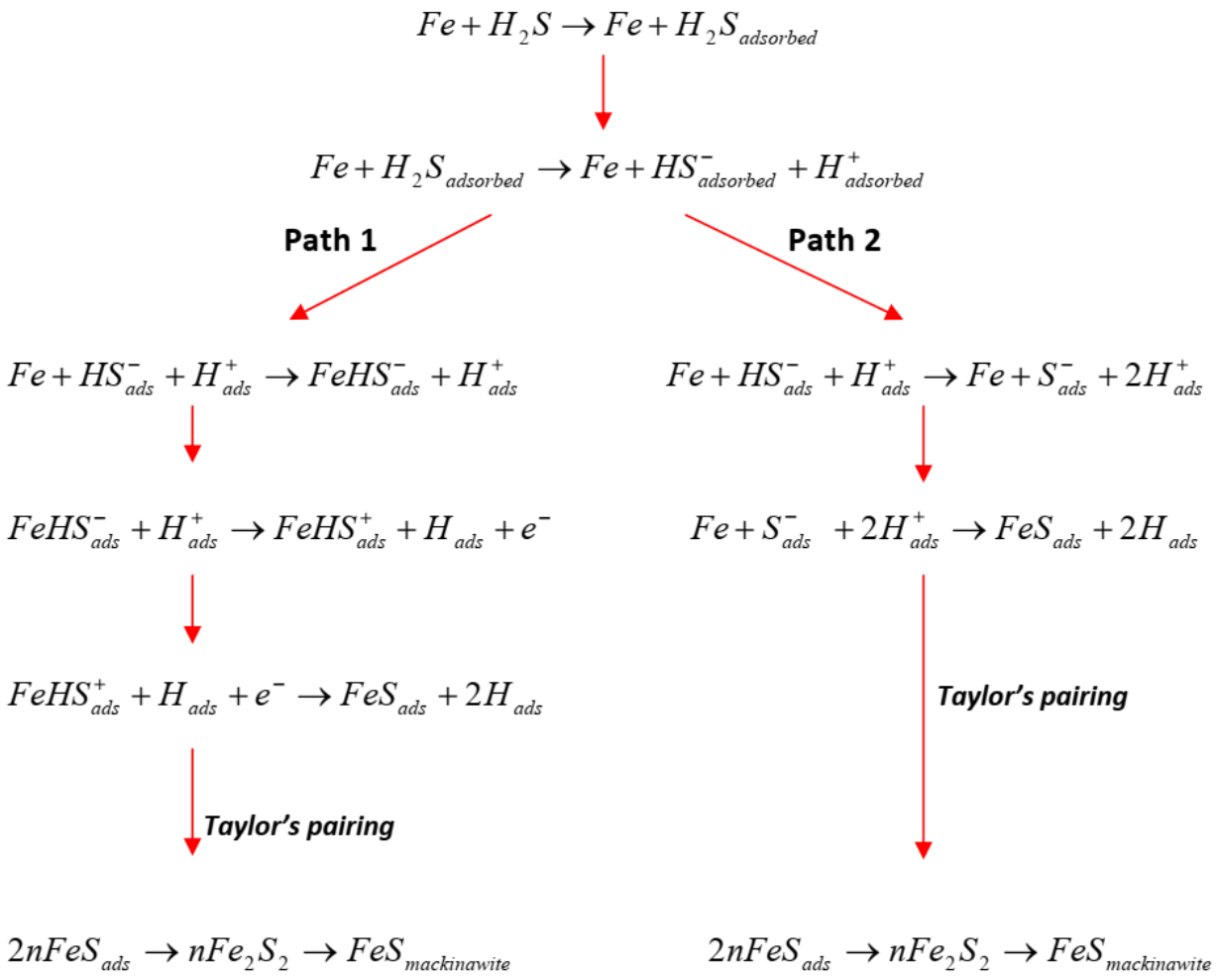

Fig. 2.10. The mechanism presented for H_2S corrosion based on mackinawite film formation [46].

2.3.3.1 Factors controlling H_2S corrosion

Similar to sweet corrosion, a number of parameters affect H_2S corrosion and severity. The factors are interdependent and act interactively. The main factors controlling sour corrosion are as follows:

2.3.3.1.1 The H_2S partial pressure effect

Hydrogen sulfide concentration in the environment has a huge effect on the severity and failure resulted from sour corrosion. The H_2S partial pressure influences the corrosion in two ways. First, an increase in the partial pressure of hydrogen sulfide decreases the pH and could cause a type of hydrogen embattlement called sulfide stress cracking through a cathodic cracking mechanism. If the H_2S pressure is kept lower than 0.3 kPa, SSC can be controlled and would not be an issue [56]. As the second way, H_2S partial pressure is also important in the characteristics of the formed sulfide corrosion product layer so that by increasing H_2S in the environment the corrosion film is looser and less adhesive and therefore has less contribution in corrosion prevention [80].

2.3.3.1.2 The temperature effect

At low-temperature ranges (~<100°C) and short term exposure, the effect of temperature is negligible and corrosion is controlled by the protective corrosion product film in the form of pitting and general corrosion. By increasing the temperature of more than 110°C the protective iron sulfide film tends to be porous and the effect of temperature would be higher [56,77].

2.3.3.1.3 The pH effect

pH is an important factor affecting the corrosion product layer and its composition. Similar to CO_2 corrosion, low pH values (pH<2) drive iron to be dissolved more into the solution. The formed iron sulfide product is highly soluble at low pH and does not precipitate on the steel surface. At higher pH values (pH=3-5), the iron sulfide film forms and precipitates on the surface to protect it against corrosion [81].

2.3.3.2 Types of damages caused by sour corrosion

At addition to typical damages caused by sour corrosion, i.e. general and pitting corrosion, hydrogen sulfide is able to deteriorate oil and gas facilities through other forms of damages among which the most prevalent types are sulfide stress cracking (SSC), hydrogen-induced cracking

(HIC), and stress oriented hydrogen induced cracking (SOHIC). The first two types are the main reasons for the failure of oil and gas pipelines [56].

Sulfide stress cracking (SSC), defined as "brittle failure by cracking under the combined action of tensile stress and corrosion in the presence of water and H_2S", starts from surface pits [82]. This type of cracking is a form of hydrogen embrittlement acting by the cathodic cracking mechanism. The diffusion of hydrogen from the environment through the bulk of steel decreases the ductility. If tensile stress is combined, cracks can initiate and propagate perpendicular to the stress direction [56].

Hydrogen-Induced cracking, also called stepwise cracking (SWC) and hydrogen pressure-induced cracking (HPIC), is a type of cracking caused by the accumulation of hydrogen molecules into the bulk of the steel which can also appear as blistering on the surface. The cracks direction is parallel to the rolling direction of the steel pipes which may not need any external or residual stress to be created. Hydrogen in the atomic form is very small and easily diffuses into the bulk of the steel. The hydrogen atoms recombine to make hydrogen molecules at the trap sites which are normally defects such as inclusions and voids of segregated bands of the microstructure. The trapped hydrogen molecules initiate local cracks which then can propagate and link to other cracks and finally cause failure of the equipment [56,83].

The last type (SOHIC) is related to the previous one, i.e. the interaction between the external or residual stresses and the local straining around the hydrogen-induced cracks and blisters. The appearance of the crack in ladder-type which is a crack array perpendicular to the applied or residual stress. This type of cracking is observed at longitudinally welded pipes. Although this cracking type caused failure in the pipelines in the past, it has not been reported to cause any failure in the modern micro-alloyed pipes [56,83]. Fig. 2.11 depicts a schematic of the discussed cracks.

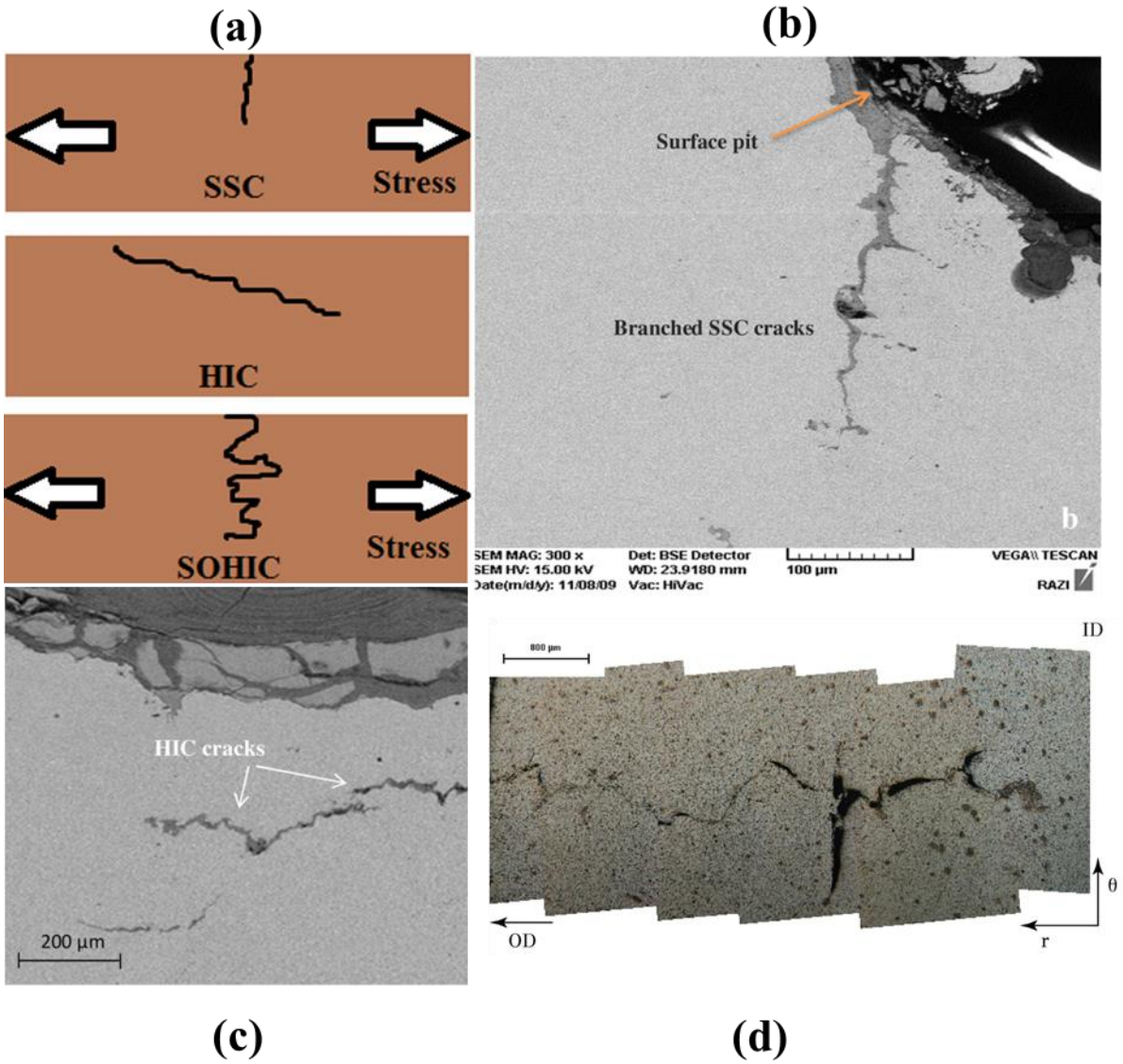

Fig. 2.11. (a) Schematic view of SSC, HIC, and SOHIC (b) SEM micrograph of SSC (c) SEM micrograph of HIC (d) SEM micrograph of SOHIC (taken from [84,85]).

2.4 OCTG used for pipelines in the downhole oil and gas environment

In the last decades, due to the special conditions in the downhole environment and the importance of using corrosion resistance alloys, the pipe manufacturers have been demanded to develop materials with the required characteristics applicable in downhole service conditions. The pipes of interest must be able to operate under high pressure in the oil and gas fields and offer the highest safety while economically affordable. Therefore, the ideal pipes should have high strength, high toughness, good corrosion properties, and optimized geometry. During the last decades, different

grades of high strength steels have been developed. The longitudinally welded pipes are the most common types used in the oil and gas industry [86]. Fig. 2.12 shows the developed API-grades and their attributed toughness.

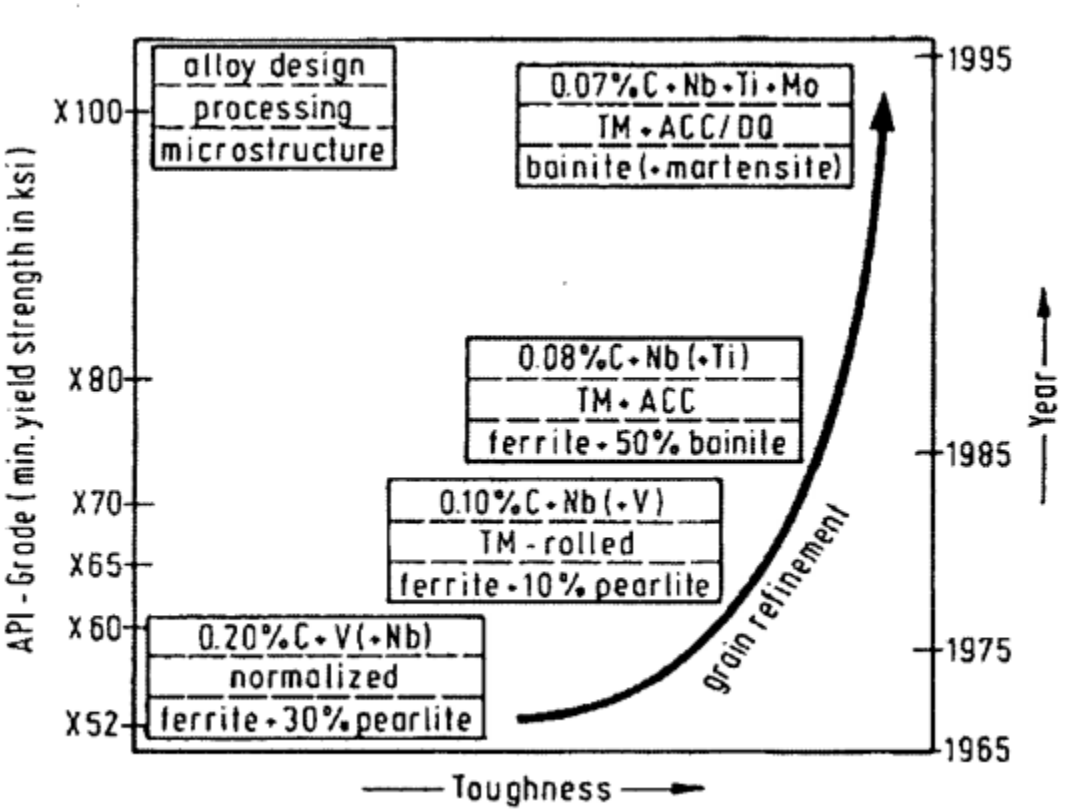

Fig. 2.12. High strength low alloy steels developed from 1965-1995 (taken from [86]).

In the seventies, the adopted new method of thermo-mechanical rolling rather than using the old hot rolling and normalizing one, allowed the pipe manufacturers to reduce the carbon content and add niobium and vanadium in the micro-alloying process which leads to the production of steels up to X70. During the next decade, the thermo-mechanical rolling method was combined with subsequent rapid cooling which resulted in developing higher strength steels like X-80. This new type of steel has better weldability due to its less carbon content. By modifying the production method and also the addition of more alloying elements such as molybdenum, copper, and nickel the higher strength steel of API X-100 was born [86]. Table 2.3 includes the mechanical properties of API steels used in oil and gas industry.

Table 2.3. Mechanical properties required for API steels grade (taken from [73]).

Group	Grade	Type	Total elongation under load (%)	Yield strength (ksi)		Tensile strength Min. (ksi)	Hardness[a] Max.		Specified wall thickness (in)	Allowable hardness variation[b] (HRC)
				Min.	Max.		HRC	HBW		
1	2	3	4	5	6	7	8	9	10	11
1	H40	-	0.5	40	80	60	-	-	-	-
	J55	-	0.5	55	80	75	-	-	-	-
	K55	-	0.5	55	80	95	-	-	-	-
	N80	1	0.5	80	110	100	-	-	-	-
	N80	Q	0.5	80	110	100	-	-	-	-
	R95	-	0.5	95	110	105	-	-	-	-
2	M65	-	0.5	65	85	85	22	235	-	-
	L80	1	0.5	80	95	95	23	241	-	-
	L80	9Cr	0.5	80	95	95	23	241	-	-
	L80	13Cr	0.5	80	95	95	23	241	-	-
	C90	-	0.5	90	105	100	25.4	255	≤0.500 0.501 to 0.749 0.750 to 0.999 ≥ 1.000	3.0 4.0 5.0 6.0
	T95	-	0.5	95	110	105	25.4	255	≤0.500 0.501 to 0.749 0.750 to 0.999 ≥ 1.000	3.0 4.0 5.0 6.0
	C110	-	0.7	110	120	115	30	286	≤0.500 0.501 to 0.749 0.750 to 0.999 ≥ 1.000	3.0 4.0 5.0 6.0
3	P110	-	0.6	110	140	125	-	-	-	-
4	Q125	-	0.65	125	150	135	b	-	≤0.500 0.501 to 0.749 ≥ 0.750	3.0 4.0 5.0

a In case of dispute, laboratory Rockwell C hardness testing shall be used as the referee method.

b No hardness limits are specified, but the maximum variation is restricted as a manufacturing control with 7.8 and 7.9

The term OCTG is the abbreviation for oil country tubular goods which covers a group of welded and seamless pipes for use in the oil and gas industry such as tubing, casing, and drilling pipes. The most known international standard for OCTG industry is ISO 11960. According to the standard, each grade of the steels is named as a two-part name including a prefix letter which is meaningless and a number which represents the minimum yield strength (KSI) of the material. The OCTG materials are categorized into four groups as follows [73]:

a) The first group in which steels come with letters of H, J, K, N, and R includes low strength steels with no resistance to sour corrosion.
b) The steels in the second group with M, L, C, and T letters have 50% reduced yield strength than the first group which can be applied for the sour environment.
c) The third one, which comes with the only letter of P is a high strength grade, not useful for the sour environment.
d) The fourth class with Q letter includes very high strength steels, which are not suitable for H_2S containing environment.

2.4.1 Selection of the appropriate materials for oil and gas fields

It is very significant to select suitable materials in oil and gas industry, which are resistant to corrosion attacks and meet the special mechanical requirements [76]. Stainless steels are a big family of materials that cover a wide range of mechanical and corrosion properties. Many different grades of stainless steel are using in the oil and gas industry depends on the environment condition. The most known and useful types of stainless steel in this area are 13Cr, super 13Cr, 22Cr duplex, 25 Cr duplex, 28 Cr, 825 nickel alloy, and nickel alloys grade of 625, 2550, and C276 [87]. Table 2.4 shows a list of the common alloys used oil and gas industry according to the study of process and operating circumstances.

The selection procedure of corrosion-resistant alloys (CRA) could be very complex for a specific service environment. It is always recommended that before making a final selection for the suitable CRA for a specific environment, it is desirable to test the selected material in a simulated service environment. CRAs are typically resistant to be used in sweet environments however if H_2S and chloride are present in the environment, the maximum service temperature in which they can work without local corrosion is limited. In addition, if the H_2S partial pressure exceeds a certain amount,

which this limit is dependent on the pH, temperature and chloride concentration, they can face sulfide stress cracking. Each group of CRAs shows the maximum susceptibility to SSC in a range of temperatures. For instance, martensitic stainless steels show the highest susceptibility at ambient temperatures. This range for duplex stainless steels is around 80°C in which a combination of SSC and SCC can occur. The above temperature ranges are determining in the maximum allowed partial pressure of H_2S in the environment [87].

Table 2.4. The most common materials used in the oil and gas industry (taken from [46]).

Material specification	Oil and gas applications
Carbon steels	Bulk fluids, crude pipelines, flow lines, water and steam injection lines, production and test separators, KO drums, storage tanks
Low- and medium-alloy steels	Well head items, chokes, manifolds and well components with sour and high-temperature applications
Straight chromium steels (chromium 12% to 18%)	Christmas trees, well heads, downhole rods, valves and casing pipes
Chromium-nickel steels (chromium >18%, nickel >8%)	Valve trims, instruments and materials of separators and tanks, low-chloride levels
Nickel steels (2.5%, 3.5%, 9% nickel)	Rarely used in oil and gas sectors, LNG storage tanks, piping and pumps
Duplex stainless steels (22% chromium duplex, 25% chromium super, duplex)	Piping, vessel and tank internals where a very high level of chlorides is present
Nickel-chrome (inconels) Ni-Cr-Fe alloys	Well head and flow lines, manifolds with high sour and temperature applications
Nickel-iron (incolys) Ni-Fe-Cr alloys	Well head and flow lines, manifolds with high sour and temperature applications

The maximum service temperature for the above-mentioned alloys is more than these ranges so that at that temperature the uniform and pitting corrosion rates are extremely high. The austenitic stainless steels are selected according to the highest temperature in which pitting or SCC may occur [87]. Table 2.5 shows the service limits of using the various classes of alloys in the oil and gas industry.

Table 2.5. Service limits of using various classes of alloys in the oil and gas industry (taken from [87]).

Material	PH_2S (bar)	Temperature (°C)	%NaCl	Comment
9Cr1Mo (grade 80, 552 MPa max. yield strength (YS))	0	…	…	Similar or slightly lower performance to 13Cr but not recommended for tubing
	0.1	Room Temp. (RT)	5	
13Cr(l-80)	0	150	…	Max. Temp. depends on chloride and CO_2 content
	0.001	RT test	5	pH<3
	0.01	RT test	5	3<pH<3-5
	0.1	90	2	pH>3-5, grade 90, 620 MPa max. YS Ni<0-2%
13Cr5Ni2Mo	0.03	150	5	Tested with 30 bar CO_2, superior resistance to SSC than 13Cr
	0.1	150	0.01	Limit of H_2S is a function of chloride content
15Cr	0	180	12	Up to 210°C at lower chloride content
	0.05	200	20	
	0.1	RT test	5	
22Cr duplex	0	200	20	NKK data
and 25Cr duplex	0	250	5	
with PREN <37*	0.1	80	≤1	A lower level of H_2S tolerable at higher levels of chloride or if cold worked above grade 125, 1035, MPa YS
25Cr superduplex	0	250	20	Extrapolated from 22Cr data
PREN ≥ 40	0.375	80	4.6	Grade 110, 965 MPa YS, pH<4
	0.7	80	10	pH>4 (pass data)
UNS N08028	5	100	6.2	Pass data
	13.1	204	2.5	No cracking in the absence of acetic acid
Nickel base alloys	0	…	…	No apparent restrictions within the normal operating temperature range
UNS N09925	5	150	5	SSR tests +47 bar CO_2 (fail)
and N07718	14	150	15	C ring tests +26 bar CO_2 (pass)
UNS N06950	10	170	Any	Also resists elemental sulphur
UNS N08825	60	200	25	Cabval data, NKK data, and Ref. [88]
and N06625				
UNS N10276	660	260	Any	Also resists elemental sulphur
Titanium base alloys	0	…	…	No apparent restrictions within the normal operating temperature range
UNS R58640	66	160-190	20	Temp. limit depends on strength (cold work and heat treatment), also resists elemental sulphur
UNS R56320	10	260	25	Grades 110-190, 965-1310 MPa YS, also resists elemental sulphur
R56400				
R56260				
R58640+Pd				

***PREN is pitting resistance equivalent= %Cr+3.3% Mo+ 16%N**

2.5 13Cr stainless steel

Generally speaking, the addition of 12wt% of chromium or more to carbon steel produces the big family of the stainless steels with a wide range of corrosion resistance properties. Stainless steels are usually classified according to their microstructure as martensitic, ferritic, austenitic, duplex, and precipitation hardened. The hardenable martensitic grade containing minimum chromium content (11-13wt% Cr) has superior atmospheric corrosion resistance than other types of steels. This grade, however, has limited corrosion behavior comparing high alloyed grades in harsh environments [89]. 13Cr tubing stainless steel is typically used in oil and gas industry, particularly in CO_2 containing environment, due to the special performance in terms of good corrosion resistance, good mechanical properties, and more cost-effectiveness compared to other stainless steel grades such as duplex one. However, due to the significant effect of temperature, the corrosion resistance of 13Cr stainless steel is not satisfactorily at high temperatures (>150°C). In addition, if the chloride ions concentration in the environment is more than 50 ppm, this steel is prone to pitting corrosion [4,90–92]. Numerous research works have been performed on corrosion properties, weldability, hydrogen permeation, and SCC of 13Cr stainless steel and many efforts were focused to improve and determine the corrosion resistance. The motivation for working on the alloy has been its potential in cost-effectiveness so that it would replace other expensive stainless steel [93].

Hashizume et al [94] investigated the pH limit for de-passivation of low carbon 13Cr stainless steels with different molybdenum content (0-1.9 wt%) immersed in a solution of 5% NaCl and 0.5 % acetic acid. The pH of the environment was controlled by adding NaOH to the solution. The partial pressure of the corrosive cases of CO_2 and H_2S were 0.0965 MPa and 0.0035 MPa, respectively. The test performed at 24°C for four days. The criteria to distinguish the depassivation pH value were corrosion rate and visual inspection. The results showed that changing the microstructure has a small effect on the de-passivation pH. Changing Mo content in the mentioned range changes the depassivation pH from 3.6 to 3.8.

In a similar study, Linne et al. [95] through a different experimental procedure, which was immersing the samples into a solution of 120 gr/Lit. NaCl and measuring the anodic current density found that the depassivation pH value for modified 13Cr stainless steel is 1.3 while 3.5 for the conventional one.

Fig. 2.13 illustrates the corrosion rate of conventional and modified 13Cr stainless steel versus temperature and chloride content of the solutions. For the conventional steel (AISI 420) when the temperature range and chloride concentration were changing in the ranges of 150-200°C and 5-20 wt%, respectively, the corrosion rate was estimated from 1mm/year to 4 mm/year. In a constant chloride content of 10wt%, by increasing the temperature from 150°C to 200°, the corrosion rate of the modified 13Cr increased from 0.1 mm/year (the criterion limitation for selection) to around 1 mm/year. At a constant temperature of 200°C, for the same alloy, differing the chloride concentration from 5wt% to 20wt% increases the corrosion rate from 0.2 mm/year to 0.7 mm/year [96]. It should be mentioned that the tests performed at 10wt% NaCl, which were in the presence of CO_2 partial pressure of 3 MPa and H_2S partial pressure of 0.005 MPa. All the rest of the tests were done under 4 MPa CO_2 partial pressure.

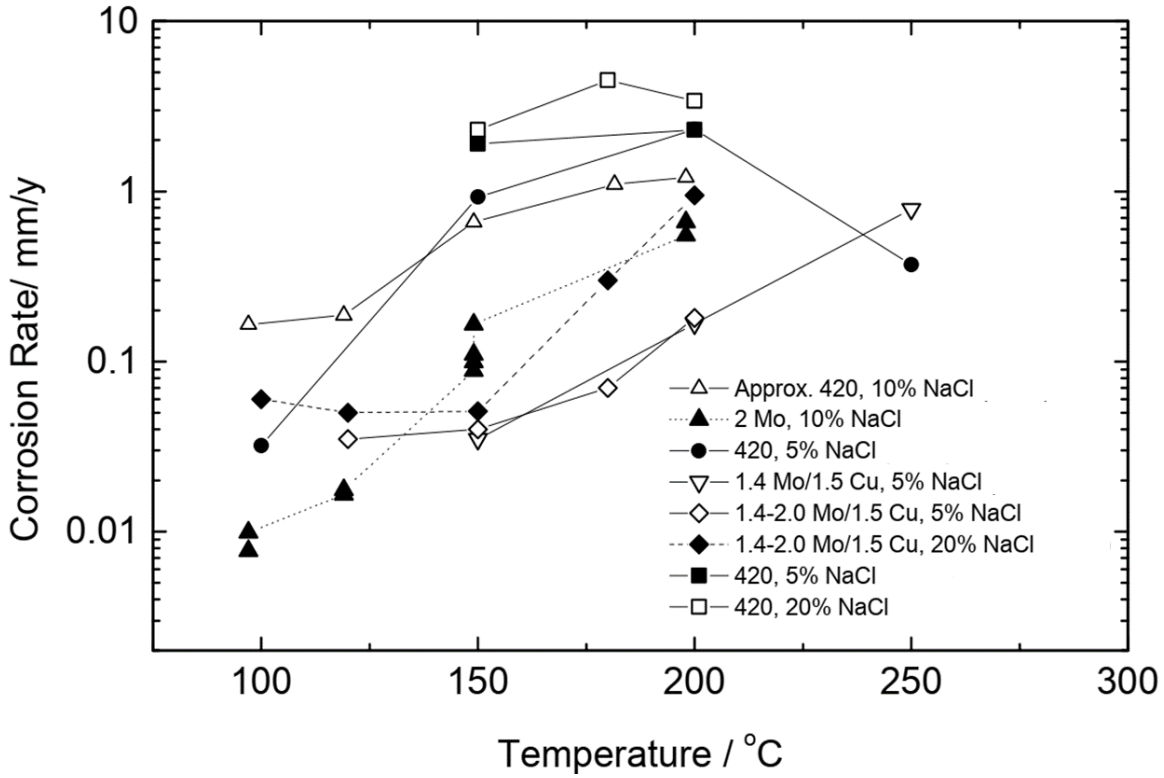

Fig. 2.13. The corrosion rate dependence of conventional (AISI 420) and modified 13Cr stainless steel to temperature and chloride concentration (taken from [96]).

Sakamoto et al [97] investigated the effect of environmental factors on the corrosion properties of API-13Cr and modified 13Cr stainless steels through a series of immersion tests in autoclave. The results showed that at the temperature of 150°C and H_2S partial pressure less than 0.1MPa,

corrosion rate is approximately independent of the H_2S content and pH value is not affected. Nonetheless, they reported some sensitivity at a higher temperature of 200°C.

Miyata et al [98] pointed out the effect of lowering carbon from and adding nickel to the composition in decreasing the general corrosion rate of two new types of martensitic stainless steel in CO_2 environment. They also showed the improvement effect of the addition of Cu to the composition on pitting resistance and Mo addition on SSC resistance. Fig. 2.14 shows the effect of composition, which is introduced as a CO_2 corrosion index, on the corrosion rate.

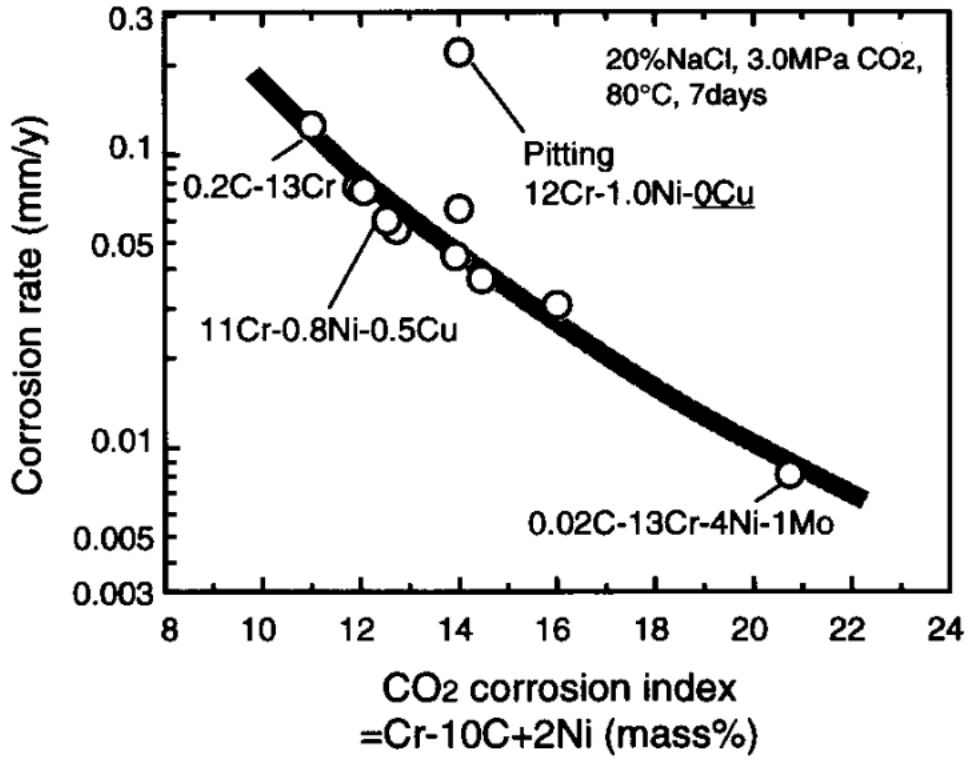

Fig. 2.14. The relation between chemical composition and corrosion rate of stainless steels at 20wt% NaCl and CO_2 partial pressure of 3 MPa (taken from [98]).

Kimura et al [99] studied the effect of retained austenite on the corrosion rate and pitting sensitivity of a modified 13Cr stainless steel with different amounts of retained austenite, which were obtained through quenching and tempering heat treatment process. The CO_2 and H_2S partial pressures were constant values of 0.1 MPa and 0.004 MPa, respectively, while chloride concentration and pH value vary in the experiments. They concluded no relationship between the retained austenite and the corrosion characteristics of the steel in the tested parameters ranges.

Huizinga and Like [100] studied the corrosion rate of a conventional 13Cr stainless steel, with 0.2% carbon content, in varying temperature, chloride concentration, and CO_2 partial pressure. The obtained mathematical model showed that for 0.1 mm/year, the threshold for selection, at 150 gr/Lit. chloride concentration, the studied steel can be used at temperatures up to 125°C.

Ueda et al [101] studied the dependence of corrosion rate, pitting potential, and SSC to temperature for conventional 13Cr, super 13Cr, and weldable 13Cr stainless steels in constant values of 5wt% chloride concentration, 3 MPa CO_2 partial pressure, and 0.001 MPa H_2S partial pressure. Fig. 2.15 shows the results as a graph.

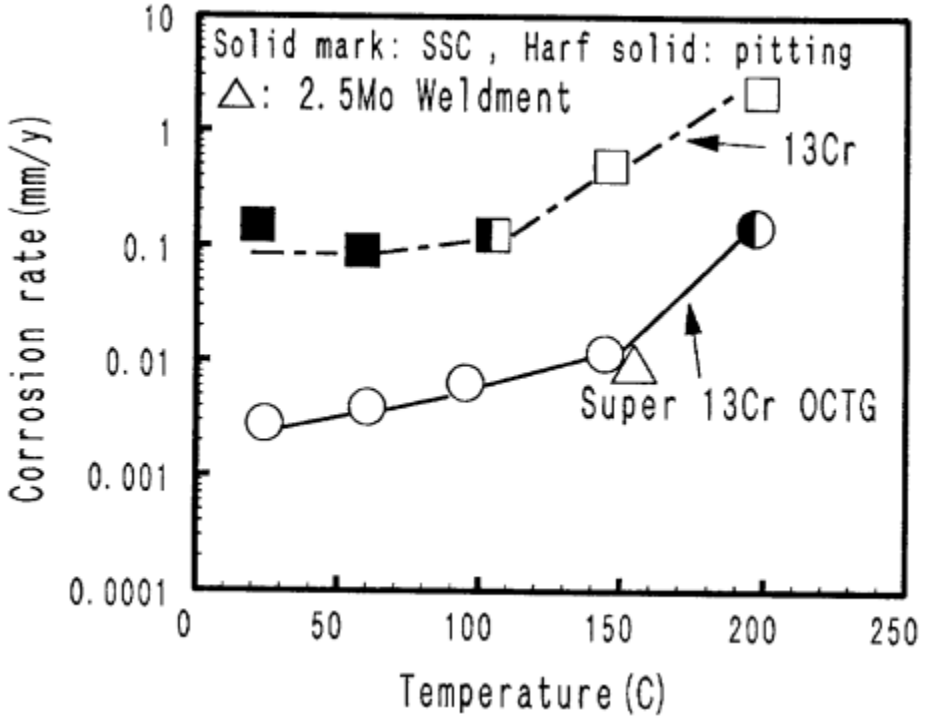

Fig. 2.15. The temperature dependence of 13Cr, super 13Cr, and weldable super 13Cr to corrosion rate, pitting potential and SSC (taken from [101]).

Abayarathna and Kane [102] performed a comprehensive set of tests on a family of 13Cr stainless steels. The tests were done in different environmental conditions as long term exposure to corrosion samples. For all the 13Cr samples tested in different environments, pitting corrosion was the common corrosion type. The corrosion severity was less for super 13Cr type. Table 2.6 presents the details and results of the conducted experiments.

Table 2.6. Corrosion results of a group of 13Cr stainless steels (taken from [102]).

ACE and SSR Data for MSS Alloys

Env. # (temp)	Cl⁻ (ppm)	H_2S (kPa)	CO_2 (kPa)	HCO_3^- (meq/ℓ)	pH	Material	Temperature (C)	Pitting (ACE) 60 days	SSC/SCC† (ACE) 30 days	SSC/SCC† (ACE) 60 days	EC†† (SSR) (Y / N)	CR††† (mpy)
1	1,000	0.7	1.4	20	5.0	13 Cr	93	Y	N	N	--	0.6
							204	Y	N	N	--	1.4
						Super 13 Cr	93	Y	N	N	--	0.1
							204	Y	N	N	--	0.9
						15 Cr	93	Y	N	N	--	0.6
							204	Y	N	N	--	2.1
						410 SS (A)	93	Y	N	N	--	0.2
							204	Y	N	N		0.8
						410 SS (B)	93	Y	N	N	--	0.1
							204	Y	N	N		1.2
2	10,000	0.7	4.1	20	4.3	13 Cr	93	Y	N	N	--	1.1
							204	Y	N	N	--	3.6
						Super 13 Cr	93	Y	N	N	--	0.1
							204	Y	N	N	--	1.5
						15 Cr	93	Y	N	N	--	1.1
							204	Y	N	N	--	2.8
						410 SS (A)	93	Y	N	N	--	0.2
							204	Y	N	N		4.3
						410 SS (B)	93	Y	N	N	--	1.4
							204	Y	N	N		3.0
3	10,000	6.9	1.4	20	5.0	13 Cr	93	Y	N	N	--	1.4
							204	Y	N	N	--	2.3
						Super 13 Cr	93	Y	N	N	--	0.1
							204	Y	N	N	--	1.6
						15 Cr	93	Y	N	Y	--	1.1
							204	N	N	N		1.6
						410 SS (A)	93	Y	N	N	--	0.5
							204	Y	N	N		2.1
						410 SS (B)	93	Y	N	N	--	0.3
							204	Y	N	N		1.3
4	10,000	6.9	4.1	20	4.3	13 Cr	24	--	N	--	N	--
						Super 13 Cr	24	--	N	--	N	--
						15 Cr	24	--	N	--	N	--
						410 SS (A)	24	--	N	--	N	--
						410 SS (B)	24	--	--	--	--	
5	10,000	6.9	4.1	0	3.1	13 Cr	24	--	N	--	Y	--
						Super 13 Cr	24	--	Y	--	Y	--
						15 Cr	24	--	Y	--	Y	--
						410 SS (A)	24	--	Y	--	Y	--
						410 SS (B)	24	--	--	--	--	

† SSC/SCC - Cracking data (yes/no) based on ACE (30 and 60 day) tests

†† EC - Environment cracking (yes/no) based on SSR tests

††† CR - Corrosion Rate

Felton and his colleague Scholfield [103] conducted a similar study on a group of 13Cr stainless steels with different compositions, in different environmental conditions to determine the general and pitting corrosion rates of the investigated materials. The studied materials were categorized into three main groups including conventional 13Cr stainless steel (AISI 420), low carbon 13Cr type (AISI 410) and the alloyed 13Cr stainless steel containing low carbon content and Mo and Ni additions which are super martensitic 13Cr stainless steels. Table 2.7 and 8 show the results of the general and pitting corrosion rate, respectively.

Table 2.7. The general corrosion rate of a group of 13Cr stainless steels tested in different conditions (taken from [103]).

	Test 1	**Test 2**	**Test 3**	**Test 4**	**Test 5**	**Test 6**	**Test 7**	**Test 8**
Chloride	90000	90000	500	90000	30000	121370	121370	121370
pH	4.3	4.3	3.5	3.5	3.5	3.5	3.5	3.1
Temp (°C)	150	130	150	130	180	180	180	200
H_2S (bar)	0.1	0.1	0.1	0.1	0.1	0.1	0.1	0.01
CO_2 (bar)	10	10	10	10	10	10	10	30
420	0.2	0.039		0.088				
13Cr-80(B)	0.13	0.047		0.091				
13Cr-80(C)	0.181	0.06		0.108				
13CrLC-L80(D)	0.08	0.012	0.031	0.035				
13CrLC-C95(D)	0.08	0.019	0.037	0.032	0.35			
410	0.06	0.022		0.031				
17-4	0.002	0.002	0.001	0.005	0.009		0.011	0.037
450	0.003	0.01	0.002	0.007			0.012	0.071
S13Cr-80(E)	0.007		0.003		0.012	0.04	0.061	
S13Cr-95(C)	0.005		0.002		0.013	0.049	0.037	0.189
S13Cr-110(F)	0.007		0.015		0.066	0.102	0.082	
S13Cr-95(A)	0.005		0.021				0.044	
S13Cr-95(E)						0.056		0.148
S13Cr-110(E)						0.057		0.157
S13Cr-80(B)	0.006		0.031					
S13Cr-95(B)						0.053		0.119
13-5-2							0.094	0.186
913							0.057	0.195
S13Cr-95(F)							0.111	

Table 2.8. Pitting corrosion rate of a group of 13Cr stainless steels tested in different conditions (taken from [103]).

	Test 1	Test 2	Test 3	Test 4	Test 5	Test 6	Test 7	Test 8
Chloride	90000	90000	500	90000	30000	121370	121370	121370
pH	4.3	4.3	3.5	3.5	3.5	3.5	3.5	3.1
Temp (°C)	150	130	150	130	180	180	180	200
H_2S (psi)	0.1	0.1	0.1	0.1	0.1	0.1	0.1	0.01
CO_2 (psi)	10	10	10	10	10	10	10	30
420	0.17	0.02		0.14				
13Cr-L80(B)	0.38	0.12		0.02				
13Cr-L80(C)	0.19	0.02		0.05				
LC-L80	0.19	0.04	0.07	0.05				
LC-C95	0.22	0.04	0.07	0.24	0.47			
410	0.10	0.05		0.29				
17-4	0.13	0.01	0.02	0.38	0.42		0.09	0.37
450	0.32	0.05	0.13	1.06			0.04	0.17
S13Cr-80(E)	0.04		0.02		0.16	0.42	0.17	
S13Cr-95(C)	0.19		0.02		0.10	0.31	0.09	0.56
S13Cr-110(F)	0.20		0.02		0.63	0.26	0.09	
S13Cr-80(A)	0.04		0.02				0.09	
S13Cr-95(E)						0.42		0.12
S13Cr-110(E)						0.68		0.63
S13Cr-80(B)	0.16		0.02					
S13Cr-95(B)						0.052		0.19
13-5-2							0.11	0.24
913							0.11	0.19
S13Cr-95(F)							0.09	

The pH value for each test was considered as its room temperature equivalent. The real pH value was determined around 0.4 higher. They observed that the impact of temperature and pH on the corrosion is more than the effect of chloride concentration. They also obtained fewer pits growth rates, which is measured through the depth of the deepest pit, with time. The reasons were mentioned as the slower mass transfer into the pits with increasing the depth, also increasing the number of pits with immersion time, which slows the corrosion and growth rate of a single pit.

There is almost no systematic investigation on the electrochemical properties of 13Cr stainless steel in simultaneous varying parameters of chloride concentration, pH, temperature, and partial pressures of H_2S and CO_2, but in individual environmental conditions [96].

In a study, Linter and Burstein [104] investigated the effect of dissolved CO_2 in the electrochemical reactions of a 13Cr stainless steel through polarization of the samples from open circuit potential in both cathodic and anodic directions in a 0.5 M NaCl solution and constant pH of 4. The results suggested that CO_2 in the environment had a small effect on the polarisations curve.

Huizinga and Like [105] studied the polarization behavior of 13Cr stainless steel in 2 different solutions. The first solution contained a combination of 150 gr/Lit of Cl^- and 234 gr/Lit of $CaCl_2$ and the second one 10 gr/Lit of Cl^- and 16 gr/Lit of $CaCl_2$. The tests were performed after different immersion times. The results showed that, under testing in the second solution, the corrosion potential decreased by increasing the immersion time while the re-passivation potential increased. Moreover, at longer immersion times, the passivity behavior of the steel improved and the pitting potential increased, suggesting slow cathodic reactions. According to the results, although having less corrosion potential, the steel showed a more stabilized oxide layer at higher pH conditions of solution 2.

Since welded parts are always an important part of OCTG, Case et al [106] studied the effect of H_2S gas concentration (0.001 and 0.01 MPa H_2S) on the weld and base metal of a modified 13Cr stainless steel. The polarization experiments were conducted at room temperature in a solution containing 7% sodium chloride and 0.4 gr/Lit sodium acetate. The pH was kept 4.5 through adding hydrochloric acid. Despite showing a lower passive current, the weld metal higher re-passivation potential showed more susceptibility to pitting than the base metal. They concluded that H_2S plays a significant role in the pitting, particularly at the weld metal. They mentioned fewer pits growth rate at higher temperatures since the pits are less open, H_2S diffusion to the pits is more difficult, and the oxide layer functionality is higher.

2.6 Electrochemical methods

Several different electrochemical techniques have been developed during the last decades to evaluate corrosion mechanism, corrosion rate, electrochemistry and electrochemical reactions occurring on the surface of the metals in corrosion. The most common types are explained below.

2.6.1 Open circuit potential

When an electrode is immersed in an electrolyte without applying any external potential or current, the measured potential between the metal electrode and the reference electrode is called open

circuit potential (OCP) or mixed corrosion potential (E_{corr}) where both the cathodic and anodic reactions have the same rate. In this state, the current for forwarding and backward reactions are equal so that the net current passing through the electrode is zero. At potentials above the OCP value, the electrode is in anodic region and below that, it is in cathodic area. OCP measurement is not able to provide much corrosion information because it does not give any kinetic properties of the corrosion process. Nonetheless, some corrosion properties of a sample can be determined by OCP measurement over time. After immersion of the electrode, the surface is adjusted with the new environment of the electrolyte through different processes and reactions including dissolution, passivation, hydration, adsorption, corrosion product formation, etc. These phenomena on the surface change the measured potential, which will reach an approximately constant value after several minutes or hours due to the equilibrium with the electrolyte environment. Generally speaking, over a period, increasing the potential toward noble positive values indicates the metal surface is less being corroded due to the formation of a corrosion barrier. Instead, if the potential trend falls down to the negative values, the metal is in corrosion active state and is dissolving into the electrolyte. The OCP measured curves are not usually smooth and contain some fluctuations, which can be due to, for instance, either environmental noises or the localized corrosion damages followed by re-passivation of the metal surface [93,107,108].

2.6.2 Potentiodynamic polarization technique

In potentiodynamic polarization (PDP) method the potential of the electrode is scanned in a defined range, from some hundred millivolts below to several hundred millivolts above the OCP value, at a special rate (usually 0.166 mV/sec, according to ASTM G61-86 (2009) standard) and the electrical current is simultaneously measured. This measurement needs three electrodes including working electrode (WE) (the metal understudy), counter (auxiliary) electrode (CE) which closes the electrical circuit and establish the current along with WE, and the reference electrode (RE) which does not conduct any electrical current and is used as the base for measuring and controlling the WE potential. The results of the test are plotted at potential versus the current density (current per unit area of the WE). This method provides main information including corrosion rate, passivity (immunity) region, passivation current and potential, corrosion current and potential, cathodic and anodic behavior, and pitting potential. The last one is an important parameter at which the passive oxide film on the surface of metals breaks down, determines the

susceptibility of the metals to pitting corrosion. PDP is a type of destructive test because the applied potential is large enough to damage the metal's surface [86,93,108,109].

2.6.2.1 The anodic polarization scan

Fig. 2.16a shows a schematic anodic scan for stainless steel. Numbers 1 and 2 in the figure indicate the beginning and ending points of the scan, respectively. Point A is the corrosion potential in which the cathodic and anodic reaction rates equal. In the B region in which by increasing the potential, the current passing through the metal increases, the metal oxidation (dissolution) reaction occurs. From point C which is called passivation potential, the surface of the metal starts to passivate and oxide layer forms and all the way in the region D the layer grows and increasing the potential leads to current density decrease. Region E is called passive area in which current density is constant (passive current density) while the potential is increasing until point F where the potential is high enough so that the formed passive layer breaks down and the current density rapidly increases in the region G which based on the metal and environment nature can be due to either activation of other anodic reactions (e.g. oxygen evolution) where the oxide layer is very strong, pitting events on the surface (e.g. on stainless steels, aluminum alloys), or transpassive dissolution [86,93,109].

2.6.2.2 The cathodic polarization scan

Fig. 2.16b shows the schematic view of the cathodic scan. According to the figure, in the reverse direction of the anodic polarization, the cathodic scan starts from point 1, followed by a potential decrease, and ends at point 2. In this scan, the point A represents again the open circuit potential. Depending on the solution properties such as pH value and oxygen concentration, region B may depict oxygen reduction, which, as a mass transfer controlled reaction, is highly dependent on the oxygen dissolution rate. Therefore, the rate of the reaction and the corresponded current is limited, which is known as limiting current density, so that decreasing the potential cannot change the current density and region C is seen as a vertical line. At point D, the potential is low enough to actuate other cathodic reduction reactions becoming dominate to control the overall current density as shown in the region E [86,109].

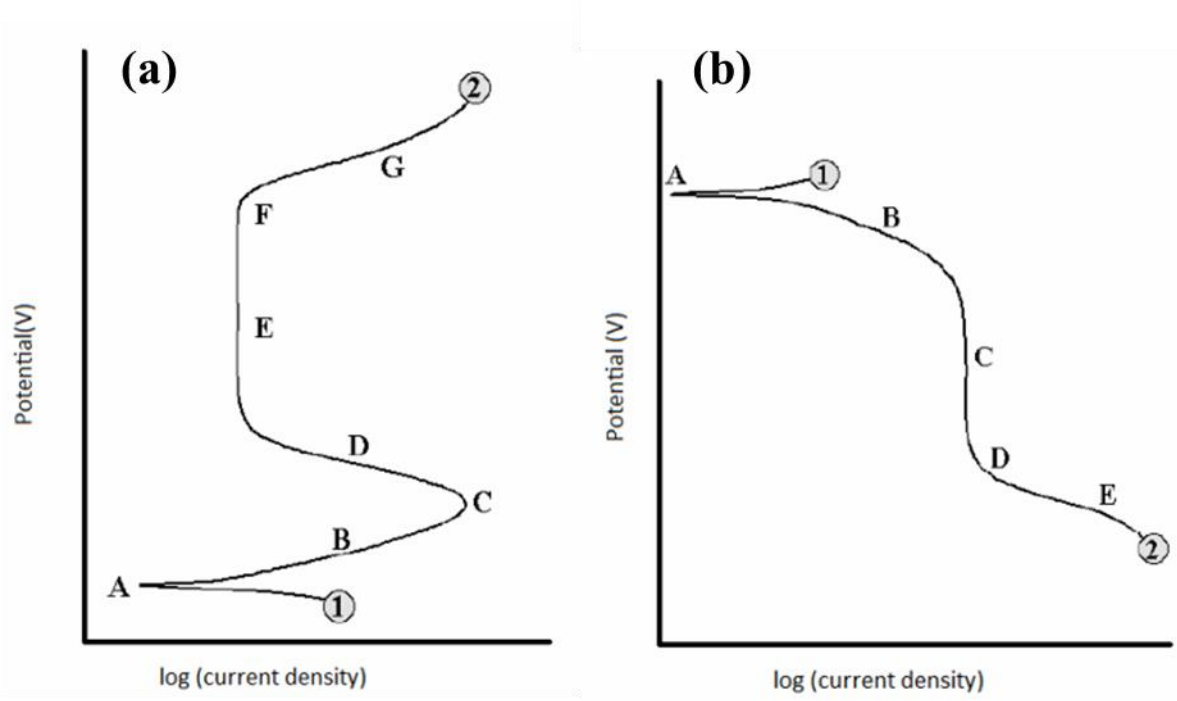

Fig. 2.16. Schematic of (a) Anodic (b) Cathodic polarization test (taken from [109]).

2.6.3 Electrochemical impedance spectroscopy (EIS)

Processes occurring during corrosion events are complex reactions and phenomena which can not be fully understood through traditional and simple electrochemical measurements. Electrochemical impedance spectroscopy or alternating current impedance, as a non-destructive test, is one of the newest and most powerful tools widely used to study electrochemical and corrosion on the metal surface, coatings, corrosion inhibitors, etc. This method is able to provide useful information about the transport characteristics of the species in the solution near the metal surface, film or coatings properties, thickness and morphology of the corrosion products, etc. In this technique, the electrochemical system should be in its steady state. A small amplitude of AC sinusoidal potential (~5-10 mV) in a wide range of frequencies (typically 10^{-3}-10^{6} Hz) is applied to the system to excite the electrochemical interface and the output current signal is measured. In this method, the results are as the impedance of the interface between metal and the solution and the data are modeled with an equivalent electrical circuit containing electrical elements such as inductor, resistor, capacitor, etc., so that the physical phenomenon at the interface can be better interpreted and explained. Fig. 2.17 illustrates a typical equivalent circuit used to model and interpret the EIS measured data. In Fig. 2.17, R_{Sol} shows the solution resistance which is the

resistance of ionic flow between the working and reference electrode. CPE_{dl} is the constant phase element (imperfect capacitor) regarding the capacitance of the double layer formed at the interface between the metal surface and the solution as a charged interface of the polarized water molecules and metal surface which mimics the behavior of an electrical capacitor. Many different factors can affect the capacitance of the double layer such as surface roughness of the electrode, temperature, species concentration, etc. R_{ct} is charge transfer resistance which is proportional to the kinetics and rates of the reactions on the metal surface so that the higher R_{ct}, the less corrosion rate. CPE_{film} and R_{film} are the capacitance and resistance related to the oxide film on the metal surface, respectively [93,107–110].

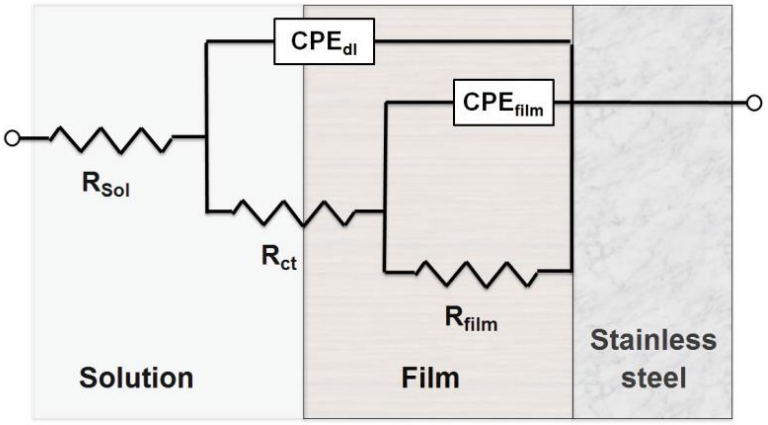

Fig. 2.17. Schematic of an equivalent circuit used to analyze EIS data (taken from [110]).

2.7 Research background

As before discussed, corrosion can be controlled by environmental factors, also materials microstructure. Accordingly, the study was focused on both aspects: the effect of environmental factors and microstructure/phase constituents of the 13Cr martensitic stainless steel.

2.7.1 Environmental factors study

In comparison with the other types of CRAs, such as dual-phase duplex stainless steels, 13Cr (AISI 420) martensitic stainless steel is widely used as the casings and tubing material for harsh oil and gas downhole environment at elevated temperatures up to 150°C due to its good corrosion and mechanical properties with lower cost [5].

As before mentioned, the behavior of stainless steel over time in a corrosive environment is controlled and affected mainly by two groups of parameters. Firstly, the material's inherent characteristics which include mechanical and microstructural properties such as hardness and tensile strength, and as the second one, environmental conditions and parameters which can be temperature, pH of the environment, aggressive ion concentration such as chloride, partial pressure of H_2S and CO_2. By controlling these factors, corrosion in a structure can be managed [9]. Considering all the factors, the first three parameters, *i.e.*, chloride concentration, temperature and pH of the environment, play important roles in the failure of oil and gas pipelines, particularly in the harsh downhole environment [10]. Hence, failure analysis, service life prediction, and corrosion control of OCTG such as 13Cr stainless steel require a good understanding of the effect of these parameters [9,10].

A small change in the environment circumstances can have a profound effect on the corrosion behavior of 13Cr stainless steel [4]. Developing a comprehensive model predicting the corrosion behavior of 13Cr stainless steel in the downhole environment requires determining the relationship between the corrosion response and the affecting parameters. Generally speaking, modeling and optimization are affordable and low-cost methods for systematic degradation prediction of materials under corrosion in oil and gas downhole environment [111]. However, Due to the complex nature of the electrochemical reactions in a real environment, the failure prediction of stainless steels is difficult so that usually the developed models are empirical and based on a statistical analysis of the real recorded data [112]. For instance, the real data of the maximum pit depth were measured and correlated to the environmental factors to assess the pitting corrosion [112]. In addition, obtaining real data for developing an empirical model from the oil and gas structures during operation is highly challenging [113]. During an investigation, Galvele [114] developed a logarithmic relationship between the pitting potential and the concentration of chloride ion in the solution. This correlation was assessed and confirmed also in various temperatures from ambient to higher temperatures [6]. Contrary to this research, a linear relationship between pitting potential and chloride concentration was developed and reported [115].

The correlation between two environmental parameters of pH and temperature with the corrosion rate of 13Cr stainless steel in the presence of CO_2 was developed by Sakamoto *et al* [116].

According to the obtained results in their study, at temperatures lower than 200°C, an increase in the temperature increased the corrosion rate, while at higher temperatures of 200°C, it decreased. The developed equation depicted a logarithmic relationship between the pH and the corrosion rate [116]. In another study, Ossai *et al.* [117] utilized pipeline operational factors such as temperature, CO_2 partial pressure, pH, fluid flow rate, chloride ion, and sulfate ion, along with maximum pit depth to develop a multivariate regression model.

In spite of developing some corrosion prediction models in the past decades, most of them were developed for a particular case study and are not comprehensive models, so that almost there is no standard model or approach to predict the pitting corrosion of stainless steels in the harsh downhole environment [113].

Therefore, following the previous research works for the prediction of corrosion behavior of stainless steels, the design of experiment (DOE) methodology is used to develop a mathematical model as the first step of establishing a comprehensive model for the prediction of corrosion behavior and service life of OCTG. In this study, three environmental parameters of temperature, chloride concentration and pH are considered as the input factors of the model to predict the corrosion behavior of 13Cr stainless steel. The pitting potential results obtained from cyclic potentiodynamic polarization tests in various levels of the input parameters are also considered as the response or output of the model.

2.7.2 Microstructural study

Microstructure is one of the most important facets controlling the characteristics of stainless steels [19]. Accordingly, modification of martensitic stainless steels has been performed during the last decades to improve their service life [118–121]. In the severe environmental conditions of high stress and corrosive environment, increased resistance to cracking, particularly SSC and SCC, would be one of the aspects of the modifications [122–124]. For instance, modification in the corrosion and mechanical properties of 13Cr stainless steel is possible through changing the chemical composition and doing heat treatment which leads to a different microstructure and micro-phase constituents. Many studies have been conducted on the relationship of chemical composition change and their application limits of martensitic stainless steels [20]. It has been shown, as an example, the addition of the same amount of Ni and Mo to the chemical composition

of a common 410 stainless steel can increase both its toughness, pitting, and SSC resistance [20–22].

In order to meet the martensitic stainless steel requirements of working in special service conditions, heat treatment is a significant and well-known technique to gain the mechanical and corrosion characteristics of interest. For the suitable microstructure and phases, proper cycles of heating, quenching, and tempering should be taken. The common phases in martensitic stainless steels after the quenching from the initial austenite phase include hard martensite, some amount of retained austenite, and carbide precipitations [23,24]. The tempering post-process can reduce the hardness and brittleness of the formed martensite, meanwhile increasing the ductility and toughness. The details of the process such as austenitizing temperature and time, quench medium, tempering time and temperature should be adjusted in a proper manner to obtain the desired microstructure. In this regard, while the effect of austenitizing temperature on the mechanical properties of martensitic stainless steel is well known, the results around the corrosion properties are controversial [25]. Candelaria et al. [26] in a study on AISI420 martensitic stainless steel figured out how increases in corrosion rate were affected by higher austenitizing temperatures.

In contrast, Rosemann et al. [27], working on the same steel, observed an improvement in the critical pitting potential while increasing the austenitizing temperature. The same results were reported by Lu et al. [125] by working on martensitic stainless steels. Heat treatment also could change the carbides' dissolution, grain growth, and various phase transformations that each one would have different effects on the corrosion properties [25]. For example, it was observed that in ferritic/martensitic steels, the corrosion processes rate is proportional to the martensite fraction in NaCl solution[126].

One of the determining factors in martensitic stainless steels is the fraction of retained austenite in microstructure [20]. Kimura et al. [127] investigated the pitting resistance and corrosion rate of a modified 13Cr SS samples containing 3-40% retained austenite and concluded that this phase has a small effect on the SSC resistance. Lei et al. [128] performed a research on the samples with and without retained austenite and resulted that samples containing retained austenite phase depicted nobler pitting potential, lower corrosion current, and higher pitting resistance.

During quenching and tempering processes, some types of Cr-rich carbides may form, which lead to Cr- depleted zones in the martensitic stainless steels. It would prevent the formation of a strong

and thick chromium protective passive film and deteriorate the corrosion resistance. The existence of retained austenite in the microstructure prevents the formation of carbides through carbon diffusion from retained austenite to the martensite phase and decreases the corrosion susceptibility [129].

In addition to the common phases found during heat treatment, stainless steels containing a high amount of ferrite stabilizing elements such as Cr and Mo are prone to the formation of an additional delta ferrite phase. Under equilibrium conditions, delta ferrite is not stable at room temperature and does not exist; however, martensitic stainless steels may have less or more content of the phase that usually forms due to inappropriate chemical composition or non-equilibrium solidification of the steels slabs, which is inevitable during industrial production [130–132]. The formation and presence of delta ferrite phase in martensitic stainless steels have been reported in other research works [130]. The effect of delta ferrite on the properties of martensitic stainless steels is controversially reported [131]. In some studies, delta ferrite is mentioned as a deteriorating phase for the mechanical properties due to its non-coherency with the matrix [133,134]. Wang et al. [131] during investigating the effect of delta ferrite on impact properties of a 13Cr-4Ni martensitic stainless steel showed that delta ferrite increases the brittle/ductile transition temperature and lowers the crack initiation and propagation energy, which causes brittle fracture of the tempered martensitic matrix. On the contrary, some reported that it improves ductility and toughness due to its soft nature [135]. Eliminating the formed delta phase is not possible or convenient through conventional heat treatment, but it is at high-temperature annealing [131].

According to the literature, the presence of all the discussed phases in the martensitic stainless steels would be possible so that considering all of them in a specific stainless steel for deep studying of the microstructural effect on the corrosion properties is necessary. Because delta ferrite is a high-temperature phase which typically forms from melt state, therefore, in this part of the study, tungsten arc melting was applied to locally melt a wire of 13Cr stainless steel. In order to have all the possible phases in different fractions, six layers were deposited as layer by layer upon each other so that the heating effect of the upcoming layers changed the microstructure and phases fractions in the previously deposited layers.

Chapter 3. Experimental Procedure

3.1 Materials

According to the type of the research, the materials used in this study were supplied from two different sources: the material used in the design of experiment (DOE) study was provided from a 13Cr-L80 stainless steel tube, provided by Suncor Energy, while for the microstructural study the 13Cr wire used for the local melting was purchased from US Welding Corporation. Table 3.1 shows the nominal chemical composition of the feedstock materials.

Table 3.1. The nominal chemical composition of 13Cr stainless steels used in the current study (wt.%)

Materials	C	Mn	Si	S	P	Cr	Ni	Mo	Cu	Al	Sn	Fe
AISI 420SS (13Cr) wire	0.3-0.4	<1.00	<1.00	<0.03	<0.04	12-14	<0.5	<0.5	<0.5	<0.5	<0.5	Bal.
13Cr (AISI 420)-Tube	0.19	0.85	0.8	0.004	0.003	13.4	0.42	-	0.24	-	-	Bal.

3.2 Sample preparation

The samples used for the DOE part were cut out from the tube as small cubes (~ $1\times1\times1 cm^3$). Each cube was hot-mounted into an epoxy resin so that only one surface of that was apparent for the next evaluations (see Fig. 3.1). A hole was drilled on the side of each sample aimed for the corrosion tests, and a stainless steel screw was used in there to build the electrical connection between the mounted sample and the corrosion test device. Then, through a step-by-step procedure, all the samples were ground by desired SiC sandpapers and mechanically polished using different solutions to a mirror-like final surface, which was followed by an ultrasonic surface cleaning in ethanol.

For the microstructural study, a six-axis automatic robotic weld arm equipped with a gas metal arc welding torch was used to deposit a six-layered wall as each layer on top of the previous one. The deposition was performed on an AISI 420 stainless steel base plate (see Fig. 3.3a). The deposition direction was reversed after the deposition of each layer. Before ensuring that a deposited layer is in the room temperature, the next layer deposition was not started. The deposited wall was

sectioned perpendicular to the deposition direction into several parts, and one of the middle parts were selected for future investigations (Fig. 3.3b). The selected piece was cut layer by layer along the deposition direction and the obtained layers were prepared similar to the DOE samples (Fig. 3.4).

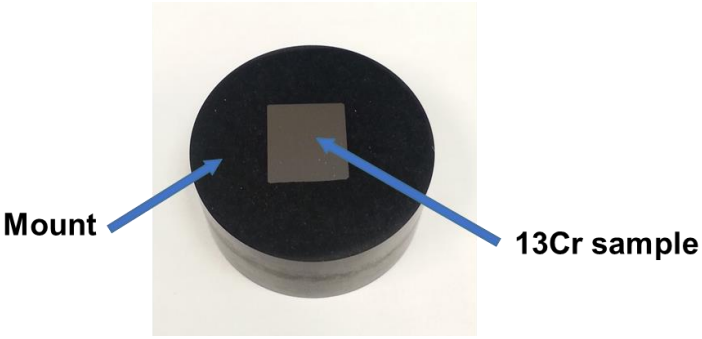

Fig. 3.1. The image of one of the mounted samples.

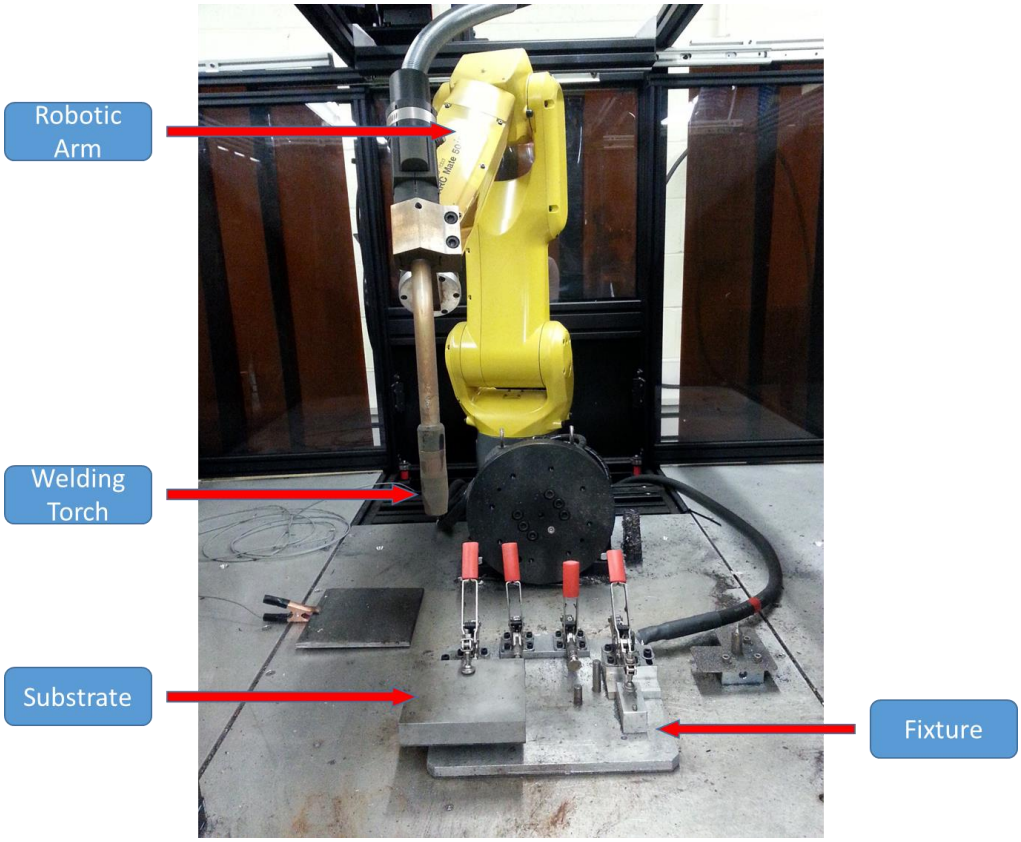

Fig. 3.2. The Robotic weld arm

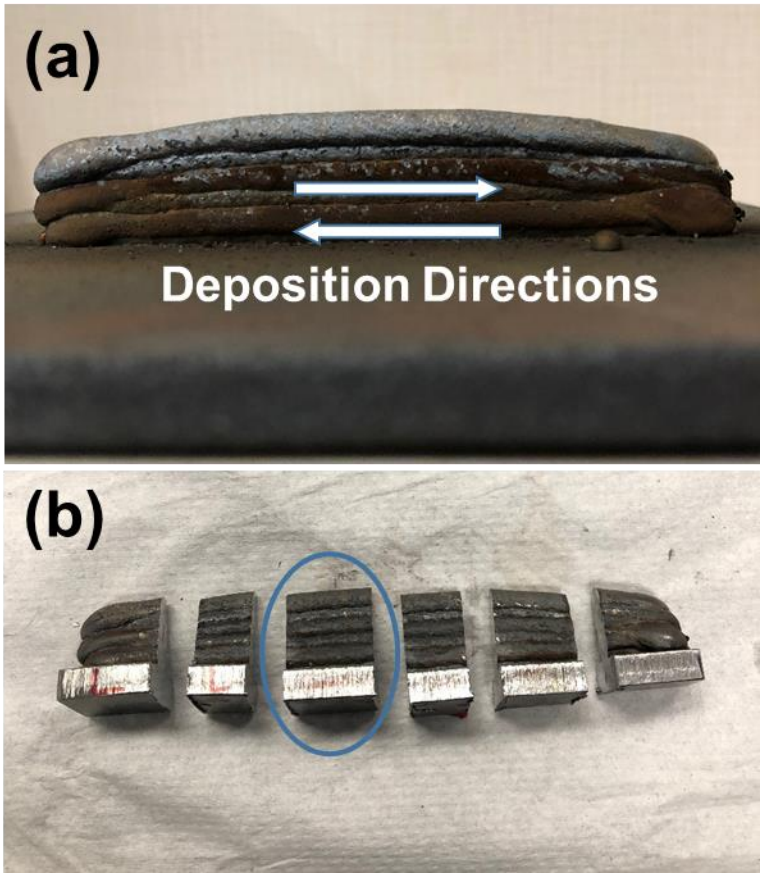

Fig. 3.3. The deposited layers (a) As-deposited (b) sectioned; the circled part was used for further studies.

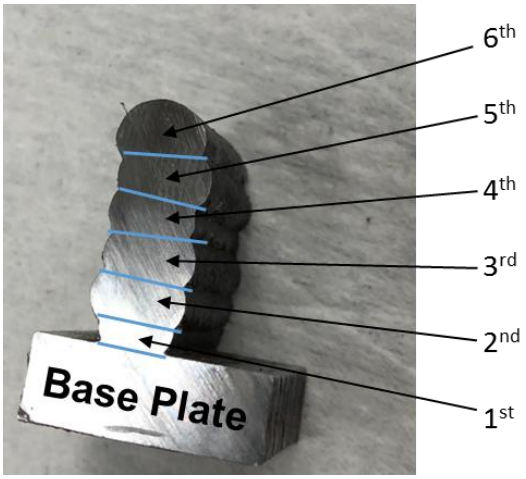

Fig. 3.4. Cross-section of the deposited layers

3.3 Materials characterization

In this investigation, the materials were characterized through an optical microscope, a scanning electron microscope equipped with energy-dispersive X-ray spectroscopy, and X-ray diffractometer as following.

3.3.1 Optical microscopy (OM)

In order to initial study of the microstructure, the 13Cr SS prepared samples were etched using Villela's reagent to reveal the microstructure and micro phases and structure were investigated through optical microscopy. This microscopy analysis was helpful for an overview of the probable present phases in the microstructure. Further microstructural studies were performed by scanning electron microscopy.

3.3.2 Scanning electron microscopy (SEM)

The scanning electron microscope, FEI-MLA-650F model, was used to investigate the microstructure of the prepared samples at higher magnifications. In this analysis, the surface of the etched sample was carbon-coated to set the required electrical conductivity of the samples. In addition, energy-dispersive X-ray (EDX) analysis was used for elemental map analysis of the microstructure of the samples.

3.3.3 X-ray diffraction analysis

To identify the phases formed in the microstructure, XRD analysis was performed using an Ultima-IV XRD machine. In all the experiments Cu-Kα radiation (λ=1.54Å) in a scanning rate of 1 deg./ min at 2θ range of 20° and 100° was used.

3.4 Corrosion study

The procedures and conditions in which corrosion tests were done, were defined according to the type of the study. For the environmental study, only cyclic potentiodynamic tests in different environmental conditions were carried out on the samples, while potentiodynamic polarization and electrochemical impedance spectroscopy tests were performed on the samples for microstructural study. The common conditions in all the experiments are as follows:

Before doing the tests, the samples were polished up to a mirror-like surface and the mounting resin/metal interfaces were covered by non-conductive nail polish to prevent the edge effects during the experiments (Fig. 3.5). All the tests were done using an IVIUM apparatus and in a standard three-electrode corrosion cell containing the samples as the working electrode, an Ag/AgCl as the reference electrode, and a graphite rod as the counter (auxiliary) electrode (Fig. 3.6). Before all the experiments, the samples were run under open-circuit condition for 1h to ensure that the samples were in the stable condition in the electrolyte.

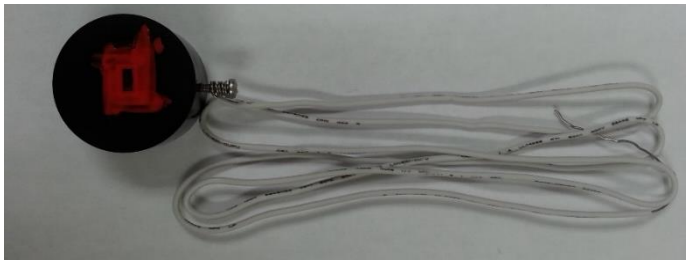

Fig. 3.5. The corrosion coupon

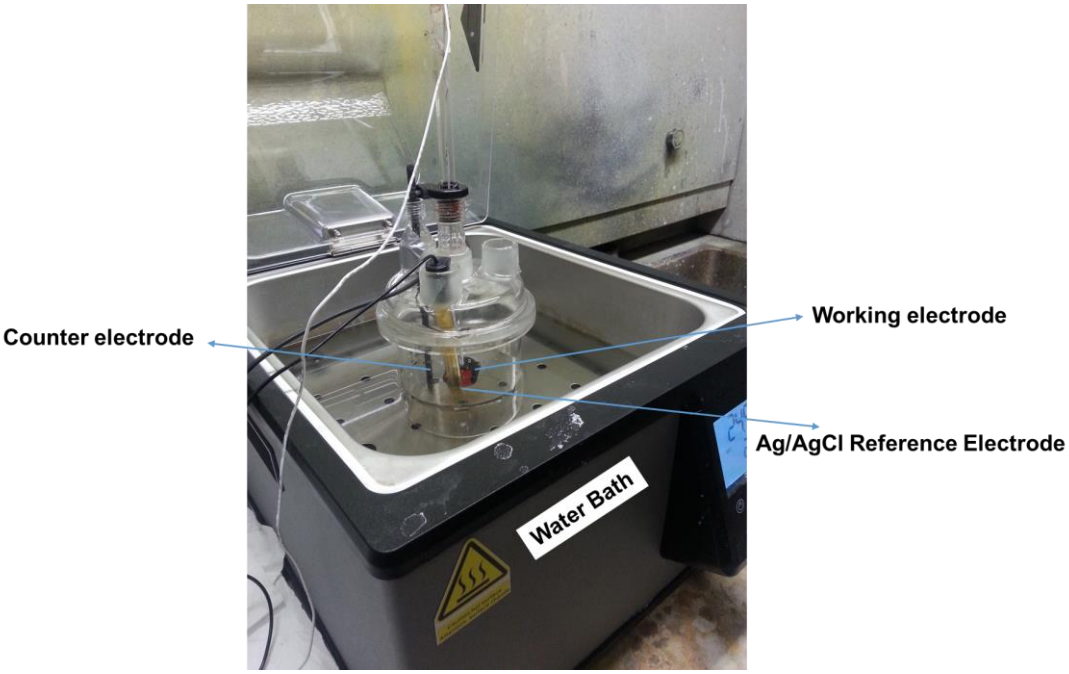

Fig. 3.6. The micrograph of the corrosion cell and the water bath.

3.4.1 Potentiodynamic polarization (PDP)

In order to determine the cathodic/anodic behavior, pitting potential, corrosion current density and potential of the samples, the PDP test was done on the deposited layers. An aerated 3.5wt% NaCl solution was used as the electrolyte solution for all the experiments. The temperature of the tests was kept on 25°C through an auto-controlled water bath. Before running the test under open circuit conditions, the samples were initially polarized in the cathodic potential of -0.5 V for 10 min to clean the surface from previously formed oxide films. The tests were done in the potential range of -0.2 up to 0.3 V versus open circuit potential (OCP) in the scanning rate of 1mV/s.

3.4.2 Electrochemical impedance spectroscopy (EIS)

This experiment was carried out to determine the characteristics of the protective oxide layer formed on the samples surfaces also the mechanisms occurring during the corrosion tests. The experiments were done in aerated 3.5wt% NaCl solution at the temperature of 25°C. The samples here again were cathodically polarized in the same conditions as PDP test. The EIS tests were conducted in the frequency range of 10^{5}-10^{-2} Hz and sinusoidal perturbation signal voltage of 10 mV.

3.4.3 Cyclic potentiodynamic polarization (CPD)

The CPD tests were done on 13Cr samples in varying values of temperature (22-80°C), pH (4-7), and chloride concentration (1000-22000 mg/Lit.). The parameters ranges were provided by Suncor Energy and calculated according to the real conditions in the wells downhole environment. Different solutions with various chloride concentrations were prepared through dissolving a sufficient amount of sodium chloride. The pH of the prepared solutions was first measured and according to the required values then either sodium hydroxide or hydrochloric acid was added to the solutions to meet the required pH values. The desired temperature of the solutions was set by the water bath. In each experiment, after running of the cell under OCP condition for 1 hour, the CPD test was carried out from the starting potential of -0.2 V (vs. OCP) up to the vertex current of 1 mA at the scanning rate of 1mV/s and then the scanning direction was reversed.

3.5 Design of experiment method

In order to investigate the effect of each environmental factor (temperature, pH, chloride concentration) and their interaction on the corrosion behavior of 13Cr stainless steel and developing a mathematical model for foreseeing a special environmental situation, the response surface methodology (RSM) with a Box-Behnken experimental design was applied. Using regression analysis on the data, RSM is principally a statistical method that was used to find the governing mathematical correlation between the input environmental factors and the defined outputs. The result of applying the method is a second-order polynomial model, which is capable to predict the output value in the investigated range of the input values. The general form of an RSM mathematical model is as equation 3.1:

$$y = \beta_0 + \sum_{i=1}^{k} \beta_i x_i + \sum_{i=1}^{k} \beta_{ii} x_i^2 + \sum_{i=1}^{k-1} \sum_{j=2}^{k} \beta_{ij} x_i x_j + \varepsilon \qquad (3.1)$$

Where x_i and x_j are input parameters, y represents the input or model response, ε is the modeling error, βi, βii, βij are the linear coefficients, quadratic coefficients, and the interaction coefficients, respectively. The design of the experiment and the statistical analysis were performed by Design-Expert version 11. The significant parameters and interaction were determined through analysis of variance (ANOVA) in which a confidence level of 95% (p-value < 0.05) was considered as the criterion for the model's parameters significance.

Chapter 4. Results and discussions

As before discussed, the study contains two different parts including the effect of the environmental factors on the corrosion properties of the 13Cr stainless steel and the effect of microstructure and phase constituents on the corrosion behavior of 13Cr SS as the second part. Therefore, this chapter presents the respective results of the aforementioned parts in two sections.

4.1 DOE results and discussion

Table 4.1 shows the Box-Behnken design of the experiments including 17 individual tests in different levels of the input parameters and the response of each experiment which defined as the pitting potential. The response for each test was obtained from its CPP graph. Fig. 4.1 shows some CPP graphs of the performed experiments. The higher pitting potential means higher pitting and corrosion resistance. A glance at the obtained responses induced that the highest pitting resistivity occurred at the lowest temperature 22°C, medium pH level of 5.5, and chloride concentration of 1000 mg/L, respectively, while the worst corrosion condition took place at the environmental conditions of medium temperature, lowest pH value, and highest chloride content of 51°C, 4, and 22000 mg/L, respectively. However, modeling of the obtained data and the subsequent optimization process shows the exact values of the parameters, which lead to the lowest, and the highest pitting resistivity reaction. Using Design-Expert software, a quadratic (second-order) regression model was matched with the obtained data. To evaluate the model and determine the significance of every single factor and their interaction in the estimated model analysis of variance (ANOVA) with a level of significance of 5% (confidence level of 95%) was done on the model. According to the considered level of significance in the analysis, the significance of each expression in the model was determined with their P-values and the significance of the quadratic model was evaluated by F value. The factors or interactions with smaller p-value had higher significance in the model and if they are less than 0.05, they were considered statistically significant in the estimated model. The adequacy of the model was determined by lack of fit parameter; i.e. it compares the significance of the replicated error with the model-dependent error. In a good model, this parameter has to be not significant. If not, It means that in the modeling some contributions between the independent variables and the response is not considered.

Table 4.1. Box-Behnken experimental design layout and the corresponding experimental results.

Run	A: Chloride Concentration (mg/L)	B: Temperature (°C)	C: pH	Pitting Potential ($V_{Ag/AgCl}$)
1	22000	51	7	0.029
2	11500	51	5.5	0.098
3	1000	51	7	0.17
4	1000	80	5.5	0.15
5	1000	51	4	0.164
6	22000	80	5.5	0.038
7	1000	22	5.5	0.235
8	11500	80	4	0.058
9	11500	51	5.5	0.083
10	11500	22	4	0.12
11	11500	51	5.5	0.079
12	22000	51	4	-0.07
13	11500	51	5.5	0.072
14	22000	22	5.5	0.044
15	11500	22	7	0.17
16	11500	51	5.5	0.094
17	11500	80	7	0.14

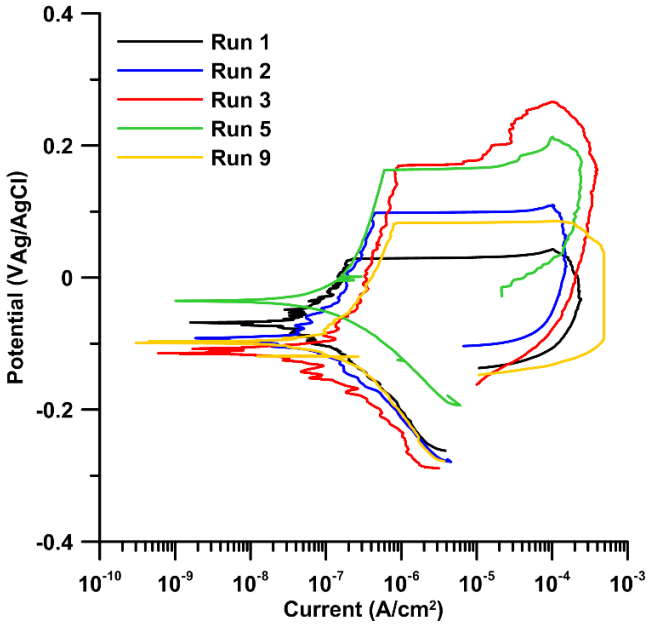

Fig. 4.1. Cyclic polarization graphs of Runs 1, 2, 3, 5, and 9 experiments.

R-square (R^2) or the coefficient of determination is a parameter that shows the quality of the model and how well the real data fit the predicted values by the regression model. If a model obtains an

R^2 more than 80%, it can be considered as a model with good fitness capability and the predicted values by the model would be acceptable. Since R^2 is not sensitive to the number of the variables and usually remains the same or increase by adding more variables, the Adjusted value of R^2 (R^2_{adj}) is introduced as a parameter which decreases by increasing the number of terms in the model if the added terms do not add value to the model. The other parameter R^2_{pred} is a criterion to measure how much variation in the predicted data by the model is expected. The ideal case for a model, i.e. high model accuracy in prediction, is when all types of the discussed R^2 reach 100% and looks identical with each other. Adequate precision which in a desirable model should be more than 4, is a parameter measuring the signal to noise ratio which is a comparison between the range of the predicted values in a design and the average model prediction.

By looking at the values obtained in the ANOVA table, it is clear that the developed regression model with an F-value of 72.08 and the corresponding p-value of less than 0.0001 is significant and there is only a 0.01% chance that such large F-value has occurred due to the noise. It is also noticeable that all the factors and interactions included in the model, A, B, C, AB, AC, and B^2 have the p-values of less than 0.05 which means all are significant. The F-value of 1.99 for the lack of fit means it is insignificant and there is a 26.37% chance that a Lack of Fit F-value this large could occur due to the noise.

All the obtained R-squares including R^2, R^2_{adj}, and R^2_{pred} have the high values of 0.9774, 0.9638, and 0.9046, respectively, which are indicating good fitness of the experimental data with the predicted values and sufficient adequacy of the model. The value of 35.11for the adequate precision which is much higher than 4, showing a reasonable signal to noise ratio for the model that means it is applicable for the considered design ranges of the factors. Equation 4.2 is the final quadratic model correlating the response, pitting potential, to the input parameters of pH, temperature, and chloride concentration.

$$E_{pit} = 0.357844 - 0.000019A - 0.006324B + 0.002774C + 6.48604 \times 10^{-8}AB + 1.47619 \times 10^{-6}AC + 0.000047B^2 \qquad (4.2)$$

For more statistical evaluation of the model and the ANOVA analysis, the residuals plots were analyzed. The normal probability plot of the residuals, shown in Fig. 4.2(a), follows a straight line meaning that the data and the corresponding errors have a good normal distribution. The random

distribution of the data in the plot of the residuals versus the predicted values (Fig. 4.2(b)) approves the constant variance assumption in the model. The next plot, Fig. 4.2(c), which is showing a random scattering without any special trend, is applied to investigate the independency of the experiments and check if any hidden variable was affecting the response by time passing.

Table 4.2. ANOVA and regression analyses for the proposed quadratic model.

Source	Sum of Squares	df	Mean Square	F-value	p-value	
Model	0.0790	6	0.0132	72.08	< 0.0001	significant
A-Chloride	0.0575	1	0.0575	314.59	< 0.0001	
B-Temp.	0.0042	1	0.0042	22.92	0.0007	
C-pH	0.0070	1	0.0070	38.44	0.0001	
AB	0.0016	1	0.0016	8.54	0.0152	
AC	0.0022	1	0.0022	11.84	0.0063	
B^2	0.0066	1	0.0066	36.15	0.0001	
Residual	0.0018	10	0.0002			
Lack of Fit	0.0014	6	0.0002	1.99	0.2637	not significant
Cor Total	0.0808	16				
R^2	0.9774					
Adjusted R^2	0.9638					
Predicted R^2	0.9046					
Adeq.	35.11					

Fig. 4.2(d) shows the plot of the experimental responses versus the values predicted by the developed model. It depicts that all the data are fallen almost on a straight line with a 45°angle regarding the plot axis which illustrates good consistency between the predicted and the measured results.

As before discussed, the expressions in the model possessing a p-value less than the level of significance are considered significant factors or interactions. By looking at the ANOVA analysis, two important interactions of AB and AC are revealed. Fig. 4.3 depicts these interactions plots. Fig. 4.3(a) shows the AC which is the interaction between pH and chloride concentration. It is evident that in the different levels of pH, pitting potential lowers with increasing chloride concentration. However, the pitting potential is less sensitive to the chloride concentration at

higher pH values. The AB interaction which is between temperature and chloride concertation is shown in Fig. 4.3(b). According to the figure, this interaction has the same trend as the previous one. It shows that at different levels of temperature, increasing the chloride concentration decreases pitting resistivity. At the upper level of temperature, the variations of the pitting potential to the chloride concentration are less.

Fig. 4.4 illustrates the 3D surface plots of the pitting potential versus the independent factors of the temperature and the chloride concentration at three different levels of pH value. The general trend of all the graphs in this figure is almost identical in a way that in all the graphs increasing the chloride concentration degrades the pitting potential. Furthermore, the lowest pitting potential occurs at medium temperatures. The effect of pH on the results was considerable. All the graphs show the same values at the three different pH values at low chloride concentrations. However, at higher pH values, the variations of the pitting potential with temperature are faster at high chloride concentrations levels.

In order to obtain the conditions in which the best (highest pitting resistance) and the worst (lowest pitting resistance) corrosion behavior take place, optimization was performed with the criteria of maximum and minimum pitting potential, corresponding to the best and the worst conditions, respectively. As expected, the best conditions occur at the lowest levels of both the temperature and the chloride concentration and at the highest pH value. However, the worst corrosion behavior was estimated to be at the highest chloride concentration and the lower limit of pH and at the medium temperature of 51°C.

It is shown very well in the literature that the pH of the environment has a significant effect on the corrosion products' films of the steels [136]. Usually, the formation and accumulation of corrosion products on the surface of the steels can act as a barrier against the diffusion of aggressive ions in the environment through the passive film. Nonetheless, when pH decreases, the stability of the corrosion product film degrades, leading to lower pitting potential [52]. Moreover, obviously higher chloride concentrations present more aggressive ion in the environment causing the acceleration of the metal surface corrosion [137].

Temperature always plays an important roll in all the processes. It can transform the phases and change their contents, affect the gas solubility, and corrosion product formation [138]. The general

impact of increasing temperature in the environment is an increase in the corrosion rate by accelerating the rate of the electrochemical and chemical reactions [113]. Therefore, it is expected and assumed that at higher temperatures corrosion escalates and pitting resistance drops. However, increasing the temperature catalyzes the corrosion products' precipitation process [113]. Therefore, if the temperature is sufficiently high, the corrosion products precipitation can form a protective barrier film against the aggressive environment and lowers the corrosion rate of the steels [138,139].

In addition, an increase in the environment temperature, could change and modify the microstructure of the surface products and activate the general corrosion instead of localized corrosion through decreasing pitting susceptibility [140]. According to the above discussion, at 80°C (the upper limit), the temperature is high enough for the formation of a protective product film, while not at lower medium temperatures. The effect of temperature on the corrosion product formation and transformation is very complex and is also related to the nature of the products and the layers. For instance, if a layer is physically absorbed and adhered to the surface, rising the temperature would speed up the layer’s desorption. On the contrary, if a layer is chemically absorbed to the surface, increasing the temperature up to a certain range, might enhance the electrochemical stability of the layer through strengthen the chemical band with the substrate. Higher temperatures may dissolve the layer [113].

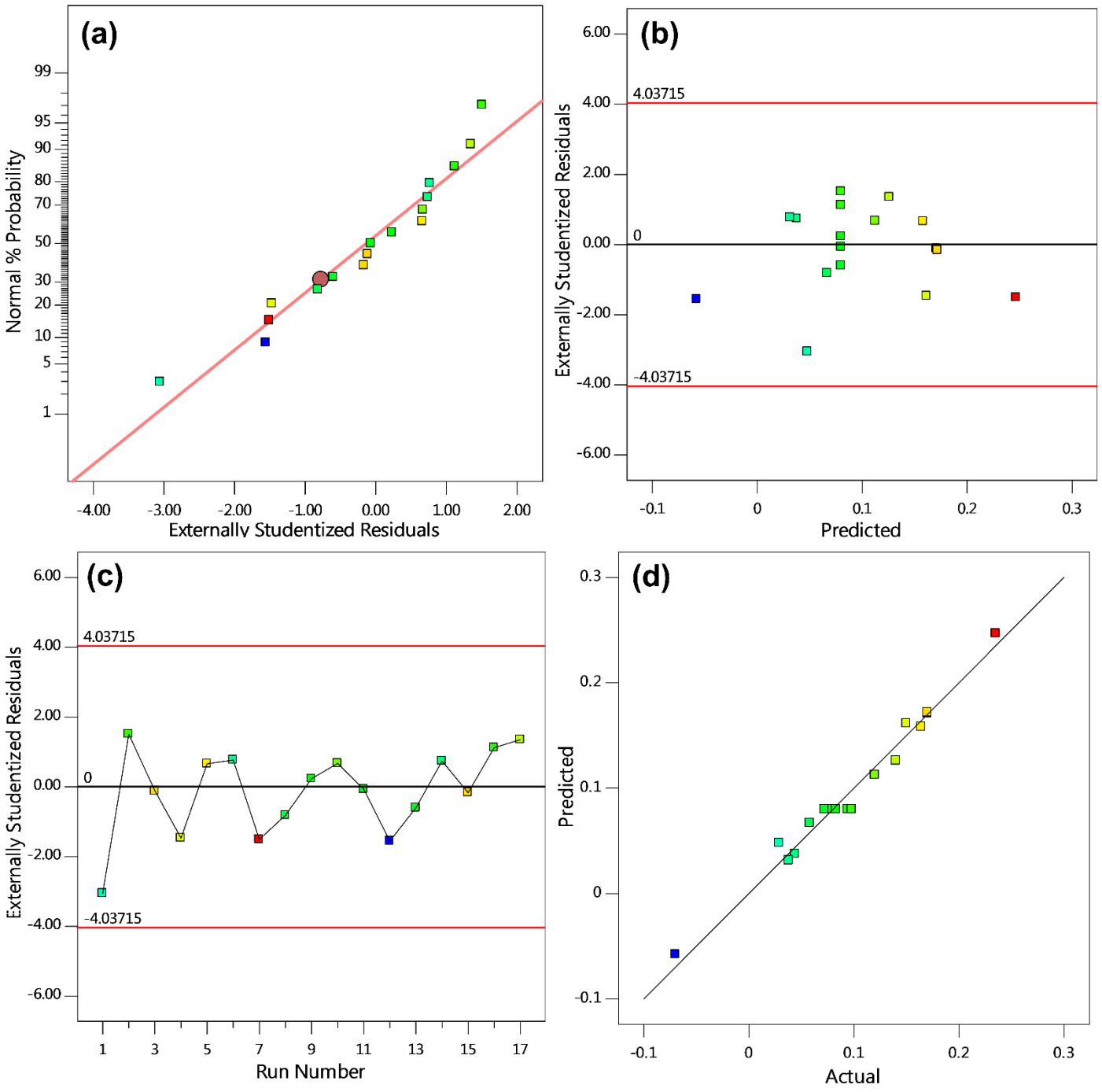

Fig. 4.2. (a) Normal probability plot of the residuals, (b) Plot of the residuals versus the predicted values, (c) Plot of the residuals versus run, and (d) Plot of the predicted values by the model versus the actual values

.

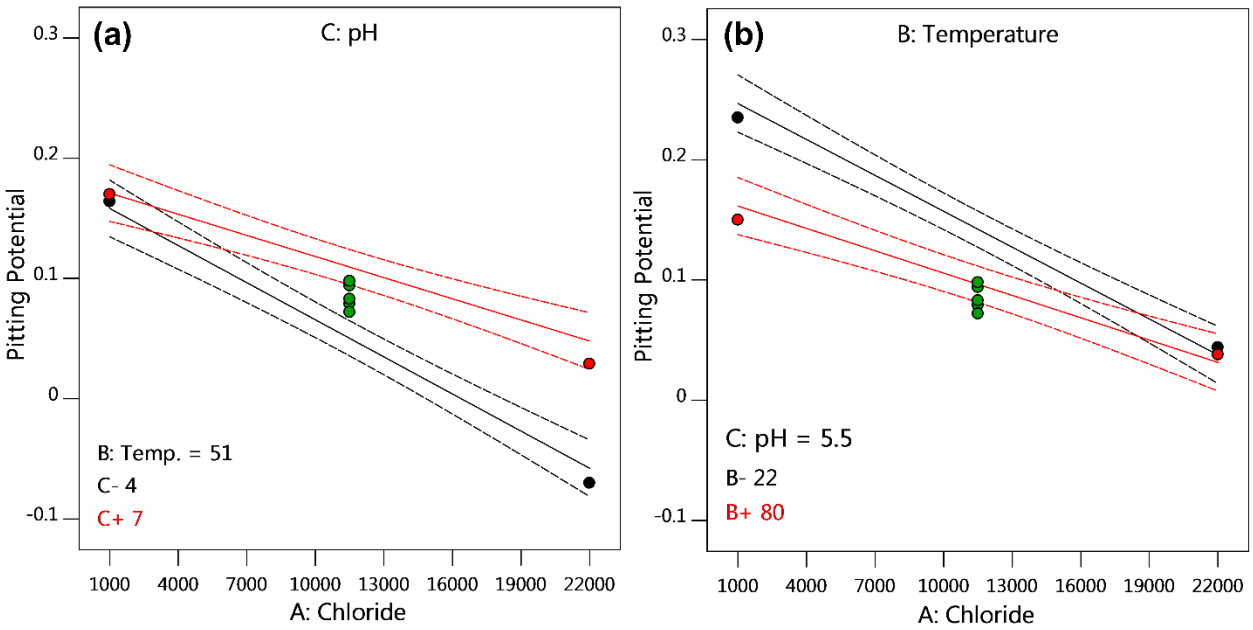

Fig. 4.3. Interaction effects between (a) chloride concentration (A) and pH (C), (b) chloride concentration (A) and temperature (B), (The red, black and green points on the graphs show pitting potential values in the upper limit, lower limit and central points of the design, respectively, and the dashed lines depict error ranges).

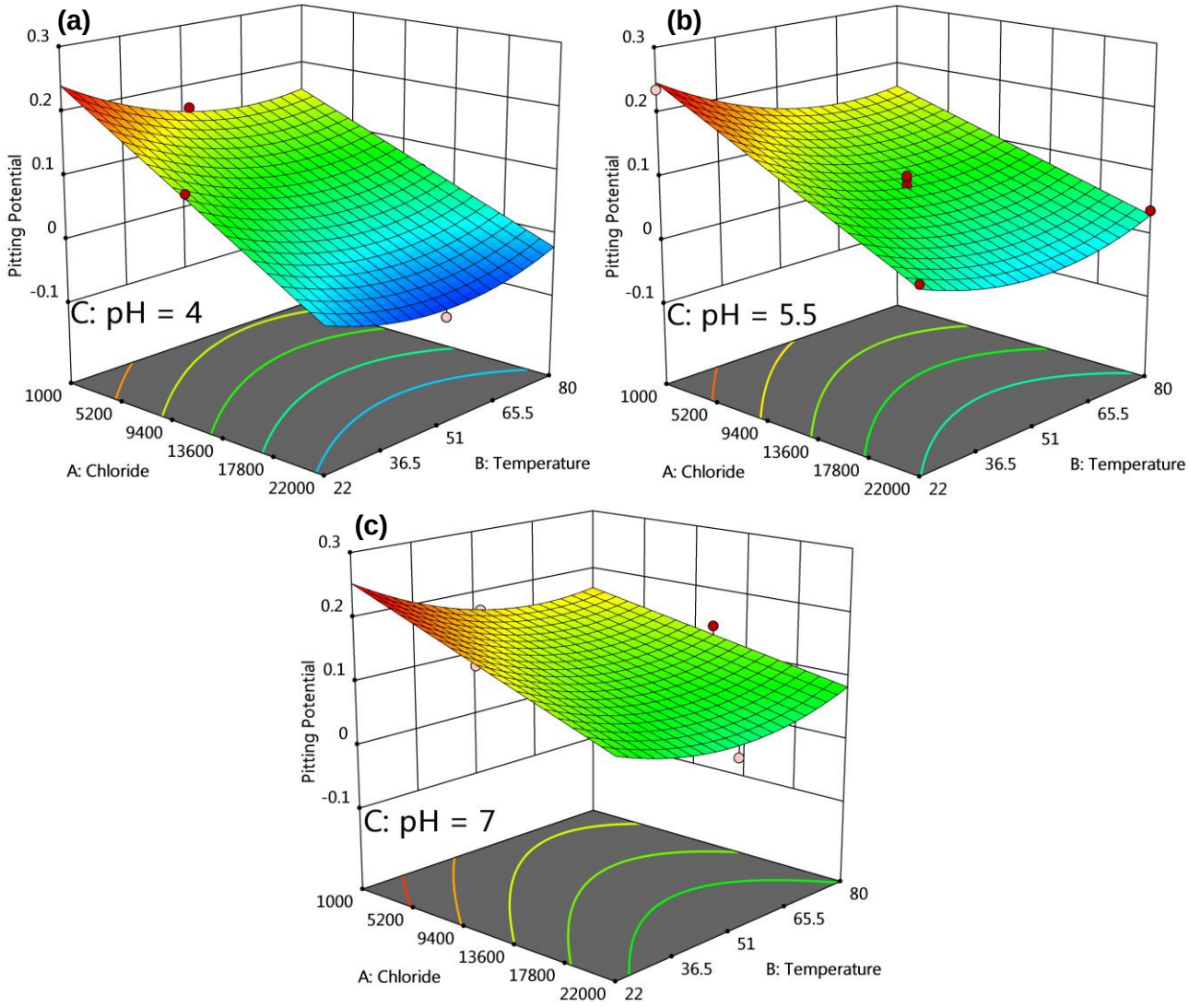

Fig. 4.4. Surface plots for the pitting potential with respect to the chloride concentration and temperature at (a) pH = 4, (b) pH = 5.5, and (c) pH = 7.

Table 4.3. The model optimization results

Optimization Criterion	**Temperature (°C)**	**Chloride Concentration (mg/Lit)**	**pH**	**Pitting Potential ($V_{Ag/AgCl}$)**
Max. Pitting Potential	23.7	2240	7.0	0.237
Min. Pitting Potential	52.1	22000	4.0	-0.058

4.2 Results and discussion of the microstructural study

4.2.1 Microstructure

The microstructural study of the deposited layers was performed through optical and scanning electron microscopy, EDX, and XRD analyses which are shown in Figs. 4.5 to 4.8, respectively. The process of locally melting and deposition of the 13Cr wire lead to a 6-layer wall whose the first layer was discarded due to dilution effects of the base plate on this layer. Therefore, the study was done on the top 5 layers. Fig. 4.5 shows the optical micrographs of the deposited layers. As can be seen, except for layer 2, all the layers have the same micro-phase constituents including a martensitic matrix and a secondary delta ferrite phase which is placed in both prior austenite grains and grain boundaries. In addition to the mentioned phases, layer 2 contains retained austenite phases as well. Within the carbon range of the used precursor (0.3-0.4), this microstructure was predictable according to the Fe-13Cr-C pseudo-binary phase diagram (Fig. 4.9). From the layer 6 (the topmost deposited layer, Fig. 4.5.a) to layer 2 (the bottommost layer, Fig. 4.5.e) the martensitic lathes of the matrix become coarser. The delta ferrite at layer 6 is almost a coherent, vermicular-shaped phase; however, by moving to the bottom layers, it is more non-coherent and irregular island-shaped. The microstructural changes including coarsening of the martensitic laths, delta ferrite shape-changing and its amount decreasing are due to the thermal cycles and history that each layer has experienced during the process [131,141–143]. Liu et al [132] investigated the effect of high-temperature heating on delta ferrite dissolution in a heat resistant steel and showed that delta ferrite dissolution rate during the first stages of heating is relatively high, but decreasing by heating time so that its complete elimination needs a long time. It can justify the disappearance of the delta ferrite phase by moving from layer 6 to layer 2. Figs. 4.6(a-e) show the SEM micrographs of the deposited layers from layer 6 to layer 2, respectively, which depict the same microstructure as the OM one. Since the chromium is the main alloying element in 13Cr SS, the distribution map of the element was obtained through EDX analysis of the layers, as shown in Figs. 4.7(a-e). The EDX results show that chromium is segregated and concentrated in the grain boundaries and inter-dendritic regions of the layers so that at the topmost layers it is more coherent. It is obvious that the chromium distribution pattern in the highly concentrated locations matches to the delta ferrite phase distribution.

In this study, the process for locally melting and solidification of 13Cr SS was purposefully chosen a high solidification-rated one (welding) so that all the possible phases could be detectable. Since chromium is a ferrite stabilizer element, in the stainless steels with high Cr content, the formation of delta ferrite during cooling from melt state, is highly possible. By looking at Fig. 4.9, during solidification, delta ferrite forms at the initial phase in the liquid. At the following, further delta ferrite phase, also austenite phase forms during a peritectic reaction, along with the initially formed delta ferrite. Then, all the delta ferrite transforms into austenite phase and at this stage, if the cooling rate is high enough, a fully martensitic microstructure will exist at room temperature. However, it is mentioned that if some amount of delta ferrite could form at the final steps of the solidification process, and if the ferrite is sufficiently enriched by its stabilizing elements such as chromium or molybdenum, it does not transform to austenite and tends to stay stable and solidify with a eutectic composition in the grain boundaries. The fraction of the delta ferrite comparing to the austenite phase is controlled mainly by their stabilizing elements. Therefore, at relatively high cooling rates, the final microstructure is a martensitic matrix along with the delta ferrite phase at the boundaries. It is also plausible that some amount of the primary delta ferrite phase stays stable during cooling to room temperature and leads to the final mentioned microstructure [130,144].

In addition to the discussed phases, the bottom layers, particularly layer 2, contain a third phase called retained austenite. It should be noted that the austenite phase is not reversed austenite. The formation of reversed austenite in the microstructure of 13Cr SS during tempering at 300°C is reported [145], but this transformation needs sufficient austenite promoting elements, especially nickel, in the composition [146]. The reheating process even for a short time can be effective in the formation of retained austenite [147]. Retained austenite fraction usually increases by temperature increase up to 550-700°C and then it decreases [148,149]. During the deposition process, the temperature at the top layers are probably high enough to prevent the formation of retained austenite, but at the bottom layers, the temperature should have been low enough so that this phase appears at layer 2. Krakhmalev et al. [150] observed the formation of more than 50 vol% of retained austenite during selective laser melting (SLM) of AISI 420 stainless steel. The presence of this amount of retained austenite was attributed to the special thermal history of the materials during the production process. Tan et al. [151] reported also the formation of 10vol% of retained austenite during the SLM process of a maraging steel.

Fig. 4.8 illustrates the XRD patterns of the deposited layers. The patterns of all the layers except layer 2, show the existence of BCC peaks with a strong peak at (110) plane. The observed peaks were considered for both martensite and delta ferrite because they have a small difference in their axis ratio (10^{-4}-10^{-5}nm) and therefore the planes of both the phases have almost the same diffraction angles [152]. Hence, the peaks belong to both martensite and delta ferrite. In the second layer pattern, a small peak is depicted which belongs to (111) plane of austenite. Therefore, the XRD patterns confirm the previous OM and SEM results.

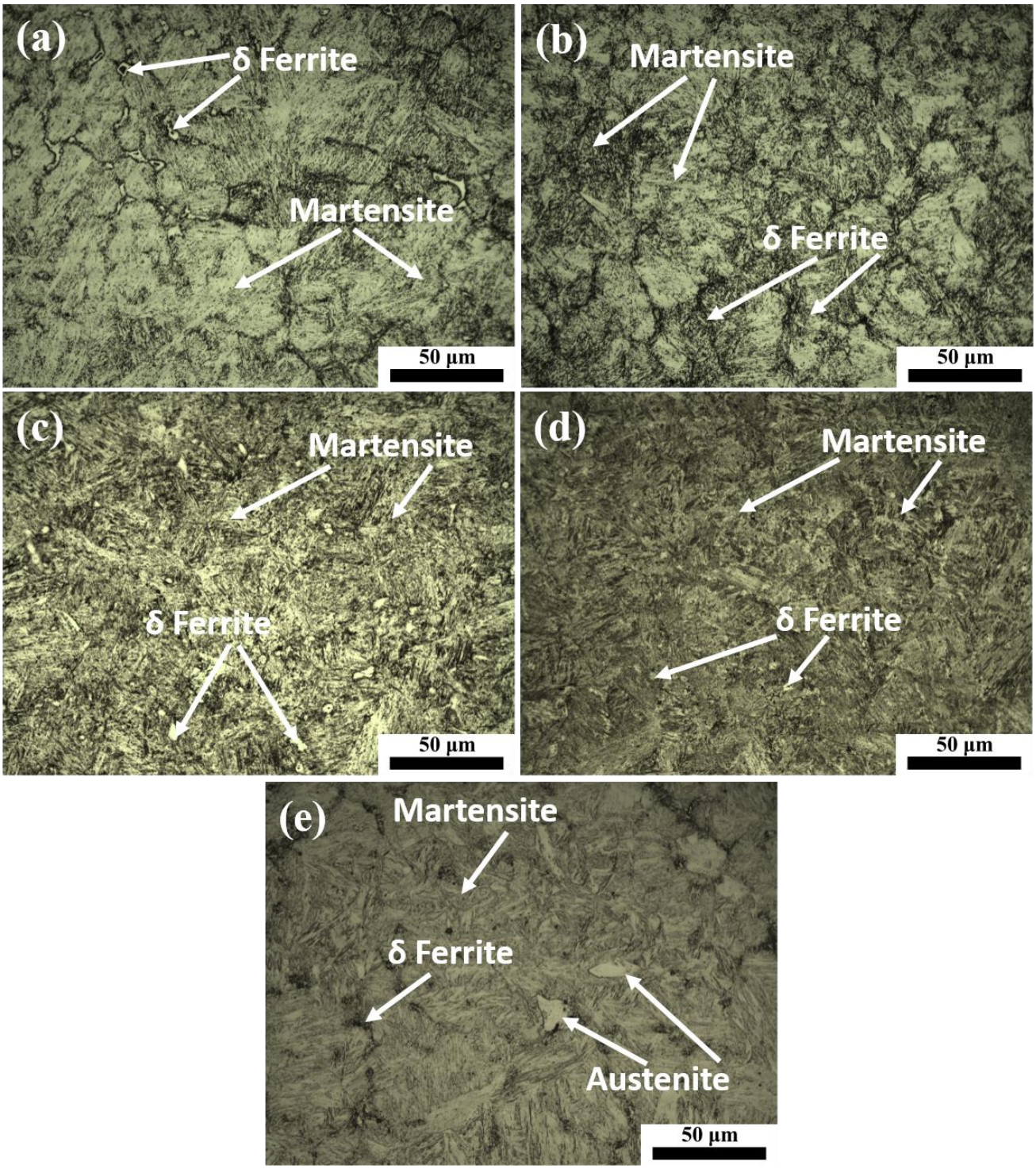

Fig. 4.5. The Optical microscopy micrographs of the deposited layers.

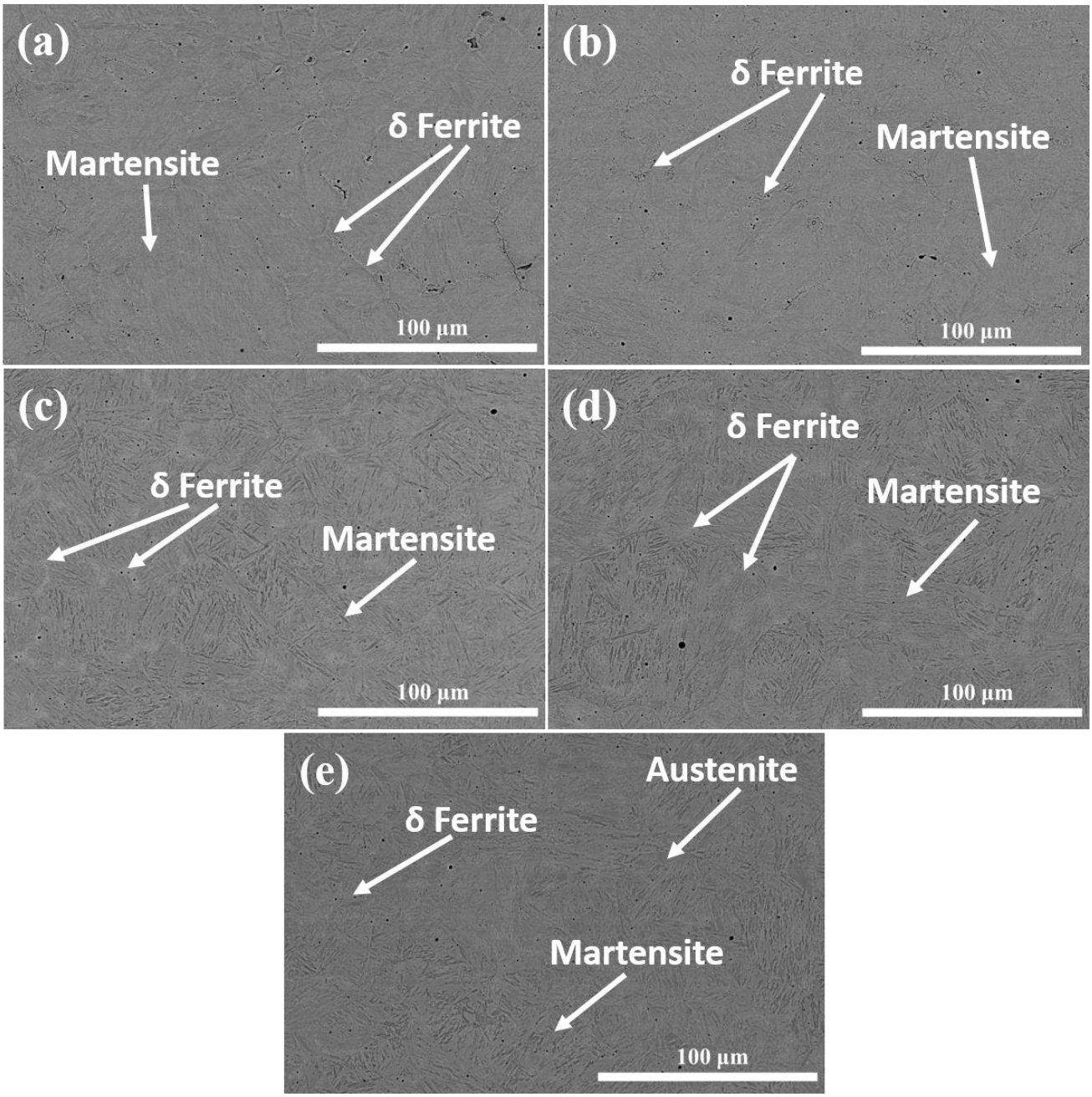

Fig. 4.6. The SEM micrographs of the deposited layers.

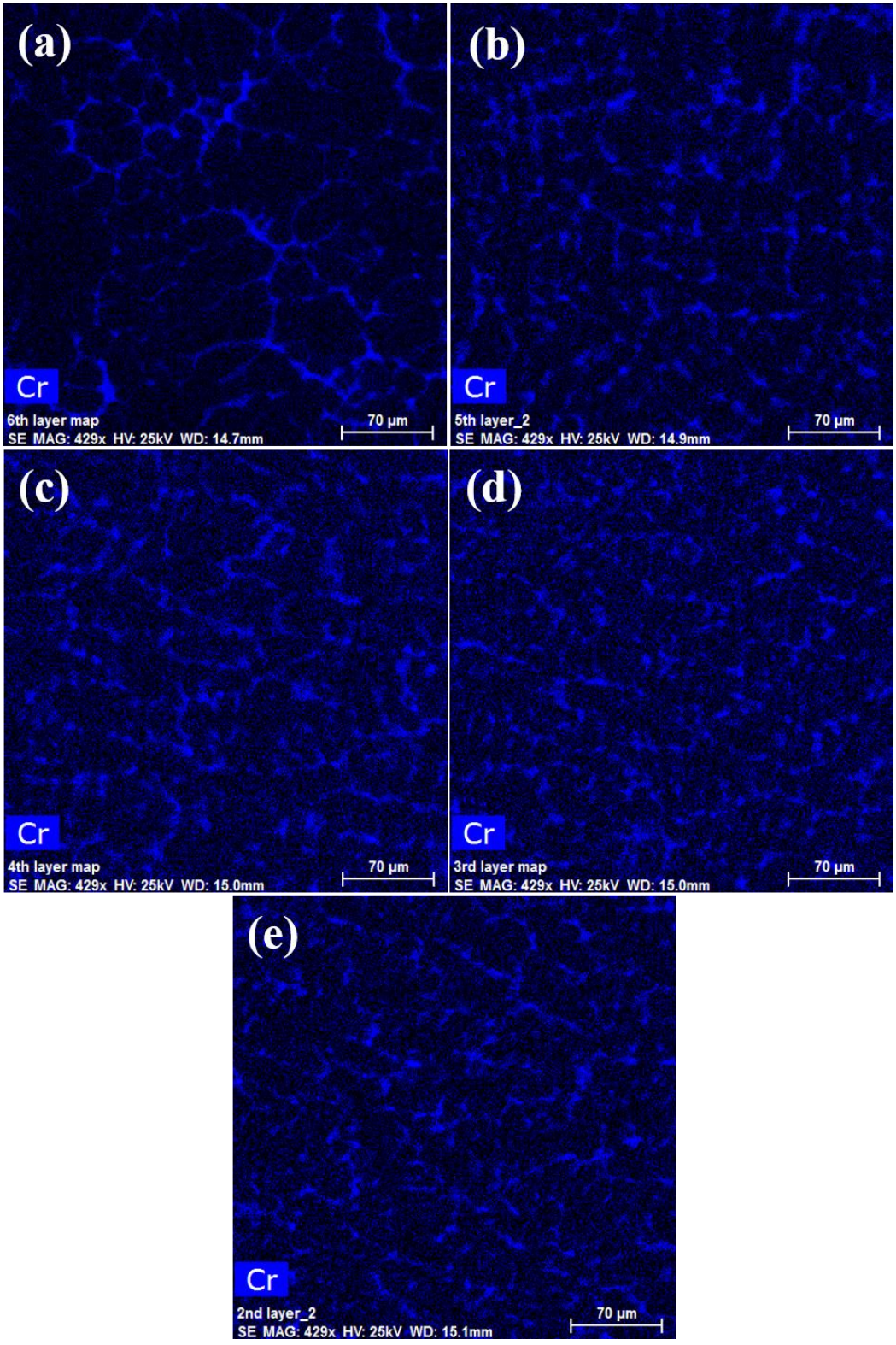

Fig. 4.7. Cr distribution, taken from EDX analysis of the deposited layers.

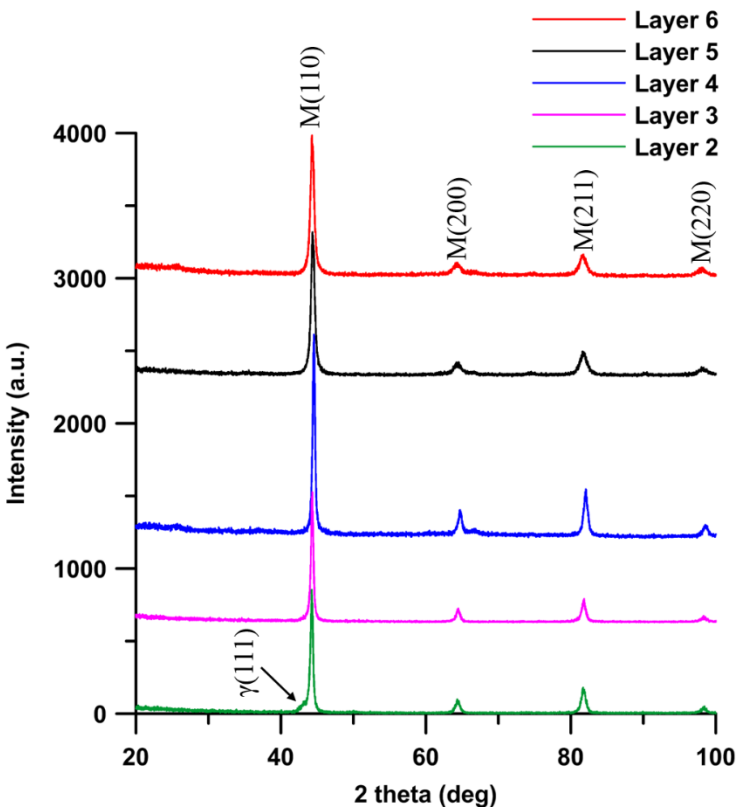

Fig. 4.8. XRD patterns of different layers of the 6-layer deposited wall.

Table 4.4. Lattice characteristics of the revealed phases

Chemical phase	Structure	Data Card JCPDS No.	Planes (Peaks)	2-theta
Martensite	BCT	00-035-1375	(110), (200), (211), (220), (310)	44.647, 64.977, 82.301, 98.882, 116.308
Gamma-Austenite	FCC	00-033-0397	(111), (200), (220), (311), (222), (400)	43.583, 50.792, 74.699, 90.697, 95.968, 118.161
Delta Ferrite	BCC	00-006-0696	(110), (200), (211), (220), (310), (222)	44.674, 65.023, 82.335, 98.949, 116.390, 137.144

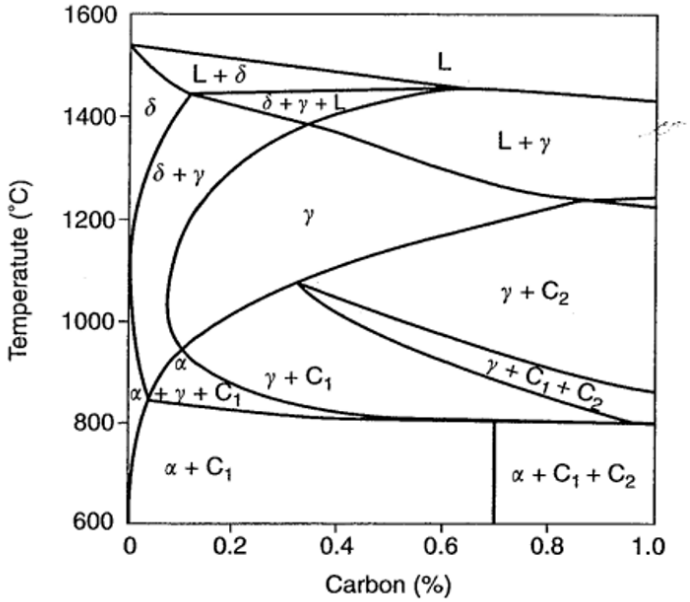

Fig. 4.9. Fe-13Cr-C pseudo-binary phase diagram (taken from [144]).

4.2.2 Electrochemical study

In order to evaluate the corrosion properties of the deposited layers and investigating its relationship with the 13 Cr micro-constituents, two common corrosion tests of potentiodynamic polarization (PDP) and electrochemical impedance spectroscopy (EIS) were performed on each layer in an aerated 3.5wt% NaCl solution at room temperature.

Figs. 4.10 and 4.11 depict the results of the PDP and EIS experiments, respectively, on each layer. All the PDP scans started at the cathodic potential of -0.2 V (vs. OCP), followed by the corrosion potential and then the pitting potential. The main parameters of the tests are corrosion potential, corrosion current and pitting potential, which are denoted by E_{corr}, I_{corr}, E_{pit}. The point where the slope of the anodic branch of the graphs suddenly changes is called pitting potential. At corrosion potential, the rate of the cathodic and anodic reactions on the surface of the steel is equal. The values of the above-mentioned parameters are shown in table 4.5. According to the EIS plots (Fig. 4.11), all the layers show two capacitive loops, which are attributed to the presence of the double layer and protective oxide film capacitances. Due to the fact that the capacitance of the passive

layer is less than the double layer, it controls the total measured impedance, especially at low-frequency region [153,154].

As shown in Fig. 4.10, at the first view, it seems that by moving from the bottommost layer to the upper layers the graphs shift upward, which means an improvement in the corrosion behavior. The first three layers, namely layers 2, 3, and 4, do not show a clear passivation area and pitting potential. However, these characteristics are relatively more obvious for the topmost layers of 5 and 6. Among all the layers, layer 5 has shown the best corrosion behavior including the highest pitting and corrosion potential and the least corrosion current. Depicting the same trend, the EIS data also confirms the PDP results as layer 5 shows the highest impedance values which correspond to a stronger protective passive film on the surface of the steel. From the layer 6 to layer 2, mainly two properties of the microstructure have been changed: the martensitic laths are coarsened, and the delta ferrite phase starts to disappear. The effect of the grains size and coarse/fine microstructure on the corrosion behavior has been controversial. Fattah-Alhosseini et al. [155] mentioned a higher possibility of the presence of point defects in the finer microstructures which leads to instability of the protective passive layer. On the contrary, Jinlong et al. [156] showed that grain refinement would help the formation of a more protective oxide film. Di Schino et al. [157,158] through working on low nickel and 304 austenitic stainless steels concluded that grain refinement improves the intergranular and pitting corrosion and weakens the general corrosion behavior. In this study, it seems that the layers with a refined martensitic structure obtained a better corrosion behavior. However, Tiamiyu et al. [159] who studied the corrosion behavior of an AISI 321 austenitic stainless steel, showed that the ultra-fine grain microstructure leads to the formation of a more stable passive film compared with the coarser grain ones. However, they concluded that the corrosion behavior is not only controlled by the ability of passivation, but the presence of the secondary phase constituents which are effective in pitting corrosion rate. By decreasing the delta ferrite content in the deposited layers, the corrosion behavior considerably is improved at layers 5, but it is deteriorated progressively from the layer 4 to the layer 2. Sarkar et al. [126] during studying the corrosion behavior of dual ferritic/martensitic phase steels observed that by increasing the fraction of the martensite in the microstructure, corrosion is intensified.

It is mentioned in the literature that tempering of martensitic stainless steels at high temperatures deteriorates the corrosion properties of the stainless steels due to the Cr depletion from the steels matrix [19,129,160,161]. Nakagawa et al. [160] mention that introducing retained austenite and reduction of delta ferrite and carbides contents can improve the corrosion properties of precipitation hardening stainless steels. In the presence of retained austenite, carbon diffuses from the martensite phase to the austenite phase and hence can improve the corrosion properties of martensitic stainless steels by the prevention of chromium carbides formation [129]. In contrast, the detrimental effect of delta ferrite on the pitting corrosion susceptibility of stainless steel has been reported previously [162–165]. This effect is mentioned to be the formation of chromium depleted zones in the microstructure and increasing the chromium nitride and carbides formation. However, in the current study it seems that in the deposited layers, since the chromium phase is mainly concentrated in the delta ferrite phase regions, chromium carbides formation is suppressed, as XRD results also do not show any carbides peaks. Wang et al. [166] in a study on a cast austenitic stainless steel mentioned that few and small ferrite grains could improve the pitting corrosion resistance. In duplex ferritic-austenitic stainless steels equal fractions of ferrite and austenite results in the optimum pitting resistance [167]. Layer 2 is the only layer showing a clear retained austenite peak. While high-temperature tempering (500 and 700°C) did not show any retained austenite, the presence of retained austenite in martensite laths interfaces at low tempering temperature of 300°C at 13Cr stainless steel is reported by Bonagani et al [19]. Therefore, the existence of retained austenite at the second layer is reasonable since it has the farthest distance from the top of the wall and the temperatures in other layers were high enough to prevent the formation of the retained austenite. However, despite the presence of retained austenite at layer 2, this layer has the worst corrosion behavior. It seems that either the retained austenite amount is not enough to considerably decrease the formation of the carbide and affects the corrosion properties, or the other microstructural changes such as delta ferrite dissolution and coarsening have had unsuitable impacts on the corrosion.

In an overall conclusion, it seems that the concentration of chromium at the delta ferrite phase could prevent carbide formation and improve the corrosion properties. Nonetheless, very fined grains and microstructure could decrease the corrosion resistance, probably due to either higher point defects in the microstructure or the lack of enough chromium in the matrix to form a good protective layer. This could justify better corrosion behavior in layer 5 comparing layer 6.

In the other layers by increasing the reheating cycles, the microstructure coarsens and delta ferrite phase starts to dissolve as the chromium distributes more evenly in the matrix, and at the same time, the formation of carbides becomes more probable. Therefore, one can say that the presence of a less tempered martensite matrix which is containing a fraction of delta ferrite could show good corrosion behavior. Meanwhile, if retained austenite can be formed along with the mentioned microstructure, an excellent corrosion behavior is expected.

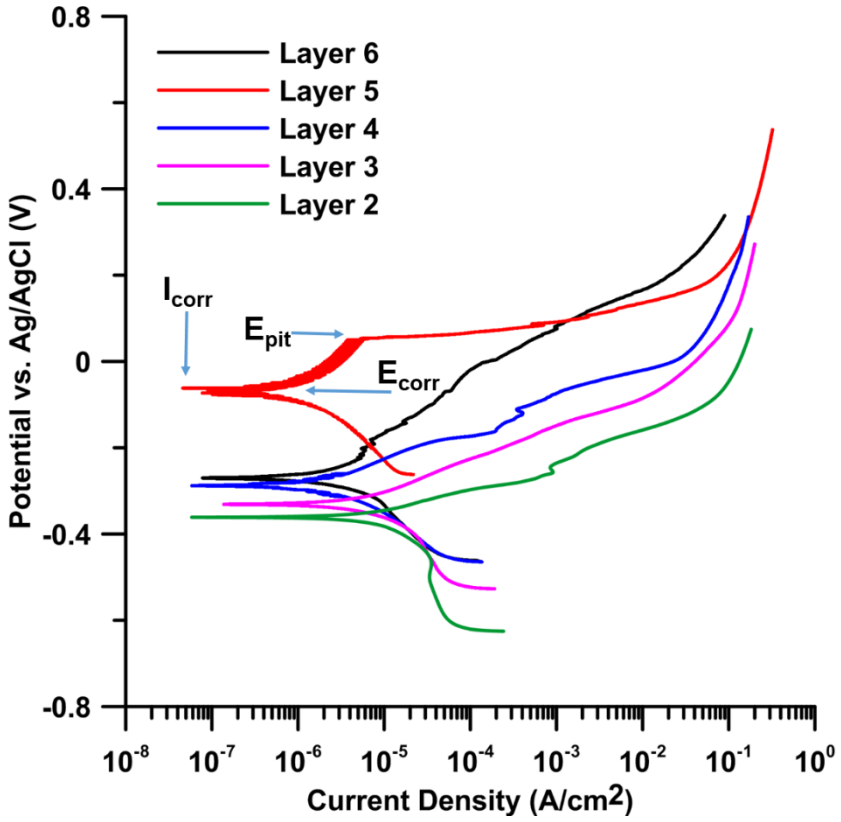

Fig. 4.10. Potentiodynamic polarization curves of the deposited layers in an aerated 3.5wt% NaCl solution at room temperature.

Table 4.5. Potentiodynamic polarization characteristics of the deposited layers

Layer	I_{corrr} (µA/cm^2)	E_{corr} (V)	E_{pitt} ×10^{-3} (V)	Corr. Rate (mm/year)
6	1.28±0.0947	-0.27233±0.00198	-1.65±1.403	0.01472±0.00108
5	0.258±0.03041	-0.0687±0.00121	53.4±4.168	0.002951±0.00034
4	1.68±0.06531	-0.28898±0.00184	-79.7±10.013	0.019545±0.00038
3	4.34±0.09817	-0.33275±0.00083	-132.4±7.749	0.04977±0.00113
2	5.53±0.37918	-0.35695±0.00168	-199.0±13.837	0.21445±0.00434

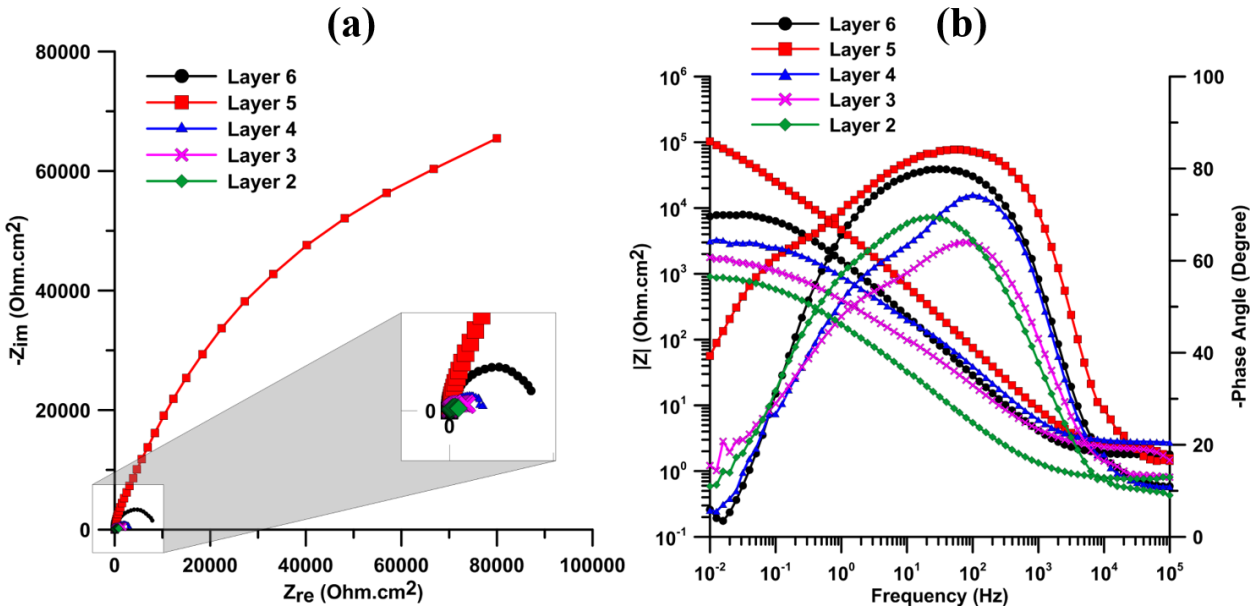

Fig. 4.11. EIS plots of the deposited layers in an aerated 3.5wt% NaCl solution at room temperature (a) Nyquist plots and (b) Bode plots.

Chapter 5. Conclusions and Recommendations

In the current research, 13 Cr stainless steel as one of the most important corrosion resistant alloys in the oil and gas environment was studied to determine its corrosion behavior in various environmental conditions, also with different microstructural characteristics. Response surface methodology using a Box-Behnken design was applied to model the corrosion response of the material in different environmental conditions. In addition, local melting and subsequent rapid solidification were used to build a 6-layer deposition of 13Cr so that each layer contained different micro-phases fractions simulating the tempering conditions of the 13Cr SS in the production process. The conclusions of the study can be summarized as follows:

1- The environmental parameters of pH, temperature, and chloride concentration were correlated to the pitting potential (resistance) of the 13 Cr stainless steel by a quadratic model.
2- The optimized results of the developed model showed that the highest pitting resistance of the material occurred at the lowest temperature of 22°C and the lowest chloride concentration of 1000mg/Lit., and at the highest level of pH of 7.
3- The worst pitting response of the materials took place at the highest amount of chloride concentration of 22000 mg/Lit., the lowest pH of 4, and the medium temperature of 51°C.
4- The best corrosion behavior of the deposited 13Cr stainless steel was observed in the microstructure with a low-tempered martensitic matrix containing less dissolved delta ferrite phase.
5- The existence of some phases such as delta ferrite and retained austenite can be beneficial for the corrosion properties of 13Cr stainless steel.
6- A coarser microstructure would be more susceptible to pitting corrosion.

The results, obtained in the current study, can be improved and developed by the following recommendations as to the future works:

1- To identify susceptible locations to pitting corrosion using the DOE optimization results and OLI software.

2- Further DOE model validation and modification.

3- Calculation of the corrosion rate in each experiment and optimization of the model based on the corrosion rates.

4- Adding H_2S and CO_2 partial pressures to the input parameters of the DOE study.

5- Investigation of the effect of retained austenite on the corrosion properties of 13Cr stainless steel.

6- Adjusting the exact amount of the present phases in the microstructure of 13Cr stainless steel to obtain the best corrosion behavior.

References

[1] M.G. Fontana, Corrosion engineering, Tata McGraw-Hill Education, 2005.

[2] M.B. Kermani, A. Morshed, Carbon Dioxide Corrosion in Oil and Gas Production-A Compendium, Corrosion. 59 (2003) 659–683.

[3] B. Luo, J. Zhou, P. Bai, S. Zheng, T. An, X. Wen, Comparative study on the corrosion behavior of X52 , 3Cr , and 13Cr steel in an O2 – H2O – CO2 system : products , reaction kinetics , and pitting sensitivity, Int. J. Miner. Metall. Mater. 24 (2017) 646–656. doi:10.1007/s12613-017-1447-9.

[4] H. Zhang, Y.L. Zhao, Z.D. Jiang, Effects of temperature on the corrosion behavior of 13Cr martensitic stainless steel during exposure to CO 2 and Cl À environment, 59 (2005) 3370–3374. doi:10.1016/j.matlet.2005.06.002.

[5] A. Dalmau, C. Richard, A.I. Mu, Degradation mechanisms in martensitic stainless steels : Wear , corrosion and tribocorrosion appraisal, Tribol. Int. J. 121 (2018) 167–179.

[6] J. Jun, Localized Corrosion of Super 13Cr Stainless Steel in 1D Pit for H 2 S-free and Sour Brines at Elevated Temperature Dissertation, The Ohio State University, 2016.

[7] S. Marcelin, N. Pébère, S. Régnier, Electrochemical characterisation of a martensitic stainless steel in a neutral chloride solution, Electrochim. Acta. 87 (2013) 32–40.

[8] M. Cristina, S. Nakamatsu, A. Laura, P. Rueda, Resistance to Pitting Corrosion in Steels Based on the Fe-Cr-Ni-C System, 20 (2017) 115–119.

[9] B. Mishra, Corrosion Characterization of Advanced Steels for Use in the Oil & Gas Industry Sweet Corrosion of Drill Pipe Steels, 2 (2013) 221–229. doi:10.5923/j.ijmee.20130202.14.

[10] Y. Prawoto, K. Ibrahim, W.B. Wan Nik, Effect of pH and Chloride Concentration on the Corrosion of Duplex Stainless Steel, Arab. J. Sci. Eng. 34 (n.d.) 115–127.

[11] Q.Y. Liu, L.J. Mao, S.W. Zhou, Effects of chloride content on CO2 corrosion of carbon steel in simulated oil and gas well environments, Corros. Sci. 84 (2014) 165–171. doi:10.1016/j.corsci.2014.03.025.

[12] Y. Wang, G. Cheng, W. Wu, Q. Qiao, Y. Li, X. Li, Effect of pH and chloride on the micro-mechanism of pitting corrosion for high strength pipeline steel in aerated NaCl solutions, Appl. Surf. Sci. 349 (2015) 746–756. doi:10.1016/j.apsusc.2015.05.053.

[13] M. Kimura, T. Tamari, K. Shimamoto, High Cr stainless steel OCTG with high strength and superior corrosion resistance, JFE Tech. Rep. 7 (2006) 7–13.

[14] S. HASHIZUME, M. Katsumi, Y. INOHARA, EFFECT OF STRENGTH ON STRESS CORROSION CRACKING RESISTANCE OF MARTENSITIC STAINLESS STEELS, in: Corrosion, 2001: p. Paper No. 01085.

[15] F. Mancia, The effect of environmental modification on the sulphide stress corrosion cracking resistance of 13Cr martensitic stainless steel in H2S-CO2-Cl- systems, Corros. Sci. 27 (1987) 1225–1237.

[16] D.D. Vitale, P.C. Drive, EFFECT OF HYDROGEN SULFIDE PARTIAL PRESSURE, PH, AND CHLORIDE CONTENT ON THE SSC RESISTANCE OF MARTENSITIC STAINLESS STEELS AND MARTENSITIC PRECIPITATION HARDENING STAINLESS STEELS, in: NACE Corros., 1999.

[17] S. Hashizume, K. Masamura, K. Yamazaki, PERFORMANCE OF HIGH STRENGTH SUPER 13%CR MARTENSITIC STAINLESS STEELS, NACE Corros. (2003) 1–12.

[18] M. Monnot, R.P. Nogueira, V. Roche, G. Berthomé, E. Chauveau, R. Estevez, M. Mantel, Sulfide stress corrosion study of a super martensitic stainless steel in H 2 S sour environments: Metallic sulfides formation and hydrogen embrittlement, Appl. Surf. Sci. 394 (2017) 132–141. doi:10.1016/j.apsusc.2016.10.072.
[19] S.K. Bonagani, V. Bathula, V. Kain, Influence of tempering treatment on microstructure and pitting corrosion of 13 wt.% Cr martensitic stainless steel, Corros. Sci. 131 (2018) 340–354. doi:10.1016/j.corsci.2017.12.012.
[20] T.J. Mesquita, E. Chauveau, M. Mantel, N. Bouvier, D. Koschel, Corrosion and metallurgical investigation of two supermartensitic stainless steels for oil and gas environments, Corros. Sci. 81 (2014) 152–161. doi:10.1016/j.corsci.2013.12.015.
[21] E. Mabruri, M.S. Anwar, S. Prifiharni, T.B. Romijarso, B. Adjiantoro, Tensile properties of the modified 13Cr martensitic stainless steels, AIP Conf. Proc. 1725 (2016). doi:10.1063/1.4945493.
[22] M.S. Anwar, T.B. Romijarso, E. Mabruri, Pitting resistance of the modified 13Cr martensitic stainless steel in chloride solution, Int. J. Electrochem. Sci. 13 (2018) 1515–1526. doi:10.20964/2018.02.13.
[23] C. García De Andrés, L.F. Álvarez, V. López, J.A. Jiménez, Effects of carbide-forming elements on the response to thermal treatment of the X45Cr13 martensitic stainless steel, J. Mater. Sci. 33 (1998) 4095–4100. doi:10.1023/A:1004424329556.
[24] L.D. Barlow, M. Du Toit, Effect of austenitizing heat treatment on the microstructure and hardness of martensitic stainless steel AISI 420, J. Mater. Eng. Perform. 21 (2012) 1327–1336. doi:10.1007/s11665-011-0043-9.
[25] I. Bösing, L. Cramer, M. Steinbacher, H.W. Zoch, J. Thöming, M. Baune, Influence of heat treatment on the microstructure and corrosion resistance of martensitic stainless steel, AIP Adv. 9 (2019). doi:10.1063/1.5094615.
[26] A.F. Candelária, C.E. Pinedo, Influence of the heat treatment on the corrosion resistance of the martensitic stainless steel type AISI 420, J. Mater. Sci. Lett. 22 (2003) 1151–1153. doi:10.1023/A:1025179128333.
[27] P. Rosemann, N. Kauss, C. Müller, T. Halle, Influence of solution annealing temperature and cooling medium on microstructure, hardness and corrosion resistance of martensitic stainless steel X46Cr13, Mater. Corros. 66 (2015) 1068–1076. doi:10.1002/maco.201408081.
[28] Z. Ahmad, Principles of Corrosion Engineering and Corrosion Control, Elsevier, Amsterdam ; Boston, Mass, 2006.
[29] Y.A. Touali, Carbon Dioxide Corrosion studies in Oil and Gas Production, International Centre for Island Technology, 2013.
[30] G. V. Chilingar, R. Mourhatch, A. Al-Qahtani, The Fundamentals of Corrosion and Scaling for Petroleum & Environmental Engineers, Elsevier Science, Burlington, 2013.
[31] W. Wallace, D.W. Hoeppner, P.V. Kandachar, Aircraft Corrosion: Causes and Case Histories, 1985.
[32] G. Palanisamy, Corrosion Inhibitors, in: IntechOpen, 2019: pp. 1–24. doi:DOI: 10.5772/intechopen.80542.
[33] R.W. Revie, H.H. Uhlig, Corrosion and Corrosion Control : An Introduction to Corrosion Science and Engineering, John Wiley & Sons, Hoboken, New Jersey, 2008.
[34] M. Di Benedetti, G. Loreto, F. Matta, A. Nanni, Acoustic emission monitoring of reinforced concrete under accelerated corrosion, J. Mater. Civ. Eng. 25 (2013) 1022–1029.

doi:10.1061/(ASCE)MT.1943-5533.0000647.
[35] K.R. Trethewey, J. Chamberlain, Corrosion for science and engineering, United States, 1995.
[36] E. Mccafferty, Introduction to Corrosion Science, Springer New York, New York, NY, 2010.
[37] R. Tubb, Pipeline & gas journal's 2013 worldwide construction report, 2013.
[38] C. Li, Effect of Corrosion Inhibitor on Water Wetting and Carbon Dioxide Corrosion In Oil-Water Two-Phase Flow, the Russ College of Engineering and Technology of Ohio University, 2009.
[39] Y.F. Cheng, Pipeline engineering, Encycl. Life Support Syst. (EOLSS),. (2010).
[40] R. Heidersbach, Metallurgy and Corrosion Control in Oil and Gas Production, N.J.: Wiley, 2011. Print. Wiley Ser. in Corrosion, Hoboken, New Jersey, 2011.
[41] L.H. Bennett, J. Kruger, R.L. Parker, E. Passaglia, C. Reimann, A.W. Ruff, H. Yakowitz, E.B. Berman, U.S.N.B. of Standards, Economic Effects of Metallic Corrosion in the United States, Department of Commerce, 1978. https://books.google.ca/books?id=-K4jxgEACAAJ.
[42] T.P. Hoar, Report of the committee on corrosion and protection : a survey of corrosion and protection in the United Kingdom, HMSO, London, 1971.
[43] B.W. Cherry, Corrosion in Australia : the report of the Australian National Centre for Corrosion Prevention and Control feasibility study, June 1983 / B.W. Cherry and B.S. Skerry, 1983.
[44] D. Webster, Pipeline Construction Drivers , Corrosion Costs and Engineering Issues, NAPCA Conv. (2010) 1–77.
[45] H.M. Shalaby, A. Al-Hashem, M. Lowther, J. Al-Besharah, Industrial Corrosion and Corrosion Control Technology, in: Proc. 2nd Arab. Corros. Conf., Kuwait, 1996.
[46] T.P. Lekan, S.G. Alhaji, K.L. Ganiyu, G. Babagana, S.B. Adebori, Corrosion Problems During Oil and Gas Production and Its Mitigation, Int. J. Ind. Chem. (2013) 1–15. http://www.industchem.com/content/4/1/35.
[47] C.I. Ossai, Advances in Asset Management Techniques: An Overview of Corrosion Mechanisms and Mitigation Strategies for Oil and Gas Pipelines, ISRN Corros. 2012 (2012) 1–10. doi:10.5402/2012/570143.
[48] Pipeline Performance in Alberta, 2013.
[49] D. V Pugh, S.L. Asher, J. Cai, W.J. Sisak, J.L. Pacheco, F.C. Ibrahim, E.J. Wright, A. Dhokte, S. Venaik, D. Robson, Top-Of-Line Corrosion Mechanism For Sour Wet Gas Pipelines, in: NACE Int. Corros. Conf. Expo, NACE International, Atlanta, Georgia, 2009: p. 15. https://doi.org/.
[50] N. International., A.P. Institute., Corrosion of oil- and gas-well equipment, (1958) 87 p. file://catalog.hathitrust.org/Record/009231366.
[51] D. Brondel, R. Edwards, A. Hayman, D. Hill, S. Mehta, T. Semerad, Corrosion in the oil industry, Oilf. Rev. 6 (1994) 4–18.
[52] S. Nešić, Key issues related to modelling of internal corrosion of oil and gas pipelines - A review, Corros. Sci. 49 (2007) 4308–4338. doi:10.1016/j.corsci.2007.06.006.
[53] R.F. Weeter, Desorption of Oxygen From Water Using Natural Gas for Countercurrent Stripping, J. Pet. Technol. 17 (1965) 515–520. doi:10.2118/933-pa.
[54] L. Garverick, Corrosion in the petrochemical industry, ASM international, 1994.
[55] P.S. Jackman, L.M. Smith, Advances in Corrosion Control and Materials in Oil and Gas

Production: Papers from EUROCORR ’97 and EUROCORR ’98, European Federation of Corrosion, 1999. https://books.google.ca/books?id=L7pRAAAAMAAJ.
[56] M.G. Kadhim, M.T. Ali, A Critical Review on Corrosion and its Prevention in the Oil Field Equipment, J. Pet. Res. Stud. (2017) 1–28.
[57] E. Bardal, Corrosion and protection, Springer, London, 2004. doi:10.5860/choice.41-5927.
[58] A. Dugstad, The importance of FeCO3 supersaturation on the CO2 corrosion of carbon steels, in: Corros. 92, Houston, 1992.
[59] M. Kermani, L. Smith, CO2 corrosion control in oil and gas production: design considerations, Inst. Mater. (1997) 53.
[60] N. International, Corrosion of oil- and gas-well equipment, Dallas: Division of Production, American Petroleum Institute, Dallas, 1958.
[61] M.B. Kermani, L.M. Smith, Prediction of Co2 Corrosion in the Oil and Gas Industry, London, UK, 1994.
[62] K. Videm, A. Dugstad, EFFECT OF FLOW RATE, pH, Fe (2+) CONCENTRATION AND STEEL QUALITY ON THE CO2 CORROSION OF CARBON STEELS, Corros. 87, NACE, Houston, TX. (1987).
[63] G. Schmitt, Fundamental aspects of CO 2 corrosion, Corros. 83, Pap. No. 43 NACE, Houston, Tx. (1984).
[64] G. Schmitt, S. Feinen, EFFECT OF ANIONS AND CATIONS ON THE PIT INITIATION IN CO2 CORROSION OF IRON AND STEEL, in: Corrosion, 2000.
[65] G. Schmitt, D. Engels, SEM/EDX Analysis of Corrosion Products for Investigations on Metallurgy and Solution Effects in CO 2 Corrosion, Corros. 88, Pap. No. 149, NACE, Houston, TX. (1988).
[66] K. Videm, A. Dugstad, Galvanic Influence of CO2 Corrosion, in: Corrosion, NACE International, Houston, TX, 89AD: p. Paper no. 468.
[67] K. Videm, A.M. Koren, Corrosion, passivity, and pitting of carbon steel in aqueous solutions of HCO3, CO2, and Cl, Corrosion. 49 (1993) 746–754. doi:10.5006/1.3316127.
[68] C. J.L., Which CO2 Corrosion, Hence Which Prediction?,” in Predicting CO2 Corrosion in the Oil and Gas Industry, in: Eur. Fed. Corros., Institute of Materials, London, UK, 1994.
[69] A. Ikeda, S. Mukai, M. Ueda, Prevention of CO2 Corrosion of Line Pipe and Oil Country Tubular Goods, in: CORROSION, NACE, Houston, TX, 84AD: p. Paper no. 289.
[70] R. Nyborg, A. Dugstad, Understanding and prediction of mesa corrosion attack, NACE - Int. Corros. Conf. Ser. (2003).
[71] T.E. Perez, Corrosion in the oil and gas industry: An increasing challenge for materials, Energy Mater. 2014, Conf. Proc. 65 (2014) 565–574. doi:10.1007/s11837-013-0675-3.
[72] T.J.A. Richardson, B.R.A. Cottis, R. Lindsay, S. Lyon, D.J.. Scantlebury, H. Stott, M. Graham, Shreir’s corrosion, Elsevier Science, 2010.
[73] L.C. Lozada, Corrosion performance of L80 , L80Cr1 % and L80Cr3 % steel grades in simulant solution with carbon dioxide and scaling, Manchester, 2015.
[74] S. Nesic, K.J. Lee, V. Ruzic, A Mechanistic Model of Iron Carbonate Film Growth and the Effect on CO2 Corrosion of Mild Steel, in: Corrosion, 2002: pp. 1–35.
[75] A. Dugstad, Formation of protective corrosion films during CO sub 2 corrosion of carbon steel, Eur. Fed. Corros. Publ. 26 (1999) 70–76.
[76] K. Nalli, Corrosion and Its Mitigation in the Oil and Gas Industries, Process Plant Equip. (2012) 673–679. doi:10.1002/9781118162569.app6.
[77] W. Sun, S. Nesic, A mechanistic model of H2S corrosion of mild steel, in: NACE Int.

Corros. Conf. Expo, 2007: pp. 1–26. doi:10.1016/j.clinph.2008.07.213.
[78] G. V. Chilingar, C.M. Beeson, Surface Operations in Petroleum Production, Elsevier Publishing Co., New York, London, Amsterdam, 1969. doi:10.1017/S0016756800059550.
[79] W. Sun, Kinetics of iron carbonate and iron sulfide scale formation in CO2/H2S corrosion, Russ College of Engineering and Technology, 2006.
[80] D.W. Shoesmith, P. Taylor, M.G. Bailey, D.G. Owen, The Formation of Ferrous Monosulfide Polymorphs during the Corrosion of Iron by Aqueous Hydrogen Sulfide at 21°C, J. Electrochem. Soc. 127 (1980) 1007–1015. doi:10.1149/1.2129808.
[81] H. Ma, X. Cheng, G. Li, S. Chen, Z. Quan, S. Zhao, L. Niu, The influence of hydrogen sulfide on corrosion of iron under different conditions, Corros. Sci. 42 (2000) 1669–1683. doi:10.1016/S0010-938X(00)00003-2.
[82] J.R. Davis, Corrosion: Understanding the basics, ASM International, Materials Park, OH (US), 2000.
[83] M. Institute of Materials and Mining, A working party report on guidelines on materials requirements for carbon and low alloy steels for H_2S-containing environments in oil and gas production., 3rd ed.., Leeds, UK : Published for the European Federation of Corrosion by Maney Publishing on behalf of the Institute of Materials, Minerals & Mining, Leeds, UK, 2009.
[84] S.M.R. Ziaei, A.H. Kokabi, M. Nasr-Esfehani, Sulfide stress corrosion cracking and hydrogen induced cracking of A216-WCC wellhead flow control valve body, Case Stud. Eng. Fail. Anal. 1 (2013) 223–234. doi:10.1016/j.csefa.2013.08.001.
[85] G.N. Haidemenopoulos, H. Kamoutsi, K. Polychronopoulou, P. Papageorgiou, I. Altanis, P. Dimitriadis, M. Stiakakis, Investigation of stress-oriented hydrogen-induced cracking (SOHIC) in an amine absorber column of an oil refinery, Metals (Basel). 8 (2018). doi:10.3390/met8090663.
[86] M.S. Alwaranbi, CHLORIDE PITTING CORROSION OF API X-80 and X-100 HIGH STRENGTH LOW ALLOY PIPELINE STEELS IN BICARBONATE SOLUTIONS, University of British Colombia, 2006.
[87] L. Smith, Control of corrosion in oil and gas production tubing, Br. Corros. J. 34 (1999) 247.
https://nickelinstitute.org/~/Media/Files/TechnicalLiterature/ControlofCorrosioninOiland GasProductionTubing_14052_.pdf.
[88] B. Craig, J. Collins, R. Patrick, T. Gilbert, TESTING AND EVALUATION OF CORROSION-RESISTANT ALLOYS, Mater. Perform. 30 (1991) 51–55.
[89] C.P. Dillon, Corrosion resistance of stainless steels, New York : M. Dekker, New York, 1995.
[90] N. Chermat-Aourasse, R. Kesri, Corrosion-Electrochemical behavior of 13% chromium (Cr) martensitic stainless steel in hydrochloric acid (HCl) solutions, Prot. Met. 43 (2007) 344–352. doi:10.1134/S0033173207040054.
[91] L. Calabrese, M. Galeano, E. Proverbio, D. Di Pietro, F. Cappuccini, A. Donato, Monitoring of 13% Cr martensitic stainless steel corrosion in chloride solution in presence of thiosulphate by acoustic emission technique, Corros. Sci. 111 (2016) 151–161. doi:10.1016/j.corsci.2016.05.010.
[92] L. Xu, Y. Meng, Y. Shi, Y. Liu, Effects of temperature on the corrosion behavior of 13Cr martensitic stainless steel during exposure to CO2 and Cl- environment, Acta Metall. Sin. (English Lett. 26 (2013) 271–276. doi:10.1016/j.matlet.2005.06.002.

[93] T.R. Hernandez, STUDY OF CORROSION OF 13 Cr STAINLESS STEEL UNDER ALTERNATING CURRENT IN ARTIFICIAL SEAWATER, 2011.
[94] S. Hashizume, Y. Inohara, K. Masamura, Effects of pH and PH2S on SSC Resistance of Martensitic Stainless Steels, in: Corrosion, 2000.
[95] C.P. Linne, F. Blanchard, G.C. Guntz, CORROSION PERFORMANCES OF MODIFIED 13Cr FOR OCTG IN OIL AND GAS ENVIRONMENTS, in: Corrosion, 97AD.
[96] A. Turnbull, A. Griffiths, Corrosion and cracking of weldable 13 wt-%Cr martensitic stainless steels for application in the oil and gas industry, Corros. Eng. Sci. Technol. 38 (2003) 21–50. doi:10.1179/147842203225001432.
[97] S. Sakamoto, K. Maruyama, H. Kaneta, CORROSION PROPERTY OF API AND MODIFIED 13CR STEELS IN OIL AND GAS ENVIRONMENT, in: Corrosion, 96AD: p. Paper no. 77.
[98] Y. Miyata, M. Kimura, T. Koseki, T. Toyooka, F. Murase, MARTENSITIC STAINLESS STEEL SEAMLESS LINEPIPE WITH SUPERIOR WELDABILITY AND C02 CORROSION RESISTANCE, in: Corrosion, 1997.
[99] M. Kimura, Y. Miyata, T. Toyooka, K.S. Corporation, K.S. Corporation, C. Works, EFFECT OF RETAINED AUSTENITE ON CORROSION PERFORMANCE FOR MODIFIED 13% Cr STEEL PIPE, in: Corrosion, 2000.
[100] S. Huizinga, W.E. Liek, LIMITATIONS FOR THE APPLICATION OF 13CR STEEL IN OfL AND GAS Production ENVIRONMENTS, in: Corrosion, 1997: pp. 1–7.
[101] M. Ueda, H. Amaya, K. Kondo, K. Ogawa, T. Mori, CORROSION RESISTANCE OF WELDABLE SUPER 13CR STAINLESS STEEL IN HZS CONTAINING C02 ENVIRONMENTS, in: Corrosion, 1996: p. Paper no. 58.
[102] D. Abayarathna, R.D. Kane, DEFINITION OF SAFE SERVICE USE LIMITS FOR USE OF STAINLESS ALLOYS IN PETROLIUM PRODUCTION, in: Corrosion, 1997: p. Paper no. 34.
[103] P. Felton, M.J. Schofield, Extending the limits of corrosion behaviour of modified 13%Cr martensitic OCTG at high temperature, in: Supermartensitic Stainl. Steels, Belgian Welding Institute, Brussels, 1999: pp. 272–282.
[104] B.R. Linter, G.T. Burstein, Reactions of pipeline steels in carbon dioxide solutions, Corros. Sci. 41 (1999) 117–139. doi:10.1016/S0010-938X(98)00104-8.
[105] S. Huizinga, W.E. Liek, Corrosion behavior of 13% chromium steel in acid stimulations, Corrosion. 50 (1994) 555–566. doi:10.5006/1.3294357.
[106] R. Case, R.C. Newman, S. Olsen, G. Rorvik, Pit Growth Behaviour of Modified 13 Cr Steel In Sour Environments, Eurocorr 2000. (2000) 1–10.
[107] B.W.. Sherar, The Effect of the Environment on the Corrosion Products and Corrosion Rates on Gas Transmission Pipelines, The University of Western Ontario, 2011.
[108] F.O. Ajayi, Mitigating corrosion risks in oil and gas equipment by elefctrochemical protection: Top of the line corrosion, The University of Manchester, 2015.
[109] M. Koteeswaran, CO2 and H2S Corrosion in Oil Pipelines, University of Stavanger, 2010.
[110] J.F. Rios, J.A. Calderón, R.P. Nogueira, Electrochemical behavior of metals used in drinking water distribution systems: A rotating cylinder electrode's study, Corrosion. 69 (2013) 875–885. doi:10.5006/0848.
[111] F. Gapsari, R. Soenoko, A. Suprapto, W. Suprapto, Minimization of Corrosion Rate Using Response Surface Methodology, Eng. Rev. XX (2018) 115–119.
[112] J.C. Velazquez, F. Caleyo, A. Valor, J. m. Hallen, Predictive Model for Pitting Corrosion

in Buried Oil and Gas Pipelines, Corrosion. (2009) 332.
[113] S. Papavinasam, A. Doiron, R.W. Reivie, V. Sizov, Model predicts internal pitting corrosion of oil , gas pipelines, Oil Gas J. (2007) 68.
[114] J.R. Galvele, Transport Processes and the Mechanism of Pitting of Metals, (1976) 464–474.
[115] C. Mohammad, M. Islam, Effects of Concentration of Sodium Chloride Solution on the Pitting Corrosion Behavior of AISI-304L, 17 (2011) 477–483. doi:10.2298/CICEQ110406032A.
[116] S. Sakamoto, K. Maruyama, Corrosion Property of API and Modified 13Cr Steels in Oil and Gas Environment, in: NACE Int. Annu. Conf. Expo., 1996.
[117] C.I. Ossai, B. Boswell, I.J. Davies, Predictive Modelling of Internal Pitting Corrosion of Aged Non-Piggable Pipelines, 162 (2015). doi:10.1149/2.0701506jes.
[118] C. Krishna S, N.K. Gangwar, A.K. Jha, B. Pant, K.M. George, Microstructure and properties of 15Cr-5Ni-1Mo-1W martensitic stainless steel, Steel Res. Int. 86 (2015) 51–57. doi:10.1002/srin.201400035.
[119] R. Fan, M. Gao, Y. Ma, X. Zha, X. Hao, K. Liu, Effects of Heat Treatment and Nitrogen on Microstructure and Mechanical Properties of 1Cr12NiMo Martensitic Stainless Steel, J. Mater. Sci. Technol. 28 (2012) 1059–1066. doi:10.1016/S1005-0302(12)60173-X.
[120] B. Ravi Kumar, S. Sharma, P. Munda, R.K. Minz, Structure and microstructure evolution of a ternary Fe-Cr-Ni alloy akin to super martensitic stainless steel, Mater. Des. 50 (2013) 392–398. doi:10.1016/j.matdes.2013.03.035.
[121] I. Calliari, M. Zanesco, M. Dabalà, K. Brunelli, E. Ramous, Investigation of microstructure and properties of a Ni-Mo martensitic stainless steel, Mater. Des. 29 (2008) 246–250. doi:10.1016/j.matdes.2006.11.020.
[122] B.M. Schönbauer, S.E. Stanzl-Tschegg, A. Perlega, R.N. Salzman, N.F. Rieger, S. Zhou, A. Turnbull, D. Gandy, Fatigue life estimation of pitted 12% Cr steam turbine blade steel in different environments and at different stress ratios, Int. J. Fatigue. 65 (2014) 33–43. doi:10.1016/j.ijfatigue.2013.10.003.
[123] M. El May, T. Palin-Luc, N. Saintier, O. Devos, Effect of corrosion on the high cycle fatigue strength of martensitic stainless steel X12CrNiMoV12-3, Int. J. Fatigue. 47 (2013) 330–339. doi:10.1016/j.ijfatigue.2012.09.018.
[124] G. Das, S. Ghosh Chowdhury, A. Kumar Ray, S. Kumar Das, D. Kumar Bhattacharya, Turbine blade failure in a thermal power plant, Eng. Fail. Anal. 10 (2003) 85–91. doi:10.1016/S1350-6307(02)00022-5.
[125] S.Y. Lu, K.F. Yao, Y.B. Chen, M.H. Wang, Y. Shao, X.Y. Ge, Effects of austenitizing temperature on the microstructure and electrochemical behavior of a martensitic stainless steel, J. Appl. Electrochem. 45 (2015) 375–383. doi:10.1007/s10800-015-0796-1.
[126] P.P. Sarkar, P. Kumar, M.K. Manna, P.C. Chakraborti, Microstructural influence on the electrochemical corrosion behaviour of dual-phase steels in 3.5% NaCl solution, Mater. Lett. 59 (2005) 2488–2491. doi:10.1016/j.matlet.2005.03.030.
[127] M. Kimura, Y. Miyata, T. Tayooka, Y. Kitahaba, Effect of retained austenite on corrosion performance for modified 13% Cr steel pipe, Corrosion. 57 (2001) 433–439. doi:10.5006/1.3290367.
[128] X. Lei, Y. Feng, J. Zhang, A. Fu, C. Yin, D.D. Macdonald, Impact of Reversed Austenite on the Pitting Corrosion Behavior of Super 13Cr Martensitic Stainless Steel, Electrochim. Acta. 191 (2016) 640–650. doi:10.1016/j.electacta.2016.01.094.
[129] S.Y. Lu, K.F. Yao, Y.B. Chen, M.H. Wang, N. Chen, X.Y. Ge, Effect of quenching and

partitioning on the microstructure evolution and electrochemical properties of a martensitic stainless steel, Corros. Sci. 103 (2016) 95–104. doi:10.1016/j.corsci.2015.11.010.
[130] E. Mabruri, Z.A. Syahlan, Sahlan, S. Prifiharni, M.S. Anwar, S.A. Chandra, T.B. Romijarso, B. Adjiantoro, Influence of Austenitizing Heat Treatment on the Properties of the Tempered Type 410-1Mo Stainless Steel, IOP Conf. Ser. Mater. Sci. Eng. 202 (2017). doi:10.1088/1757-899X/202/1/012085.
[131] P. Wang, S.P. Lu, N.M. Xiao, D.Z. Li, Y.Y. Li, Effect of delta ferrite on impact properties of low carbon 13Cr-4Ni martensitic stainless steel, Mater. Sci. Eng. A. 527 (2010) 3210–3216. doi:10.1016/j.msea.2010.01.085.
[132] Y. Liu, J. Sun, J. Li, B. Jiang, C. Zhang, Investigation of forging process for eliminating delta ferrites in USC unites last stage blades steel 10Cr12Ni3Mo2VN, Procedia Eng. 207 (2017) 1797–1802. doi:10.1016/j.proeng.2017.10.941.
[133] S.A. Bashu, K. Singh, M.S. Rawat, Effect of heat treatment on mechanical properties and fracture behaviour of a 12CrMoV steel, Mater. Sci. Eng. 127 (1990) 7–15. doi:10.1016/0921-5093(90)90184-5.
[134] D. Carrouge, H.K.D.H. Bhadeshia, P. Woollin, Effect of δ-ferrite on impact properties of supermartensitic stainless steel heat affected zones, Sci. Technol. Weld. Join. 9 (2004) 377–389. doi:10.1179/136217104225021823.
[135] L. Schäfer, Influence of delta ferrite and dendritic carbides on the impact and tensile properties of a martensitic chromium steel, J. Nucl. Mater. 258–263 (1998) 1336–1339. doi:10.1016/S0022-3115(98)00200-1.
[136] W. Yan, P. Zhu, J. Deng, Corrosion Behaviors of SMSS 13Cr and DSS 22Cr in H 2 S / CO 2 - Oil - Water Environment, 11 (2016) 9542–9558. doi:10.20964/2016.11.13.
[137] J.O. Park, S. Matsch, H. Bo, Effects of Temperature and Chloride Concentration on Pit Initiation and Early Pit Growth of Stainless Steel, (2002) 34–39. doi:10.1149/1.1430415.
[138] S. Richter, M. Achour, K. Addis, M. Singer, S. Nesic, M. Technology, Development and Application of a Downhole Corrosion Prediction Model, in: NACE Int. Corros. Conf. Expo, 2016: pp. 1–15.
[139] M. Kazemipour, S. Salahi, A. Nasiri, On the Influence of the Environmental Factors on Corrosion Behavior of 13Cr Stainless Steel Using Box-Behnken Design, (2019) 1–9.
[140] G.X. Zhao, M. Zheng, X.H. Lv, X.H. Dong, H.L. Li, Effect of Temperature on Anodic Behavior of 13Cr Martensitic Steel in CO 2 Environment, 11 (2005).
[141] E. Mabruri, R.R. Pasaribu, M.T. Sugandi, Sunardi, Effect of high temperature tempering on the mechanical properties and microstructure of the modified 410 martensitic stainless steel, AIP Conf. Proc. 1964 (2018). doi:10.1063/1.5038314.
[142] L.Q. Xu, D.T. Zhang, Y.C. Liu, B.Q. Ning, Z.X. Qiao, Z.S. Yan, H.J. Li, Precipitation behavior and martensite lath coarsening during tempering of T/P92 ferritic heat-resistant steel, Int. J. Miner. Metall. Mater. 21 (2014) 438–447. doi:10.1007/s12613-014-0927-4.
[143] Z. Hou, R.P. Babu, P. Hedström, J. Odqvist, Microstructure evolution during tempering of martensitic Fe–C–Cr alloys at 700 °C, J. Mater. Sci. 53 (2018) 6939–6950. doi:10.1007/s10853-018-2036-7.
[144] J.C. Lippold, D.J. Kotecki, Welding metallurgy and weldability of stainless steels, Weld. Metall. Weldability Stainl. Steels, by John C. Lippold, Damian J. Kotecki, Pp. 376. ISBN 0-471-47379-0. Wiley-VCH, March 2005. (2005) 376.
[145] S.Y. Lu, K.F. Yao, Y.B. Chen, M.H. Wang, X. Liu, X. Ge, The effect of tempering temperature on the microstructure and electrochemical properties of a 13 wt.% Cr-type

martensitic stainless steel, Electrochim. Acta. 165 (2015) 45–55. doi:10.1016/j.electacta.2015.02.038.
[146] Y.Y. Song, X.Y. Li, L.J. Rong, D.H. Ping, F.X. Yin, Y.Y. Li, Formation of the reversed austenite during intercritical tempering in a Fe-13%Cr-4%Ni-Mo martensitic stainless steel, Mater. Lett. 64 (2010) 1411–1414. doi:10.1016/j.matlet.2010.03.021.
[147] B. Abbasi-Khazaei, A. Mollaahmadi, Rapid Tempering of Martensitic Stainless Steel AISI420: Microstructure, Mechanical and Corrosion Properties, J. Mater. Eng. Perform. 26 (2017) 1626–1633. doi:10.1007/s11665-017-2605-y.
[148] S.K. Bonagani, V. Bathula, V. Kain, Influence of tempering treatment on microstructure and pitting corrosion of 13 wt.% Cr martensitic stainless steel, Corros. Sci. 131 (2018) 340–354. doi:10.1016/j.corsci.2017.12.012.
[149] B.A. Tabatabae, F. Ashrafizadeh, A.M. Hassanli, Influence of retained austenite on the mechanical properties of low carbon martensitic stainless steel castings, ISIJ Int. 51 (2011) 471–475. doi:10.2355/isijinternational.51.471.
[150] P. Krakhmalev, I. Yadroitsava, G. Fredriksson, I. Yadroitsev, In situ heat treatment in selective laser melted martensitic AISI 420 stainless steels, Mater. Des. 87 (2015) 380–385. doi:10.1016/j.matdes.2015.08.045.
[151] C. Tan, K. Zhou, W. Ma, P. Zhang, M. Liu, T. Kuang, Microstructural evolution, nanoprecipitation behavior and mechanical properties of selective laser melted high-performance grade 300 maraging steel, Mater. Des. 134 (2017) 23–34. doi:10.1016/j.matdes.2017.08.026.
[152] J. Ge, J. Lin, Y. Chen, Y. Lei, H. Fu, Characterization of wire arc additive manufacturing 2Cr13 part: Process stability, microstructural evolution, and tensile properties, J. Alloys Compd. 748 (2018) 911–921. doi:10.1016/j.jallcom.2018.03.222.
[153] G. Lorang, M.D.C. Belo, A.M.P. Simões, M.G.S. Ferreira, Chemical Composition of Passive Films on AISI 304 Stainless Steel, J. Electrochem. Soc. 141 (1994) 3347–3356. doi:10.1149/1.2059338.
[154] R.K. Gupta, N. Birbilis, The influence of nanocrystalline structure and processing route on corrosion of stainless steel: A review, Corros. Sci. 92 (2015) 1–15. doi:10.1016/j.corsci.2014.11.041.
[155] A. Fattah-Alhosseini, S. Vafaeian, Influence of grain refinement on the electrochemical behavior of AISI 430 ferritic stainless steel in an alkaline solution, Appl. Surf. Sci. 360 (2016) 921–928. doi:10.1016/j.apsusc.2015.11.085.
[156] L. Jinlong, L. Tongxiang, W. Chen, D. Limin, Effect of ultrafine grain on tensile behaviour and corrosion resistance of the duplex stainless steel, Mater. Sci. Eng. C. 62 (2016) 558–563. doi:10.1016/j.msec.2016.02.008.
[157] A. Di Schino, M. Barteri, J.M. Kenny, Effects of grain size on the properties of a low nickel austenitic stainless steel, J. Mater. Sci. 38 (2003) 4725–4733. doi:10.1023/A:1027470917858.
[158] A. Di Schino, J.M. Kenny, Effects of the grain size on the corrosion behavior of refined AISI 304 austenitic stainless steels, J. Mater. Sci. Lett. 21 (2002) 1631–1634. doi:10.1023/A:1020338103964.
[159] A.A. Tiamiyu, U. Eduok, J.A. Szpunar, A.G. Odeshi, Corrosion behavior of metastable AISI 321 austenitic stainless steel: Investigating the effect of grain size and prior plastic deformation on its degradation pattern in saline media, Sci. Rep. 9 (2019) 1–18. doi:10.1038/s41598-019-48594-3.

[160] H. Nakagawa, T. Miyazaki, Effects of the amount of retained austenite on the microstructures and mechanical properties of a precipitation hardening martensitic stainless steel, Tetsu-To-Hagane/Journal Iron Steel Inst. Japan. 84 (1998) 43–48.
[161] S. Dieck, P. Rosemann, A. Kromm, T. Halle, Reversed austenite for enhancing ductility of martensitic stainless steel, IOP Conf. Ser. Mater. Sci. Eng. Pap. 181 (2017) 012034. doi:10.1088/1742-6596/755/1/011001.
[162] P.D. Bilmes, C.L. Llorente, L. Saire Huamán, L.M. Gassa, C.A. Gervasi, Microstructure and pitting corrosion of 13CrNiMo weld metals, Corros. Sci. 48 (2006) 3261–3270. doi:10.1016/j.corsci.2005.10.009.
[163] J.M. Aquino, C.A. Della Rovere, S.E. Kuri, Localized corrosion susceptibility of supermartensitic stainless steel in welded joints, Corrosion. 64 (2008) 35–39. doi:10.5006/1.3278459.
[164] M. Dadfar, M.H. Fathi, F. Karimzadeh, M.R. Dadfar, A. Saatchi, Effect of TIG welding on corrosion behavior of 316L stainless steel, Mater. Lett. 61 (2007) 2343–2346. doi:10.1016/j.matlet.2006.09.008.
[165] T.J. Mesquita, E. Chauveau, M. Mantel, N. Kinsman, R.P. Nogueira, Influence of Mo alloying on pitting corrosion of stainless steels used as concrete reinforcement, Rem Rev. Esc. Minas. 66 (2013) 173–178. doi:10.1590/s0370-44672013000200006.
[166] Y.Q. Wang, N. Li, B. Yang, Effect of ferrite on pitting corrosion of Fe20Cr9Ni cast austenite stainless steel for nuclear power plant pipe, Corros. Eng. Sci. Technol. 50 (2015) 330–337. doi:10.1179/1743278214Y.0000000229.
[167] T. Ogawa, T. Koseki, Effect of composition profiles on metallurgy and corrosion behavior of duplex stainless steel weld metals, Weld. J. 68 (1989) 181.